First Street

August 2024

First Street Technology

Table of Contents

First Street

Executive Summary

This technical methodology outlines the supporting research, data inputs, and analytical methods used in a comprehensive study of climate-induced migration patterns and their wide-ranging effects on communities across the contiguous United States (CONUS). At the center of this analysis is the First Street Climate Migration Model (FS-CMM), which projects future population changes due to various climate hazards, including floods, wildfires, smoke, drought, extreme heat, and tropical cyclone winds, under different climate scenarios. This model produces outputs expressed as absolute population changes expected for each census block group, broken down by specific hazards or combined across all hazards, for both current and future years under given climate scenarios. When converted to percentages, these population change projections are used as inputs for a series of subsequent models, each designed to explore the ripple effects of climate-induced migration. Through the creation of conversion tables, or damage functions, these secondary models translate population shifts into percent impacts on sociodemographic composition, economic indicators, and property values. Other tertiary impacts include the effects of select employment characteristics, i.e., labor force composition and downstream commercial viability across sectors using a similar conversion table technique. This interconnected modeling approach allows for a comprehensive assessment of how climate-driven population changes may reshape the social and economic aspects of affected regions, offering a robust tool for anticipating and planning for the complex consequences of climate migration. These analyses contribute to a comprehensive picture of climate change's indirect effects on the housing and financial industries, complementing the broader assessment of community-level impacts. For a full list of variables modeled, please refer to **Appendix Table 1**.

First Street

KEY TAKEAWAYS:

1. Climate Migration Model: Applies empirically derived historical relationships between climate hazards and population change using high-resolution climate risk data, historic population trends, and socioeconomic factors to adjust future population estimates at the census block group level from 2025 to 2055 under five different climate scenarios (SSP-RCPs).

2. Demographic Change Analysis: Examines how changes in community sociodemographic composition are associated with population shifts, providing insights into potential future socioeconomic and demographic trends in areas experiencing climate-induced migration.

3. Economic Implications: Assesses the relationships between population change and key economic indicators such as GDP, Housing Price Index (HPI), and Debt-to-Income (DTI) ratio across different geographic contexts.

4. Commercial Implications: Evaluates how changes in sectoral labor force composition, driven by population shifts, may impact business outcomes including employment, establishment counts, payroll, revenue, and costs across major industry sectors.

5. Property Value Analysis: Investigates both pre-exposure market impacts on property values and post-exposure effects of specific climate hazards (flood, wind, wildfire) on property transactions and values.

6. Tax Revenue Implications: Estimates potential changes in property tax revenues resulting from climate-induced population shifts and property value changes.

First Street

Abbreviations

ACS - American Community Survey

ATT - Average Treatment Effect on the Treated

BEA - Bureau of Economic Analysis

BLS - Bureau of Labor Statistics

CBP - County Business Patterns

CFPB - Consumer Financial Protection Bureau

CONUS - Contiguous United States

DTI - Debt-to-Income

ECN - Economic Census

EPA - Environmental Protection Agency

FEMA - Federal Emergency Management Agency

FHFA - Federal Housing Finance Agency

FS-CMM - First Street Climate Migration Model

GAM - Generalized Additive Model

GDP - Gross Domestic Product

HMDA - Home Mortgage Disclosure Act

HPI - Housing Price Index

IDMC - Internal Displacement Monitoring Center

IPCC - Intergovernmental Panel on Climate Change

LASSO - Least Absolute Shrinkage and Selection Operator

LTDB - Longitudinal Tract Database

NAICS - North American Industry Classification System

NHGIS - National Historical Geographic Information System

NOAA - National Oceanic and Atmospheric Administration

PLSR - Partial Least Squares Regression

PSM - Propensity Score Matching

RPs - Return Periods

RUC - Region-Urbanicity-Coastline

SSP - Shared Socioeconomic Pathway

USDA - United States Department of Agriculture

First Street

1. Climate Migration Model

1.1 Executive Summary

The development of this model relies on investigation of the impact of multiple natural hazards on population shifts across U.S. Census Block Groups from 2000 to 2020, with the primary purpose of predicting future population changes due to increasing climate exposure. By expanding on previous research conducted by Shu et al. (2023) at First Street that primarily focused on flood-induced migration, this analysis aims to provide a comprehensive understanding of how various climate risks will reshape population distributions across the United States. The study considers floods, wildfire smoke, droughts, wildfires, heatwaves, and cyclonic winds, each characterized by distinct sources, intensities, and probabilities. This multi-hazard approach allows for a more nuanced prediction of future migration patterns and population changes in response to evolving climate risks.

The study combines historical population data with current and future climate risk information and future climate projections to model population trends under all five Shared Socioeconomic Pathway (SSP) scenarios. By incorporating high-resolution climate risk data for multiple return periods and severities, the analysis allows for a more complex investigation of how populations react to various characterizations of risk. The methodology includes a temporal dimension reduction process to estimate long-term climate hazards, propensity score matching at the state level, and Least Absolute Shrinkage and Selection Operator (LASSO) regression to quantify the impact of the six climate hazards on population change. These estimates are then used to develop future population projections, providing insights into how combined climate risks are likely to impact future population growth in local communities across the U.S. The results reveal varying impacts of different climate hazards on population change, with implications for future population distributions and community resilience planning.

1.2 Background

Climate migration, the movement of people in response to environmental changes or natural disasters caused by climate change, has become an increasingly significant area of research as the impacts of climate change intensify. As global temperatures rise, increased extreme weather events, sea level rise, and altered precipitation patterns can make some areas less livable by posing safety risks, damaging infrastructure, destroying property, disrupting local economies, and compromising access to essential resources.

The scale of climate-induced displacement is significant. The Internal Displacement Monitoring Center (IDMC, 2021) reported that in 2020 alone, nearly 1.7 million Americans were displaced by natural disasters, many of which were climate-related. Furthermore, studies by the Environmental Protection Agency (EPA, 2021) indicate that regions such as the Gulf Coast and California are experiencing higher rates of out-migration as residents seek safer and more stable environments due to issues of extreme heat, flooding, and air quality.

While early studies focused primarily on international migration due to climate change (e.g., Myers, 2002; McLeman and Smit, 2006), recent research has shifted towards examining internal migration patterns within countries, particularly in the United States. A seminal study by Hauer (2017) projected that sea level rise alone could displace up to 13 million Americans by 2100. This work highlighted the potential scale of climate-induced migration within the U.S. and sparked further research into the topic. Building on this, Keenan et al. (2018) introduced the concept of "climate gentrification" in Miami-Dade County, demonstrating how flood risk influences property values and migration patterns, with higher elevations becoming more desirable as flood-prone areas are increasingly seen as uninhabitable.

More recently, Shu et al. (2023) provided a comprehensive analysis of flood-induced migration in the U.S. They found that between 2000 and 2020, flood risk at the neighborhood level directly impacted approximately 7.3 million residential moves. Notably, they identified two key patterns: "risky growth" areas where population continued to increase despite flood risk, and "climate abandonment areas" where 3.2 million people left due to flood risk and other factors.

While flood risk has been a primary focus, other climate hazards are also influencing migration patterns. Fan et al. (2016) found that drought conditions in California led to increased out-migration, particularly among agricultural workers. Similarly, Nawrotzki et al. (2017) demonstrated that wildfire events in the western U.S. resulted in short-term population displacement and longer-term migration trends. Despite these advances, current U.S.-focused research on climate migration remains predominantly centered on flood risk, neglecting the impact of other climate hazards. This narrow focus limits our understanding of the full scope of climate-induced migration and its downstream impacts on communities across various climate hazards (IDMC, 2021).

Our research aims to address this gap by examining the relationship between residential mobility patterns and increased exposure to a range of climate risks, including flooding, wildfires, wildfire smoke, extreme heat events, hurricane winds, and drought. We build upon the conceptual framework of Shu et al. (2023), which demonstrated that the relationship between flood risk and population change was both nonlinear and

confounded by the larger economic context of the local area. We extend this framework to multiple climate hazards to coin the First Street Climate Migration Model (FS-CMM), hypothesizing that similar nonlinear relationships and economic moderating effects will be observed across various types of climate risks. To test these hypotheses, we developed a series of models predicting population change from 2000 to 2020, incorporating exposure and risk data for multiple climate hazards. To explore the potential moderating effect of an area's desirability, we also explored these relationships separately for areas that experienced population gain or loss. This approach allows us to disentangle the effects of climate risks from other factors influencing migration patterns, providing a more comprehensive understanding of climate-induced residential mobility across the United States.

1.3 Methodology

The FS-CMM leverages historic data from 2000 - 2020, including population, amenity and socioeconomic information available at the community level (block or tract), as well as current and future First Street climate hazard data including flood, tropical cyclone winds, heatwaves, wildfires, wildfire smoke, and drought across CONUS. To control for extrinsic factors, we developed propensity scores to match block groups that share similar amenity and socioeconomic profiles. We then used LASSO regression to estimate the impact of the six climate hazards on population change. These estimates were then used to develop future population projections based on the climate trends under the SSP2 scenario. This provides the first insight into how combined climate risks are likely to impact future population growth in local communities across the U.S. A flow chart visualizing the steps of the FS-CMM creation is presented in **Figure 1.1**.

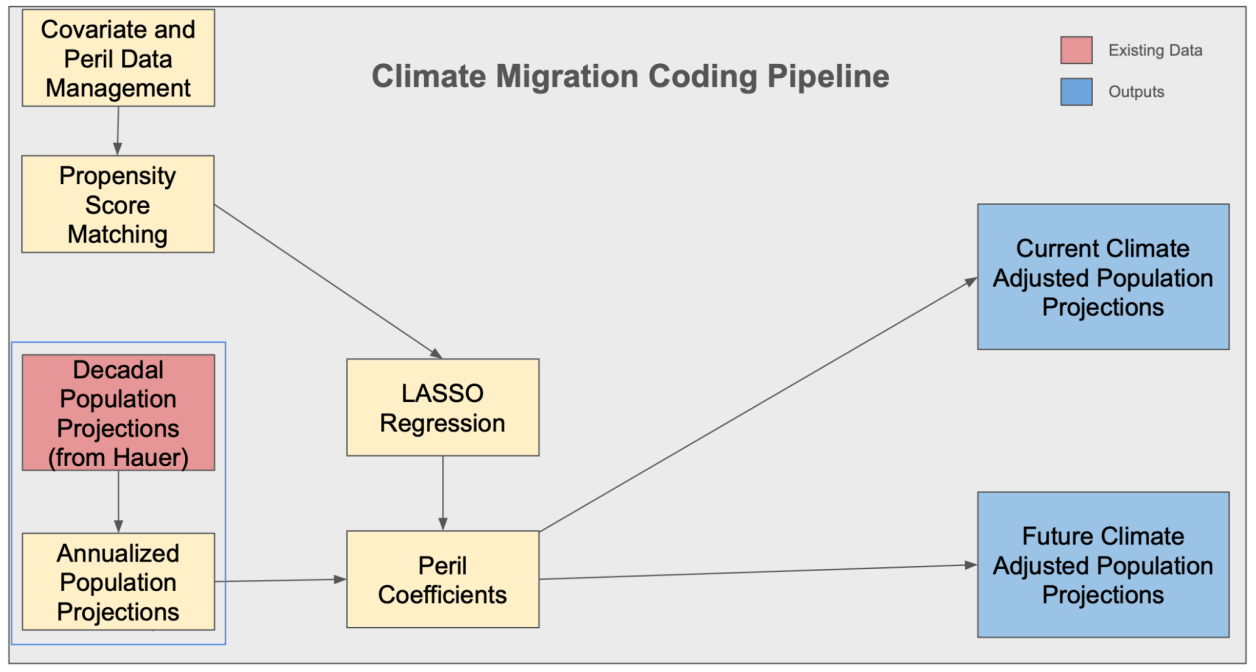

Figure 1.1 FS-CMM Pipeline tracking input data, modeling steps, and model outputs.

1.3.1 Data Inputs

FS-CMM relies on population projections, socioeconomic and geographic information, and climate projections to model climate-induced migration patterns. Socioeconomic data capture household characteristics, income levels, and employment indicators, while geographic data include topography, land use, and proximity to water bodies. Socioeconomic and geographic variables were used as covariates to match block groups that are characteristically similar, controlling for extrinsic factors and thereby isolating anticipated population changes due to climate hazards. Climate projection data encompass historic, current, and future exposure to various climate hazards at high spatial resolution.

Covariate Data

Data used to inform the covariates in our migration model was gathered from various federal and proprietary data sources. Socioeconomic data were obtained from the 2018 5-year American Community Survey (ACS) and Bureau of Economic Analysis (BEA) regional accounts datasets. Geographic characteristics were sourced from the USDA,

Lightbox, National Oceanic Atmospheric Administration (NOAA), and the UNC Global Rivers Database. **Table 1.1** provides a detailed overview of the incorporated community vulnerability and risk variables.

Table 1.1 Climate Migration Covariate Variables

Variable	Resolution	Time Period	Source
Total population	2000 and 2020 Census Tracts	2000 - 2020	5-year ACS
Total housing units	2010 Census Tract	2018	5-year ACS
Median income, persons aged 16 or older	2010 Census Tract	2018	5-year ACS
Total owner-occupied households	2010 Census Tract	2018	5-year ACS
Total 1-unit owner-occupied households, detached	2010 Census Tract	2018	5-year ACS
Total 1-unit owner-occupied households, attached	2010 Census Tract	2018	5-year ACS
Total 1-unit renter-occupied households, detached	2010 Census Tract	2018	5-year ACS
Total 1-unit renter-occupied households, attached	2010 Census Tract	2018	5-year ACS
Total properties with an active mortgage	2010 Census Tract	2018	5-year ACS
Percent of population that are single family home owners	2010 Census Tract	2018	5-year ACS
Percent of population that are single family	2010 Census Tract	2018	5-year ACS
Topography code*	County	1999	ERS USDA Natural Amenities Scale
Land area of a tract	2020 Census Tract	2020	Census 2010-2020 tract crosswalk
Water area of a tract	2020 Census Tract	2020	Census 2010-2020 tract crosswalk

First Street

Variable	Resolution	Time Period	Source
USDA amenity rank*	County	1999	ERS USDA Natural Amenities Scale
Number of jobs in climate exposed industries**	County	2001-2020	BEA Regional Economic Accounts
Total number of jobs	County	2001-2020	BEA Regional Economic Accounts
Ratio of climate-exposed jobs to total jobs	County	2001-2020	BEA Regional Economic Accounts
Number of campsites	County	2014	uscampgrounds.info
Number of schools	2010 Census Tract	2024	Lightbox
Number of fire stations	2010 Census Tract	2024	Lightbox
Number of police stations	2010 Census Tract	2024	Lightbox
Number of hospitals	2010 Census Tract	2024	Lightbox
Population density	2010 Census Tract	2018	5-year ACS
Median home value	2010 Census Tract	2018	5-year ACS
Number of individuals employed	2010 Census Tract	2018	5-year ACS
Number of individuals unemployed	2010 Census Tract	2018	5-year ACS
Number of individuals in the labor force	2010 Census Tract	2018	5-year ACS
Number of individuals not in the labor force	2010 Census Tract	2018	5-year ACS
Distance from the coast	2020 Census Tract	2013	NOAA Coastline FIle
Distance from the river	2020 Census Tract	2013	UNC Rivers Dataset

*See (https://www.ers.usda.gov/data-products/natural-amenities-scale/documentation/) for description of topography codes and amenity rank codes. Definitions appear in the raw data in rows 9-23 and 79-88, respectively.

**Climate-exposed industries include Farm proprietors employment; Farm employment; Forestry, fishing, and related activities; Mining, quarrying, and oil and gas extraction; Arts, entertainment, and recreation; Accommodation and food services

Climate Exposure Data

The FS-CMM utilizes high-resolution climate exposure data as the primary treatment variable to estimate the proportion of the population exposed to climate impacts. The model incorporates three temporal dimensions of climate exposure:

1. Historic exposure: Accounts for prior population sorting and operationalizes past experiences of climate impacts.
2. Current exposure: Captures perceived risk of potential impacts as of 2022 or 2023.
3. Future projections: Anticipates the scale and distribution of climate impacts 30 years into the future (2052 or 2053), based on the SSP2-4.5 scenario.

The FS-CMM considers six climate hazards: flood, tropical cyclone winds, wildfire smoke, drought, wildfires, and heatwaves. For most hazards, data are available for multiple return periods (RPs) and severities, allowing for a nuanced analysis of population responses to various risk characterizations:

- Flood: Proportion of inundated properties at Census block group level for 5, 20, 100, and 500 year RPs.
- Tropical Cyclone Winds: Expected wind speeds at tract level for 2, 5, 20, 100, 200 year RPs.
- Wildfire Smoke: Number of orange+, red+, purple+, and maroon AQI days in a bad year at tract level.
- Drought: Expected D2+ (D3, D4) weeks in a year for 2, 5, 10, 20, 100 year RPs at tract level.
- Wildfires: Maximum burn probability at tract level.
- Heatwaves: Probability of a relatively hot heatwave at tract level.

These data are primarily sourced from First Street Foundation (FS) models, with some exceptions. Historic flood exposure was assessed using flood event counts from Lai et al. and the NOAA Storm Events Database. Drought exposure data were obtained from the United States Drought Monitor, as no FS-based drought model currently exists.

The spatial resolution of each FS model output varies by peril, ranging from Census block group to tract level. This high-resolution data allows for a more complex investigation of how populations react to different characterizations of risk, including multiple sources (e.g., pluvial, fluvial, and coastal for flood risk) and severities. Table 1.2 provides a

detailed overview of the incorporated climate exposure variables, including their resolution, time periods, and source.

Table 1.2 Climate Migration Climate Variables

Variable	Resolution	Time Period	Source
Flood	Census Block Group	2022-2052	FS-FM
Tropical Cyclone Winds	Census Tract	2022-2052	FS-Wind
Heatwaves	Census Tract	2022-2052	FS-Heat
Wildfires	Census Tract	2023-2053	FS-Fire
Wildfire Smoke	Census Tract	2022-2052	FS-Air
Drought	Census Tract	2022-2052	USDM

The climate exposure data is then combined with the covariate data discussed above. The covariate data is largely gathered at the census tract-level with 2010 Federal Information Processing Standards (FIPS) delineations. A 2010 to 2020 tract crosswalk method was employed to reconcile changes in census tract boundaries over time so that data on covariates could be merged with climate exposure data to produce the final input data used in modeling. The crosswalk method involved relating 2010 tracts to 2020 tracts using area coverage ratios, preserving one-to-one matches where possible and assigning best matches for split or merged tracts. The method results in a crosswalk of 83,776 tracts for 2020 corresponding to 72,152 tracts from 2010, ensuring consistency with the CONUS count and facilitating analysis across changing geographic boundaries. Similarly, historic 2000 populations had to be crosswalked to 2020 FIPS boundaries, consistent with the 2020 FIPS codes used across our analysis. This was accomplished using the NHGIS 2000 to 2020 block group crosswalk obtained from: https://www.nhgis.org/geographic-crosswalks.

Furthermore, tract-level population data was downscaled to the block group level in order to align with climate exposure data and population projections data. In the absence of block group-level estimates, data for census tracts or counties are expanded to apply to each of the corresponding block groups within them. The final input into the model is

organized long for each unique block group ID and wide for each of the covariate, climate, and population variables described below.

Population Projection Data

To project the future relationship between population migration and climate exposure, future baseline population projections along SSP scenarios are integrated from Hauer et. al (2019) at the block group level. Population projections are demographically driven and do not explicitly account for climate change impacts at a local level, therefore we integrate them into our model by illustrating deviations from future projections due to climate. This study explores the impacts along all five SSPs alongside their corresponding Representative Concentration Pathways (RCPs), as defined by O'Neill et al. (2014) and van Vuuren et al. (2011). SSP-RCPs are integrated scenarios that combine socioeconomic development narratives (SSPs) with greenhouse gas concentration trajectories (RCPs) to provide a comprehensive framework for exploring potential future climate change impacts, mitigation challenges, and adaptation needs across different societal and climatic conditions. **Table 1.3** below describes the differences in these SSP-RCP climate scenarios in terms of their narrative and quantitative measures.

Table 1.3 SSP-RCP Narratives and Parameters

SSP-RCP	Narrative	Global Mean Temperature Increase by 2100	CO2 Emissions by 2100	Population by 2100
SSP1-RCP2.6	Sustainability	1.6°C (0.9-2.3°C)	Net negative	7 billion
SSP2-RCP4.5	Middle of the Road	2.4°C (1.7-3.2°C)	Reduced but not zero	9 billion
SSP3-RCP7.0	Regional Rivalry	3.6°C (2.6-4.8°C)	Continued rise	13 billion
SSP4-RCP6.0	Inequality	2.8°C (2.0-3.7°C)	Stabilized	9 billion
SSP5-RCP8.5	Fossil-fueled Development	4.3°C (3.2-5.4°C)	Continued steep rise	7 billion

1.3.2 Temporal Dimension Reduction Process for Climate Hazard Data

A single metric of long-term risk for each of the climate hazards explored in this analysis is calculated by incorporating the expected values across multiple return periods. This is particularly important for flood, wind, wildfire smoke, and drought which all have multiple categories or return periods associated with the models being used to operationalize these measures. The approach produces an expected value E(x) which is the sum of impact of the hazard (x) multiplied by the probability of the event, P(x), shown in **Equation 1.1**. **Table 1.4** denotes the climate hazard and the associated categories/return periods

evaluated with their equivalent probabilities. This framework ensures that low-probability, high-consequence events are incorporated into the developed metric, preventing the exclusion of events that significantly impact overall risk.

$$E(X) = \sum x \bullet P(x) \quad \text{(Equation 1.1)}$$

Where:

$E(X)$ is the expected value

x is the peril-specific value

$P(x)$ is the probability associated with the time-period evaluated

In addition, the probability of wildfire and probability of a heatwave are directly used as the single measures of those events.

Table 1.4 Periods and probabilities evaluated in creation of the expected value risk metric

Hazard*	Periods Evaluated	Associated Probabilities
Flood	5, 20, 100, 500 RP	0.2, 0.05, 0.01, 0.002
TC Winds	2, 5, 20, 100, 200 RP	0.5, 0.2, 0.05, 0.01, 0.005
Wildfire Smoke	Orange, Red, Purple, Maroon AQI	1, 0.5, 0.33, 0.25
Drought	2, 5, 10, 20, 100 RP	0.5, 0.2, 0.1, 0.05, 0.01
Wildfire	Burn Probability Pulled Directly from Wildfire Hazard Layer	
Extreme Heat	Probability of Heat Wave Pulled Directly from Extreme Heat Hazard Layer	

**flood (representing the average proportion of properties inundated over time), wind (the maximum expected observed speed over time), smoke (the number of expected days at or above the Orange AQI level over time), and drought (the number of expected weeks in drought stage D2 or higher (as defined by the U.S. Drought Monitor) over time.*

1.3.3 Historical Population Change

The dependent variable of our models is the annualized percentage block group population change, derived from population counts from 2000 and 2020. This data was

reconciled and described in Section 1.3.1. The calculation process involved a percent change, scaled by 5, where:

$$block\ group\ change\ = \frac{(Population_{2020} - Population_{2000})}{Population_{2000}} \qquad \text{(Equation 1.2)}$$

Where:

$block\ group\ change$ is the annualized percentage change

$Population_{2020}$ is the population value at a census block group in 2020

$Population_{2000}$ is the population value at a census block group in 2000

The historic block group population change is calculated as the annualized percentage change between 2000 and 2020, similar to the process described in Shu et. al (2023). The resulting historical population change can be visualized in **Figure 1.2**.

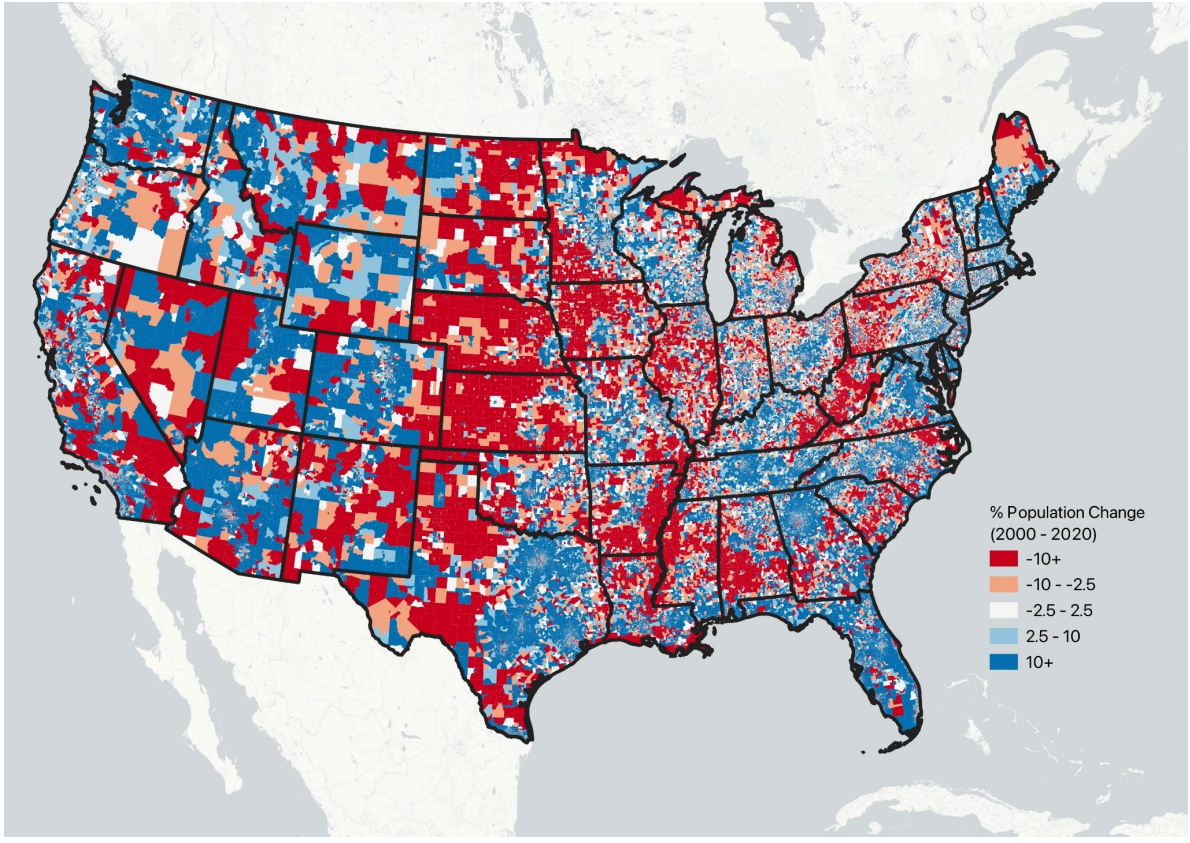

Figure 1.2 Census block group relative population change from years 2000 to 2020 (%).

1.3.4 Model Components

Propensity Score Matching

Propensity score matching (PSM) is employed in this modeling framework to mitigate selection bias and establish more robust causal relationships between population change and peril-specific climate impacts. In this model, 31 distinct 'treatment' groups are established, each representing a specific combination of exposure metrics in relation to the climate perils of interest (flood, wind, smoke, drought, wildfires, and heatwaves), as defined in **Equation 1.3**. One group serves as the control, encompassing block groups that do not meet any of the specified exposure criteria in an individual treatment group.

$$treatment = \{n \quad if\ conditions\ are\ met, \quad 0 \quad otherwise\} \qquad \text{(Equation 1.3)}$$

The matching process is performed at the state level rather than the national level. Since states across CONUS may exhibit significant variation in terms of demographics, policies, environmental factors, etc., conducting PSM at the state level can account for this variation more effectively by comparing treatment and control groups within the specific context of each state. The selected treatment thresholds are shown in **Table 1.5** below.

In this analysis, only five states had block groups that did not meet the conditions to be a part of at least one of the treatment groups, those being: DE, NJ, RI, MA, and NV. Since there was not a comparable group of control block-groups (at the state-level), we exclude these states only for the LASSO, meaning these block-groups will not contribute to the peril coefficient values.

Table 1.5 Treatment Thresholds for PSM by Hazard

Hazard	Treatment Threshold
Flood	1.6% of properties inundated in the 20yr RP or 4.2% of properties inundated in the 100 yr RP
Wind	Observed speed of 40mph or > in the 100yr RP
Smoke	7 days of Orange +
Drought	29.5 or more D2+ weeks

Hazard	Treatment Threshold
Wildfires	0.01 probability or greater
Heatwaves	0.54 probability or greater

By matching treated and untreated individuals based on propensity scores, or the likelihood of receiving treatment conditional on observed covariates (**Equation 1.4**), PSM allows for the creation of comparable groups similar to a randomized controlled trial, while also creating a simple, comparable metric that accounts for multidimensionality.

$$P(Y = 1|X) = \frac{1}{1 + e^{-(\beta_0 + \beta_1 x_1 + \beta_2 x_2 + \ldots + \beta_k x_k)}} \quad \text{(Equation 1.4)}$$

Where:

$P(Y = 1|X)$ is the probability of receiving treatment given the covariates

β_k are the coefficients estimated in the logistic regression

X_k are the covariates used in the matching process

The propensity score matching setup includes variables that could introduce bias when evaluating the relationship between climate hazards and population in areas that are characteristically different. These are variables thought to be related to climate risks and population change. For example, an area's proximity to the coast which could indicate a higher level of flood risk but also higher desirability compared to inland areas. The model also considers less apparent variables which could influence the movement into higher risk areas. For example, urban development near the coast might have additional amenities which act as pull factors (ex. schools, hospitals, and police stations). The inclusion of variables in this analysis has been informed by literature, and various model tests. The covariates ultimately used in the matching process include socioeconomic indicators such as median income, housing statistics, employment ratios, and geographic features, as presented in **Table 1.6**.

Table 1.6 Covariates used in the PSM matching process

Covariate (x)
Median Income

Covariate (x)
Percent of population that are single family
Percent of population that are single family home owners
Ratio of climate-exposed jobs to total jobs
Number of schools
Number of hospitals
Number of police stations
USDA amenity rank
Distance from the coast
Distance from a river
Topography code

Through machine learning techniques, propensity scores were computed for each block group using these observed covariate characteristics. Subsequently, these individual block groups are paired with counterparts in the control group with similar propensity scores. This algorithm calculates the absolute difference between the propensity scores of the treatment and control groups, identifying block groups with the smallest difference as the most suitable 'nearest neighbor' match. The resulting number of block groups that were matched state-by-state are presented in **Table 1.7**. Ultimately, these are the block groups used within the LASSO model to inform the hazard-specific relationships later on in this technical documentation.

Table 1.7 State-specific block group PSM matches

First Street

States	# of PSM matches
AL	4332
AZ	3076
AR	2108
CA	19032
CO	2524
CT	840
DC	728
DE	0
FL	4006
GA	9710
ID	256
IL	14718
IN	2364
IA	4280
KS	3224
KY	5092
LA	2342
ME	1388

First Street

States	# of PSM matches
MD	1176
MA	0
MI	11288
MN	6688
MS	3462
MO	6370
MT	530
NE	2360
NV	0
NH	80
NJ	0
NM	2062
NY	21574
NC	8412
ND	812
OH	10642
OK	4726
OR	286

States	# of PSM matches
PA	7656
RI	0
SC	4282
SD	1010
TN	4748
TX	662
UT	3018
VT	600
VA	5842
WA	1204
WV	2476
WI	7122
WY	698

LASSO Regression

The FS-CMM builds on the modeling approach described in Shu et al. (2023) by evaluating population changes due to climate perils beyond flooding. This analysis separately evaluated the relationship between each of the six climate hazards—flood, cyclonic winds, smoke, drought, wildfires, and heatwaves—and population change. A total of 199,806 matched blocks from PSM were included in the models, and further adjusted for nuanced social, economic, amenity, and spatial variables. These potential confounders were empirically identified, as described in Shu et al (2023), based on the

variance explained in population change. The modeling approach is expressed in **Equation 1.5**.

$$block\ group\ change\ =\ \beta_0\ +\ \beta_k Hazard_i\ +\ \beta_2 Social\ +\ \beta_3 Economic\ +\ \beta_4 Amenities\ +\ \beta_5 Spatial\ +\ \epsilon$$

(Equation 1.5)

Where each *Hazard* is modeled separately:

- *Flood* includes the expected value proportion of inundated properties at the block group level.
- *Wind* includes the expected maximum observed wind speed over time.
- *Smoke* includes expected number of days at or above the Orange AQI level over time.
- *Drought* includes the percentage of the year(# of weeks) in drought stage D2+.
- *Wildfire* includes burn probability at the block group level.
- *Heatwave* includes the probability of a relatively hot heatwave.

Social captures a set of variables, including population density and homes occupied by single families. *Economic* includes variables such as job opportunities, jobs tied to industries impacted by climate change. *Amenities* include an amenity rank, distances to natural amenities, such as proximity to coasts or rivers, and number of fire stations, police stations, hospitals, and campsites. *Spatial* is a set of variables that capture some of the spatially explicit interactions and movements of population settlements, such as longitudes and latitudes, as well as topography codes. For many of these variables, linear, interaction terms, and exponential variations (accounting for any non-linear relationships) were included in the full model and considered for selection in the final model. The model selection process was optimized to select variables that produced the most efficient model based on a LASSO approach.

LASSO, or Least Absolute Shrinkage and Selection Operator, is a powerful regularization technique that performs efficient parameter estimation as well as feature selection, an uncommon trait of other machine learning techniques. LASSO (**Equation 1.6**) works by imposing a penalty on the absolute size of the coefficients, and effectively shrinking some coefficients to zero, thereby reducing overfitting and collinearity within the model. Given the multitude of potential model features that could influence climate migration patterns, ranging from environmental to socioeconomic indicators, the ability for LASSO regression to automatically select the most relevant features allows for a better understanding of peril specific impact on population change.

$$min\left\{\frac{1}{2n}\sum_{i=1}^{n}\left(y_i\ -\ \beta_0\ -\ \sum_{j=1}^{p}x_{ij}\beta_j\right)^2\ +\ \lambda\sum_{j=1}^{p}\left|\beta_j\right|\right\}$$

(Equation 1.6)

Where,

- min : Minimization over the coefficients (β_0).

- n: Number of observations.

- p: Number of predictor variables.

- y_i: Observed value for the ith observation.

- x_{ij}: Value of the jth predictor variable for the ith observation.

- β_0: Intercept term.

- β_j: Coefficients for the predictor variables.

- λ: Penalty parameter controlling the strength of regularization and amount of shrinkage applied to the coefficients.

First, we define the dependent variable and the matrix of possible independent variables. In order to assess the model's performance and determine the optimal value of lambda (λ), or the regularization parameter, we use a k-fold cross validation. The process involves partitioning the sample into approximately equal 'folds' to undergo a training-validation process which calculates the mean squared error at each 'fold' iteration. This helps in selecting the optimal lambda value that minimizes the validation error, mitigating issues such as overfitting (or underfitting) the model. The process is run through R, and results in a sparser model where only the most relevant features, those with non-zero coefficients are retained.

The LASSO model process was operated separately for each climate peril with the model matrix in R programming taking this form:

model.matrix(~ ***climate_hazard****$_i$ +pop_density + med_inc + sfh_tot + amenity_rank + jobs_ratio + top_code + schools + tied_jobs + camps_count + fire_stations + police_stations + hospitals + labor_force + dist_coast + dist_river + noaa_cnt + hist_speed)*

Where i is each of the six climate hazards modeled separately

The full model was run, and then ran separately for areas that historically gained or lost population to account for desirability, which may overshadow changes due to climate risk (like that observed in Shu et. al (2023)). Climate hazards that were retained in either the

full model or the model restricted to areas that historically lost population are presented in **Table 1.8**.

Table 1.8 Retainment of each individual Climate Hazard in the Full Model or Loss Model (including only areas that lost population)

Hazard	Model Selection
Flood	Full
Tropical Cyclone Winds	Loss
Smoke	Full
Drought	Loss
Heatwave	Loss
Wildfire	Loss

Climate-adjusted Population Projections

Forecasting small area and subnational populations plays a vital role in comprehending enduring demographic shifts, and furthering our understanding of how population exposure to adverse natural events will change over time. Population projections have served as a valuable tool within both physical and social sciences to understand demographic transformations, strategize for future needs, and offer decision-making insights across a diverse number of contexts. While research typically works to estimate population projections at the national level, the escalating interest in granular demographic analyses, particularly in the context of climate change, underscores the significance of high-resolution, subnational forecasts.

Population projections are available decadal at the block group level along all five SSP curves, as described in Section 1.3.1. The process for calculating these population estimates are described in Hauer et. al (2019), but a summary is provided here for context. County-level population projections by age, sex, and race in five-year intervals for the period 2020–2100 for all U.S. counties. Using historic U.S. census data in temporally rectified county boundaries and race groups for the period 1990–2015,

cohort-change ratios (CCRs) and cohort-change differences (CCDs) were calculated for eighteen five-year age groups (0–85+), two sex groups (Male and Female), and four race groups (White NH, Black NH, Other NH, and Hispanic) for all U.S counties.These CCRs and CCDs were then projected using ARIMA models as inputs into a Leslie matrix population projection models and controlled to each SSP.

Hauer et. al (2019) calculated population projections at the 2010 vintage, or the delineation of the block groups for demographic and statistical purposes in 2010. The peril and covariate data we use in this analysis are in a 2020 vintage. For this reason, the NHGIS 2010 to 2020 block group crosswalk was used, which allows us to attribute 2010 block group boundaries to 2020 census boundaries based on predefined weights. Boundaries tend to change over time due to population growth, urban development, or other administrative adjustments.

Since 2020 migration and population patterns have been observed, the Shared Socioeconomic Pathway curves that delineated five varying population projections in 2020 are out-of-date. In order to correct for observed population counts in 2020, each SSP curve has been updated to include the difference between the historically observed count in 2020, and the SSP specific projection.

The residual (or error) at each block group (i) in each Shared Socioeconomic Pathway (SSP) scenario (j) in the year 2020 is given by **Equation 1.7**.

$$R_{ij} = O_{ij} - P_{ij} \quad \text{(Equation 1.7)}$$

Where:

R_{ij} represents the residual or error,

O_{ij} denotes the observed value at block group i in SSP scenario j in the year 2020,

P_{ij} denotes the projected (or predicted) value at block group i in SSP scenario j in the year 2020.

In this equation, R_{ij} captures the difference between the observed $O_{ij}$and projected P_{ij} values for each block group within each SSP scenario specifically for the year 2020. The projected population at each block group i in each Shared Socioeconomic Pathway (SSP) scenario j and in each decade t is adjusted for residuals as follows:

$$P_{ijt} = P_{ij} + R_{ij} \quad \text{(Equation 1.8)}$$

Where:

P_{ijt} denotes the projected population at block group i in SSP scenario j and decade t ,

R_{ij} represents the residual or error for block group i in SSP scenario j,

The residual R_{ij} is obtained from the equation $R_{ij} = O_{ij} - P_{ij}$, where O_{ij} is the observed population and P_{ij} is the projected population for block group i in SSP scenario j in the specific year (e.g., year 2030).

This adjustment accounts for discrepancies between observed and projected population values, ensuring more accurate projections inclusive of observed census data.

This work builds on Shu et. al (2023) to incorporate climate adjustments to 5 more climate perils in addition to flood. We modify population projections based on anticipated changes due to climate exposures. To do this, we apply the coefficients for the peril exposure variables to the future (2053) peril layer projections assuming operationally linear increases between current and future climate projections and that this gradual increase in exposure will be realized through growth rates. The coefficients for the relationship between climate variables and block group growth rates may be applied through the integration of these relationships. Where initially the future population projections are derived as age-sex-race adjusted demographic estimates along the SSP trajectories.

$$future\ growth_{baseline}\ (annual) = demographic\ indicators \quad \text{(Equation 1.9)}$$

The future projections correcting for climate exposure (i.e. integrating the climate consequence) may be similarly thought of as the contribution of and relationship between peril exposure metrics and demographic indicators, as defined in **Equation 1.10**.

$$future\ growth_{projected}\ (annual) = demographic\ indicators + climate\ impact$$

(Equation 1.10)

Where climate impact:

$$Climate\ Impact_{year,SSP} = \sum_{i=1}^{n} (Hazard\ Coefficient_{k} \times Hazard\ Value_{year,\ SSP,\ k}) \quad \text{(Equation 1.11)}$$

Projected future growth could also be expressed as:

$$future\ growth_{projected}(annual) = \frac{future\ pop_{projected} - pop_{present}}{pop_{present}} \quad \text{(Equation 1.12)}$$

Where, when combined the future population projections can be expressed as:

$$future\ pop_{projected} = (Demographic\ Indicators + Climate\ Impact_{year,SSP})\ x\ pop_{present} + pop_{present}$$

(Equation 1.13)

Peril-annualization

This methodology entails leveraging individual peril data captured at two distinct temporal points: the present and thirty years into the future. These points, described above, are the expected value and probability metrics used in the LASSO analysis to generate the coefficients, capturing the impact of each hazard on population change. We employ an annualization technique to interpolate these points to generate a dataset with 30 individual years worth of peril data. In this way, we are creating a yearly expected value metric that describes a long-term average at a point within our temporal scope for flood, smoke, wind, and drought, as well as the average probabilities for wildfire risk and heatwaves.

This model adjusts population projections to specific Shared Socioeconomic Pathways (SSPs) at the block-group level and incorporates climate effects. This adjustment may lead to a national population decrease in our forecasts over time as all of the climate impacts in this analysis are deemed to be negative disamenities. However, the “lost” population should be expected to move to other areas. To ensure consistency in population levels across different time periods, we calibrate the climate-adjusted projections. This helps us focus exclusively on capturing population movements influenced by climate effects, while minimizing interference from external factors. Conceptually, our approach is to rely on the population projection underlying drivers in the SSP scenarios, which directly integrate the larger social, economic, and political context and demographic makeup of the population (Hauer, 2019). Using well established population forecasting techniques, these estimates were produced so that they are able

to allocate population to areas with strong “pull-factors” and a demographic profile associated with growing population.

Operationally, the process involves iterating through each SSP in each decade to compute baseline and climate-adjusted populations. The difference indicates the national population decline for each decade. For block groups that experience population growth in modeled decades—driven, for instance, by SSP trends outweighing climate-related losses—they receive a portion of climate migrant populations, limited to their historical population proportion. This ensures that populations are redistributed in a manner consistent with their current size and the expectations forecasted in the SSP projections. Essentially, this research relies on the expertise provided by Hauer (2019) in order to understand what those parameters are. The redistribution process is formally stated in **Equation 1.14**.

$$Population\ Redistribution_{bg,year,SSP} = \left|NCE_{year,SSP}\right| \times Historical\ Proportion\ of\ Population_{bg}$$

(Equation 1.14)

Where:

$NCE_{year,SSP}$: National climate effect on population for a specific year and SSP scenario

$Historical\ Proportion\ of\ Population_{bg}$: Historical proportion of population for the block group

This process is utilized to adjust current and future SSP projections in a 30-year outlook as such below:

$$future\ pop_{projected} = (Demographic\ Indicators + Climate\ Impact)\ x\ pop_{present} + pop_{present} + pop_{redistribution}$$

While population projections are at the block group level along all 5 SSPs, currently peril data is mostly along SSP2 only. In this way, we are only producing climate adjustments in conjunction with a ‘middle-of-the-road’ scenario, which includes a slowing population and moderate economic development and moderate increases to energy uses and greenhouse gas emissions.

The retrospective analysis and prospective correction of population projections along the SSP2 trajectory give us the ability to take observable associations between climate risk

and exposure and integrate a high resolution climate signal into current SSP projections. Most importantly, we are interested in how areas that have been classified as highly exposed to a given climate peril are projected to change in population relative to areas that have been classified as not being highly exposed.

1.4 Results

Each of the climate hazards were shown to have a negative impact on population estimates in either the full or the restricted models including areas with population loss. First, the impact of climate risk for both flood and wildfire smoke were negatively related to population change in the full models (controlling for all other variables in the model). However, for wildfire, tropical cyclone winds, extreme heat, and drought the full models showed no negative effect of climate risk on population change. For each of these hazards, models restricted to areas with population loss vs gain were evaluated to see if the larger context of the market played overshadowed the impact of climate. In all cases the models showed that in communities with strong growth in population over the 20 year study period, there was no negative effect of climate risk on population change. However, for communities that were seeing negative population change, there was a statistically significant negative effect of climate risk across all 4 of these hazards. These results indicate an amplification effect of climate risk as a “push factor” in areas that already have a number of other factors pushing people out of the communities. The significant negative coefficients related to the impact of climate risk on observed historic population change patterns are presented in **Table 1.9**.

Table 1.9 Coefficient estimates from LASSO regression for the overall model, and for separate models including either areas with population gain or population loss

Climate Hazard	Coefficient Estimate (all block groups)	Coefficient Estimate (gaining block groups)	Coefficient Estimate (losing block groups)
Flood	-41.74868	NA	NA
Wildfire Smoke	-0.02592867	NA	NA
Wildfire	No Effect	No Effect	-2.198713
TC Winds	No Effect	No Effect	-0.0002656105

Extreme Heat	No Effect	No Effect	-0.4162961
Drought	No Effect	No Effect	-1.036107

Following the identification of the historic relationships between each of the climate hazards and historic population change, these coefficients applied to future population projections along all 5 SSPs out to the year 2055. The population projections were created through a series of demographic and statistical techniques aimed at distributing the global scale social, economic, and political relationships along the 5 scenarios, to a higher resolution within the US context. For more information on both the techniques and framework for this down scaling, see the work by Hauer (2019) which details this process. Climate corrections to future population projections were produced by applying coefficients identified in the model results (**Table 1.9**) to block group population projections presented by Hauer (2019), and adjusted for population reallocation using the proposed downscaling framework. In order to integrate the climate correction coefficients identified in the historic models into future population projections, expectations of climate risk were estimated at the block group level over a 30 year horizon (to 2055).

Once future risk expectations were computed, the application of the climate correction coefficients (from **Table 1.9**) to the downscaled SSP scenario projections would allow for an estimation of the impact of climate risk on population over that same period. A summary of the number of CONUS block groups that are negatively impacted to some level of risk by each climate hazard are shown in **Table 1.10**. The results in the table show that flood risk overwhelmingly has the highest percentage future impact on the total number of block groups at 82.6%. This is followed by heatwaves at 47.4% coverage, drought at 46.6% coverage, wildfire at 32.7% coverage, wildfire smoke at 21.7% coverage, and tropical cyclone winds at 11.1% coverage.

Table 1.10 Count and Percentage of Block Groups with a Non-Zero Negative Effect by Climate Hazard

Climate Hazard	**Block Groups Impacted by Timing (238,193 in total)**			
	Currently	**2025 - 2035**	**2035 - 2045**	**2045 - 2055**
Flood	193,961 (81.4%)	194,815 (81.8%)	195,878 (82.2%)	196,680 (82.6%)

Tropical Cyclone Winds	20,136 (8.5%)	21,936 (9.2%)	24,948 (10.5%)	26,556 (11.1%)
Wildfire Smoke	46,941 (19.7%)	48,710 (20.4%)	49,301 (20.7%)	51,684 (21.7%)
Drought	83,772 (35.2%)	92,386 (38.8%)	104,887 (44.0%)	111,007 (46.6%)
Extreme Heat	85,777 (36.0%)	93,936 (39.4%)	106,693 (44.8%)	112,896 (47.4%)
Wildfire	47,368 (19.9%)	66,551 (27.9%)	74,237 (31.2%)	77,952 (32.7%)

When exploring the spatial distribution of these losses, we see that the areas with the largest expected absolute person losses are in the major metropolitan areas of the country. From a very practical standpoint, this makes sense given that these represent large population centers with the capacity to lose persons at the rate reflected in the model. That being said, the patterns in the figure also underscore the critical intersection between environmental vulnerabilities and demographic trends. In particular, smaller communities grappling with a convergence of climate hazards like tropical cyclones, floods, wildfires, are expected to encounter more significant challenges in sustaining population growth and even maintaining current population levels. **Figure 1.3** showcases the counties across CONUS and their associated population losses due to climate hazards in the next 30 years. Los Angeles and Miami-Dade counties which are riddled with exposure to almost all of the climate hazards in some way are those that can expect the greatest declines in population due to climate. In contrast, regions with lower exposure to these hazards may be better positioned to mitigate demographic declines and potentially foster more stable population dynamics, like counties such as Eureka, NV, Catron, NM, and Harding, SD to name a few. However, it is also important to point out that the map can be misleading in that the future projections of population growth often outpace the losses projected in the map. In order to fully understand the impact on community growth, population projections must be coupled with these negative impacts.

Figure 1.3 illustrates the intersection of projected population trends under SSP2 with the integrated climate correction factor identified from the historic model presented above. This represents a more holistic approach to understanding the impact climate might have on future population levels as it fully integrates expectations around the social, economic, and political amenities of an area as competing drivers of population change due to climate risk. In many places with high levels of climate risk, these amenities will simply outweigh the disamenity of climate risk. This relationship should be understood as a balance in which fast growing communities, with large amounts of capital, are able to allocate resources to adapt to the growing climate risk and to continue to attract businesses and populations as a result. While there is no doubt that there is a drag on the growth due to climate risk in these areas, that drag is overwhelmed by the influx of people and capital and represents a form of “risky growth”.

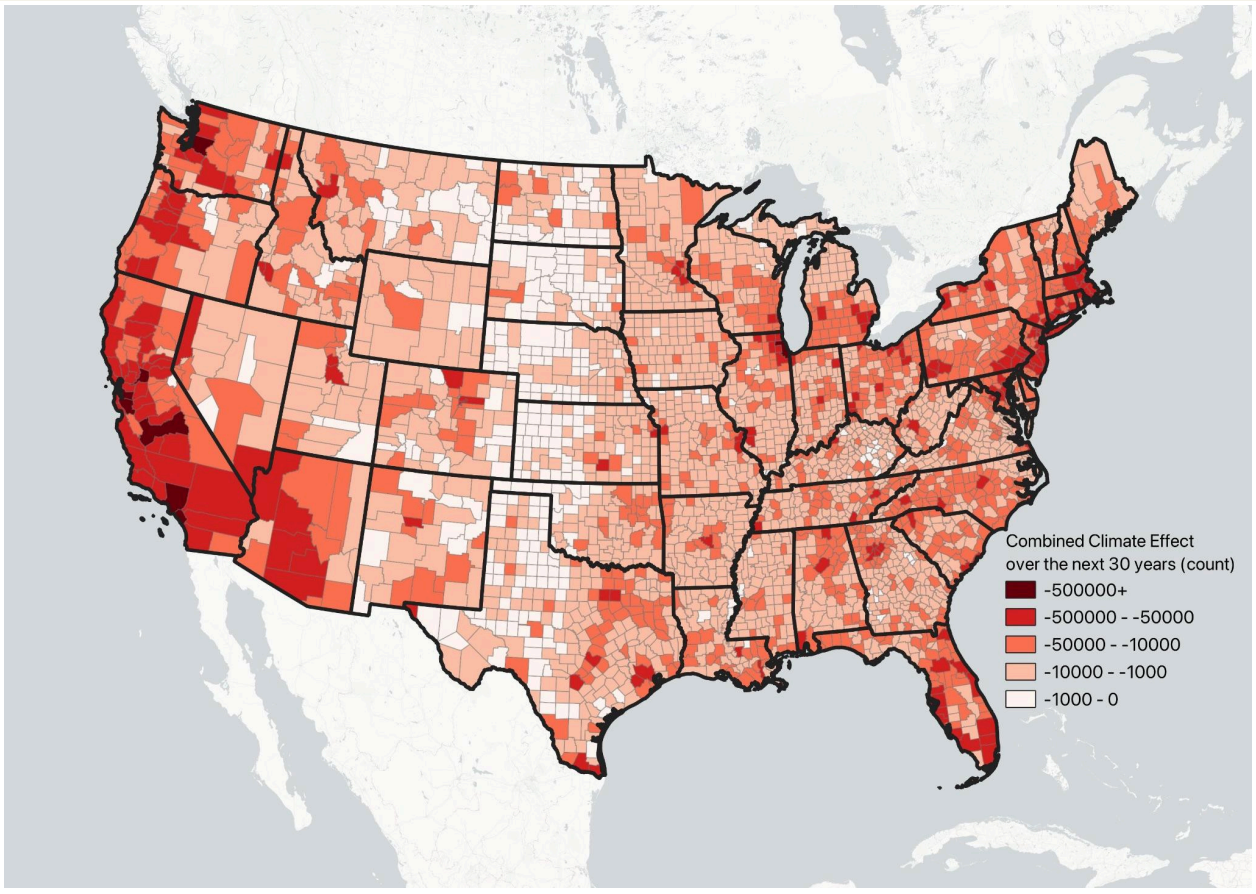

Figure 1.3 County level projected population change resulting from the combined climate effect over the next 30 years.

On the other hand, areas without these levels of capital are generally already seeing slowing growth rates, or even negative population change, and are more susceptible to

the negative impacts of climate risk. These areas make up two distinct types of communities, one in which climate abandonment is simply another factor in the general abandonment of the community and one in which there continues to be risky growth in the area but at a rate slow enough to lead to a tipping point at which the community will become a net population loser in the future. The former group represents many areas in the Midwest and Northeast where out migration due to other factors is helping to drive the amplification of the climate effect. More interesting are the areas that continue to grow in the near future, but do not have enough forecasted growth due to other factors to keep up with the negative impact of climate risk. These are the areas that can be projected to become climate abandonment areas in the next 30 years.

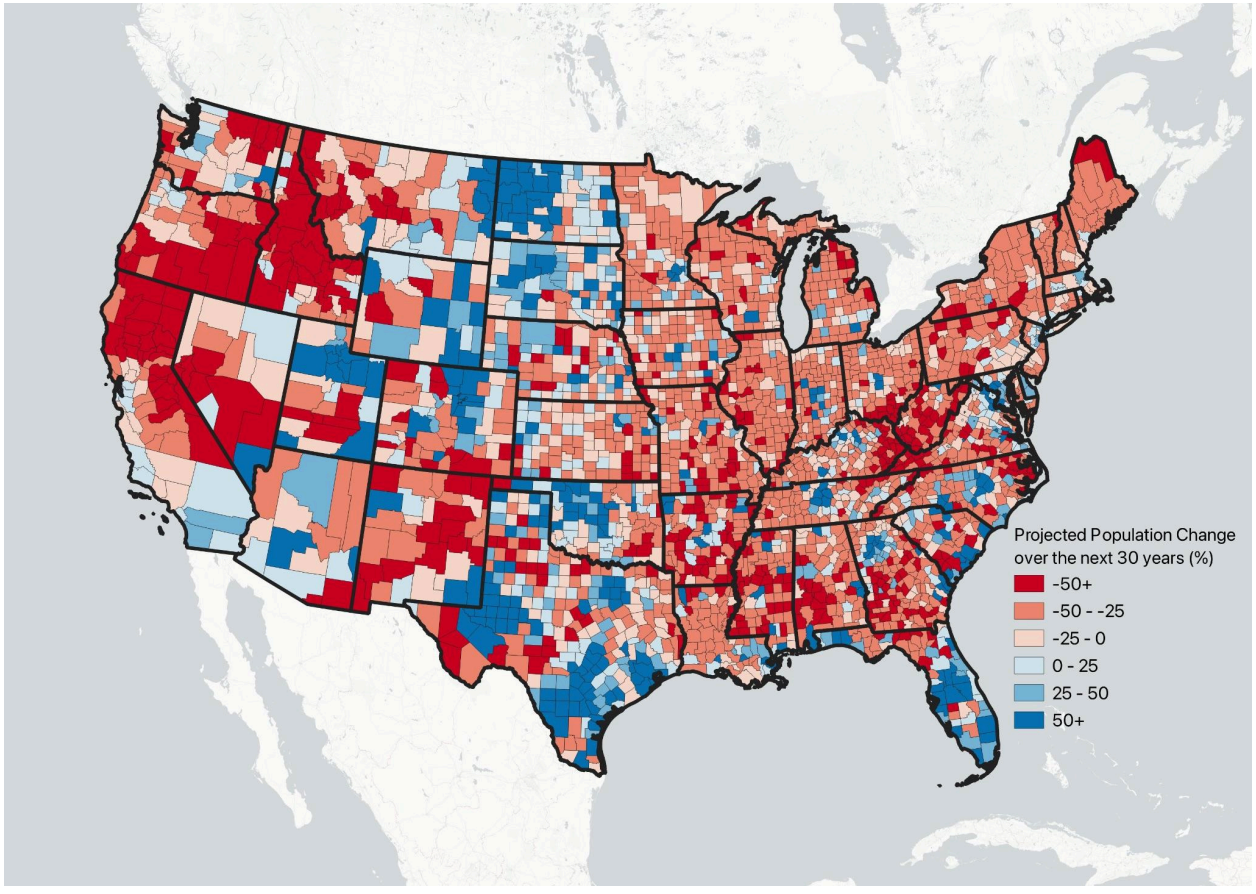

Figure 1.4 County level projected population change (%) resulting from the combined climate effect, socioeconomic impact under SSP2, and population redistribution due to climate migration over the next 30 years.

While the county level map in **Figure 1.4** highlights some of the aggregate patterns we are seeing in the data, it is hard to discern distinct patterns at the national scale. In order to fully understand the insights that can be gained from coupling the high

resolution climate risk information with the high resolution population projections, **Figure 1.5** represents a focused investigation on three distinct neighborhoods within Miami-Dade County. For context, **Figure 1.4** showed that Miami-Dade County would be an overall grower in population over the next 30 years, but if you disaggregate the data and view specific neighborhoods, one can see that all 3 of the neighborhood types mentioned in the previous paragraph exist within the county.

To illustrate this, **Figure 1.5** reports the population change forecasts for three specific census block groups which model the three trends of risky growth, declining growth with a quantifiable tipping point, and ongoing climate abandonment. In the figure you can see the three distinct trends within the county where block group (120860056001), in the Flagler neighborhood, representing an area of continued growth due to the positive population forecast and the relatively weak negative impact of climate in the area. On the other hand, the Sunny Isles Beach neighborhood (120860001071) represents an interesting case of an area which is currently growing due to the vast amount of amenities in the area (including being located directly on the coast) but that is expected to hit a tipping point in the next 2 decades in which the negative impact of climate will contribute to a decline in population. Finally, the climate abandonment area is located in the larger Doral neighborhood (120860090402), which has seen both out migration in the historic dataset (2000-2020) and is expected to continue to see out migration due, in part, to the climate risk in the area. The results presented in the figure highlight the need to investigate the process of population change and the impact of climate on a more granular level than the literature currently covers (which is generally at a county level).

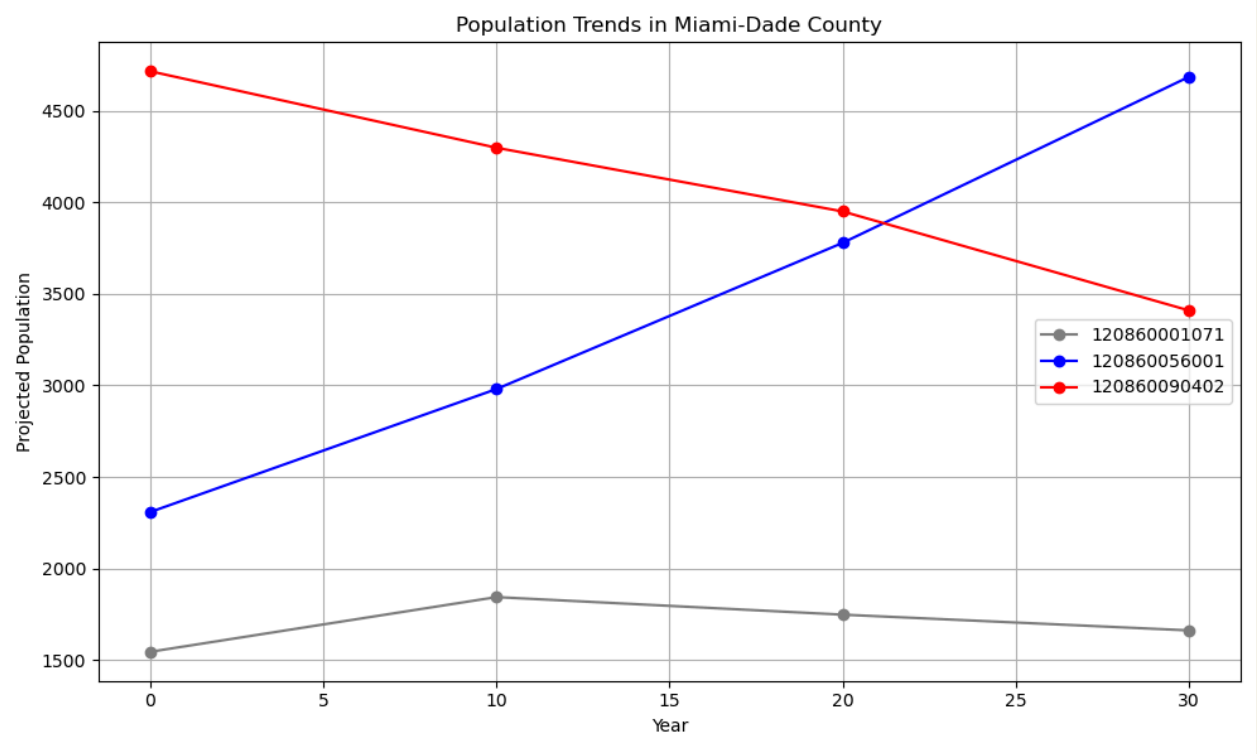

Figure 1.5 Population Projection trends in Miami-Dade county neighborhoods for areas of continual growth (blue), risky growth with tipping point (gray), and climate abandonment (red).

The variation in the results are presented across all of Miami-Dade County where the negative impacts of climate are represented in the left-hand figure and the location of the 3 archetypes presented in **Figure 1.5** are presented in the right-hand map of **Figure 1.6**. The results show that the largest negative impacts of climate risk are located along the coastal areas of Miami Beach (including the areas to the far northeast of the county), areas on mainland Miami-Dade along the coast (in the southeast part of the county), and areas along the everglades in the northwestern part of the county. These patterns underscore the impact of flood exposure in this area as these are also the communities with the largest flood levels in the underlying climate risk models. In the right-hand map, it is clear that the inland part of the county has a high concentration of areas that are growing and continuing to grow, even with the higher than average risk across the county. In contrast the coastal part of the county has a high proportion of areas that have lost population historically and are projected to continue to lose population into the future, in part due to the high level of climate risk. Finally, and perhaps the most interesting group exists in the coastal adjacent part of the county where we can see a concentration of places that are currently growing, but are expected to reach a tipping point in the next 30 years which will result in declining populations, in part due to the high level of climate risk in the area.

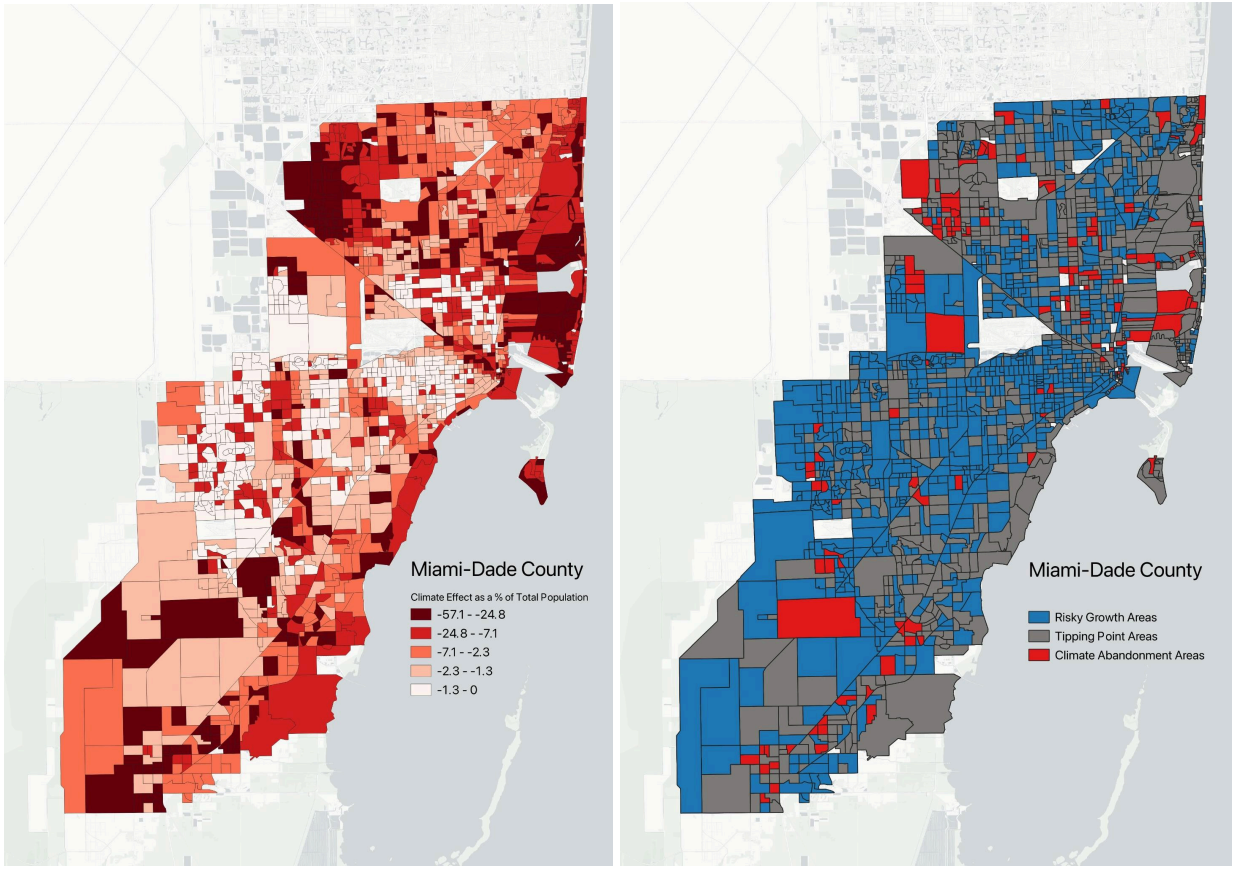

Figure 1.6 Miami-Dade county block groups' combined climate effect and projected population trend designation (risky growth, tipping point, or climate abandonment area).

2. Derivative Impacts from Population Change

The population projections developed from the First Street Climate Migration Model (FS-CMM) were combined with estimates of changes in sociodemographic composition, economic indicators, commercial viability, and residential property values, effectively predicting the downstream socioeconomic and housing consequences of climate migration across communities in the continental U.S. (CONUS). **Figure 2.1** below illustrates how FS-CMM outputs were used to derive future impacts from population change via conversion tables built from historical relationships. **Appendix Table 1** presents a list of all variables modeled over the course of this project.

"Conversion tables" refer to the way we structure our outputs to feed into a series of downstream consequences of climate migration using population migration inputs to produce relevant outputs. These tables were derived from historical relationships using

Generalized Additive Modeling (GAM) described in Section 2.2. Geographic context was explicitly incorporated into the models by separately evaluating relationships to create conversion tables based on region, urbanicity, and proximity to coastlines, as described in Section 2.1.

For a given relationship, historical change in the explanatory variable was regressed on historical change in the outcome variable to predict future changes in the outcome variable as changes in the explanatory variable are observed. In the context of the demographic change, economic implications, commercial implications, and property value change models, historical population change served as the explanatory variable, producing conversion tables with inputs along a range of population changes and resulting outcome changes for each variable modeled. To use the conversion tables developed, population change inputs were derived from the FS-CMM as percent change in the population at the block group level by dividing the difference between the climate adjusted populations from the relevant base population for a given climate scenario or timeframe by the base population. Expected percent changes in the outcome variables to these conversion tables were linked along changes in population suggested by FS-CMM outputs, allowing future predictions about the change in socioeconomic and housing factors to vary by specific climate hazard or in aggregate and by climate scenario.

The following sections of this technical document detail the development of conversion tables for each downstream consequence: 3. Demographic change, 4. Economic implications, 5. Commercial implications, and 6. Property value change.

First Street

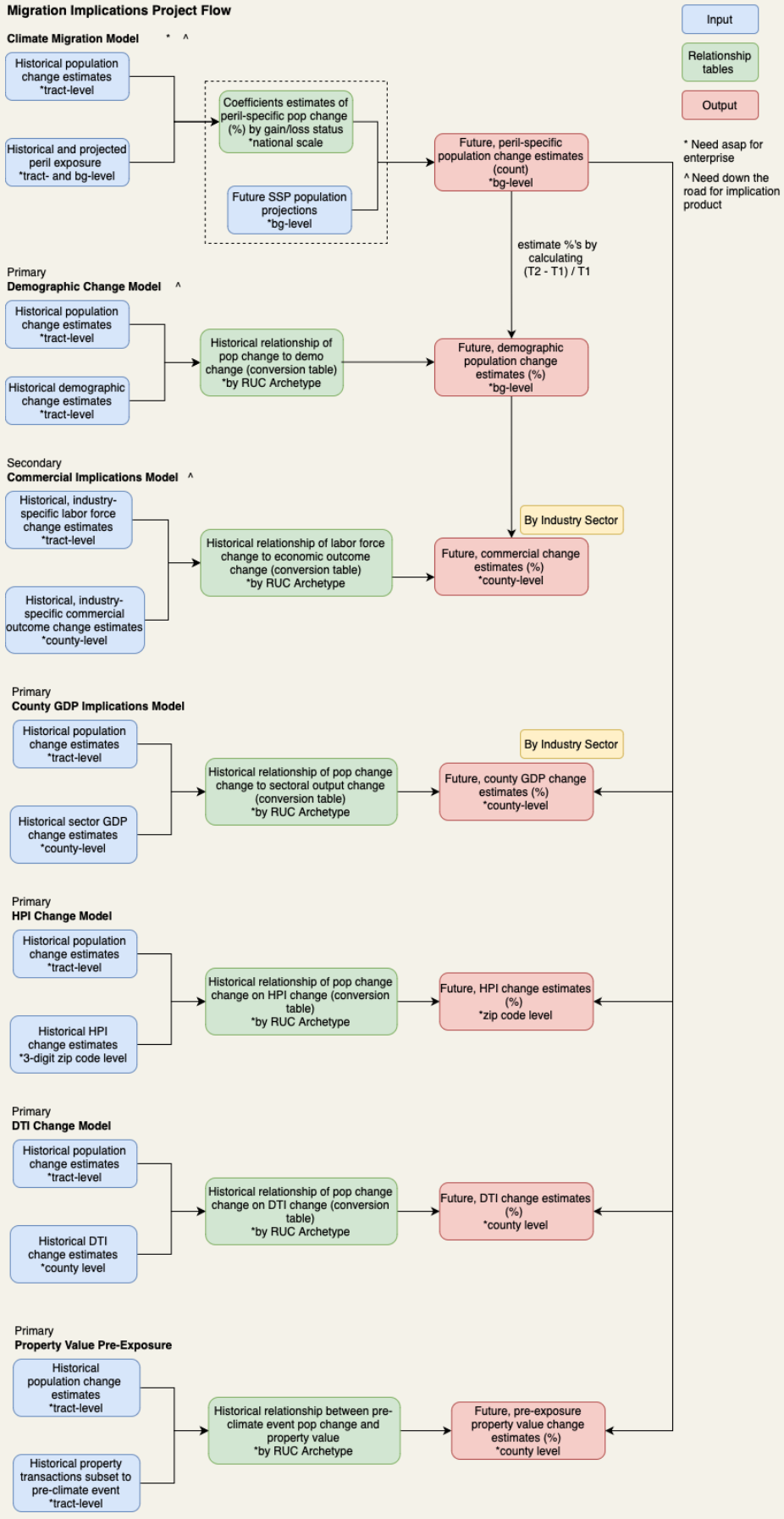

2.1 Region-Urban-Coastline Continuum

To explore the relationships modeled by geographic context, we divided tracts and their corresponding counties into Region-Urbanicity-Coastline (RUC) categories, capturing amenity profiles of geographies across the country based on three dimensions. This approach is grounded in research demonstrating that migration patterns are not uniformly distributed across geographic locations and demographic groups, but depend on various factors such as urbanicity, amenity profile, and regional characteristics (Johnson et al., 2005; Johnson and Winkler, 2015; Johnson et al., 2013; Rappaport, 2007). The three dimensions are:

1. Macro region (Northeast, South, Midwest, and West)
2. Urbanicity (metropolitan and nonmetropolitan) using Rural-Urban Continuum Codes (RUCC) for counties in 2013 (USDA, 2024). In this categorization, counties that are identified as part of a Metropolitan Statistical Area (MSA) are categorized as "metropolitan" and all other counties are classified as "nonmetropolitan" (see **Table 2.1**).
3. Coastal proximity (coastal and non-coastal) for metropolitan areas, based on whether the county border touches the coastline. There were a limited number of non-metropolitan tracts on the coastline (<1%).

These three dimensions constitute 11 distinct categories that encompass the diverse geographic contexts across the United States (**Figure 1.2**).

Table 2.1. Two levels of urbanicity defined using USDA Rural-Urban Continuum Codes for counties in 2013.

Urbanicity	RUCC Code	Description
Metropolitan	1	Counties in metro areas of 1 million population or more
Metropolitan	2	Counties in metro areas of 250,000 to 1 million population
Metropolitan	3	Counties in metro areas of fewer than 250,000 population
Non-Metropolitan	4	Urban population of 20,000 or more, adjacent to a metro area
Non-Metropolitan	5	Urban population of 20,000 or more, not adjacent to a metro area
Non-Metropolitan	6	Urban population of 2,500 to 19,999, adjacent to a metro area

Urbanicity	RUCC Code	Description
Non-Metropolitan	7	Urban population of 2,500 to 19,999, not adjacent to a metro area
Non-Metropolitan	8	Completely rural or less than 2,500 urban population, adjacent to a metro area
Non-Metropolitan	9	Completely rural or less than 2,500 urban population, not adjacent to a metro area

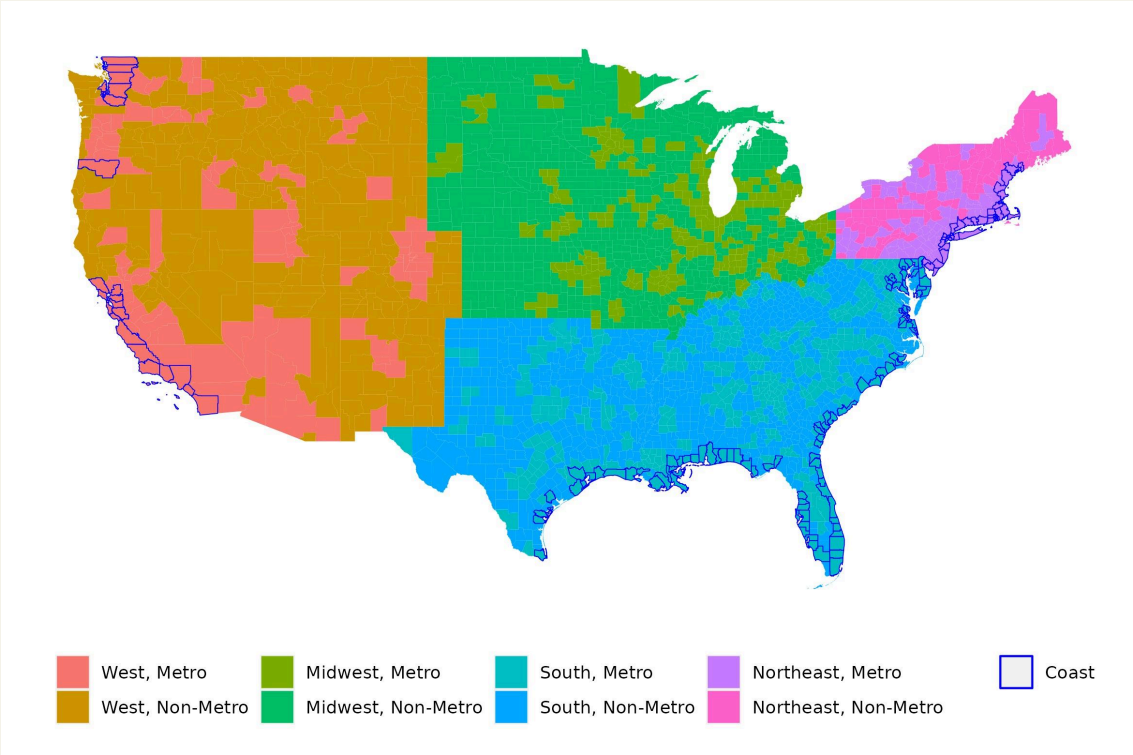

Figure 1.2 Map of the contiguous U.S. colored by Region-Urbanicity-Coastline categories. Coastline status was distinguished for metropolitan areas only, as the number of non-metropolitan tracts on the coastline were limited. There are no coastal counties in the Midwest.

The importance of these geographic distinctions is well-established in migration research. Studies have shown that migration flows of certain demographic groups vary substantially between metropolitan and non-metropolitan areas, leading to distinct demographic compositions of populations in these areas (Johnson & Lichter, 2023; Ambinakudige & Parisi, 2017). In most cases, rural-to-urban migration has historically contributed to the growth and diversification of cities while also exacerbating population decline and aging in many rural communities (Johnson & Lichter, 2019). At the same time, metro vs. non-metro migration patterns have been found to vary regionally across the U.S. with the Northeast experiencing more dramatic shifts in population (Johnson & Cromartie, 2006;

Rickman & Wang, 2017). Similarly, natural amenities, such as mild climates and coastal proximity, have emerged as important drivers of migration among particular demographic groups (McGranahan, 1999; Gosnell & Abrams, 2011). For example, amenity-driven migration has led to rapid population growth in some rural areas, such as the Rocky Mountain West and the Upper Great Lakes, while other rural regions have continued to experience population decline (Johnson & Beale, 2002).

At the same time, exposure to climate change varies along RUC divides. Most directly, all parts of the country are exposed to some type of climate hazard, which varies regionally based on the environmental conditions present in the area (First Street, 2023a; NOAA, 2024). In terms of flooding alone, FEMA (2024) has made the point that 99% of the over 3,000 counties in the US have recorded a significant flood event between the years of 1996 and 2022. More specifically, the coastal areas of the Gulf and Atlantic are particularly susceptible to tropical cyclones and storm surge, the Midwest and Northeast are seeing an increasing frequency of extreme precipitation (First Street, 2023b), the middle of the country is particularly susceptible to extreme heat exposure (Wilson et al, 2023), and the Western half of the country has seen a dramatic increase in exposure to wildfires (Kearns et al, 2022). Beyond exposure, the impacts of climate change are also expected to impact metropolitan areas differently than nonmetropolitan areas (Schifano et al, 2013; Hartfield et al, 2014). Given this variation in both exposure and responses to climate risk, our modeling framework along these RUC boundaries assumes that socioeconomic and housing responses to population change differ across the regional, urban, and coastal categories we define.

2.2 Generalized Additive Modeling

Generalized Additive Models (GAMs) are a flexible class of statistical models that allow for non-linear relationships between predictor and response variables, making them particularly useful for capturing complex patterns in the social sciences. GAMs have been successfully applied in various social science contexts, offering flexibility in modeling complex, non-linear relationships. For instance, Beck and Jackman (1998) employed GAMs to examine the relationship between democracy and economic development, revealing complex, non-linear patterns that challenge simple linear interpretations.

Across most of our analyses described in this document, we employ bivariate GAMs to evaluate the impact of population growth or decline on various outcome variables independently across different RUC classifications. This approach allows us to capture potential interaction effects between dimensions of region, urbanicity, and coastal location. Specifically, we model these relationships consistently across demographic change, economic implications, and property value using a cubic spline smoothing function limited to three knots. This results in fitting each relationship with a piecewise

cubic polynomial consisting of at most four cubic polynomial segments. By doing so, we allow for non-linear relationships between the predictor and response variables, enabling a more flexible and nuanced understanding of these relationships compared to traditional linear models.

Population change is always modeled as a percentage growth factor. Outcome changes are modeled either as percentage changes for variables that are percentage-based, or as differences over time for variables measured in dollars or counts. Subsequent sections provide the formulas used to estimate these growth factors. GAM models used across this analysis may be expressed:

$$Outcome\ Change\ (i,j)\ =\ f(Population\ Growth\ Rate(j))\ +\ \varepsilon \qquad \text{(Equation 2.1)}$$

where:

- Outcome change (*i*,*j*) is the change in the outcome variable of interest *i* from 2000 to 2020 in RUC classification *j*
- f() represents a cubic spline smoothing function with a maximum of three knots
- Population Growth Rate(*j*) is the population change from 2000 to 2020 in RUC classification *j*, expressed as a percentage
- ε is the error term

Predictions about the outcome of interest from changes in population are made using the fitted GAM model for each relationship. The values of population change are expanded into a sequence of values within the 90% central range of each variable separated into 0.05 percentage point steps. The predicted outcomes are mapped to each of the population change values to estimate the predicted value of the outcomes along with their standard errors and resulting 95% confidence intervals. The goal of formatting the results in this way is to produce a conversion table that translates changes in population into relevant outcomes across for each RUC. Importantly, the limitation to 3 knots in the GAM model serves a dual purpose: it not only captures non-linear relationships but also ensures that the model isn't overfitting the data. This balance between flexibility and complexity reduction allows for more reliable predictions by avoiding the capture of noise or idiosyncrasies specific to the historical data used, thus improving the model's generalizability to new, unseen data points within each RUC.

2.2.1 GAMs Assumptions and Limitations

While GAMs offer significant flexibility in modeling non-linear relationships, it's crucial to understand their underlying assumptions and potential limitations. These considerations inform both the interpretation of results and the scope of conclusions that can be drawn from the analysis. The key assumptions and limitations of the GAM approach used in this study include:

- Smoothness: GAMs assume that the underlying relationship between the predictor and response variables is smooth. This may not always hold in real-world scenarios, especially when abrupt changes or thresholds exist.
- Homoscedasticity: GAMs assume constant variance of residuals across the range of predictors. Violations of this assumption may lead to unreliable confidence intervals.
- Knot Selection: The choice of the number and placement of knots can influence the model's flexibility and fit. The use of three knots in this study is a simplification that may not capture all nuances in the data but allows for generalizability to make predictions based on new data.
- Temporal Consistency: The model assumes that the relationship between population change and outcomes remains consistent over the 2000-2020 period, which may not account for structural changes or shifts in these relationships as time progresses.

3. Demographic Change

3.1 Executive Summary

This analysis examines the relationship between population change and shifts in sociodemographic characteristics across the contiguous U.S. from 2000 to 2020, aiming to understand how climate-induced migration may reshape community compositions in different geographic contexts. The study utilizes sociodemographic data from the U.S. Census Bureau at the tract level, reconciled to consistent geographic boundaries. Tracts were classified into Region-Urbanicity-Coastline (RUC) categories as outlined in Section 2.1. Following the framework outlined in Section 2.2, the analysis employs bivariate generalized additive models (GAMs) to explore relationships between population change and individual sociodemographic variables for each Rural-Urban-Coastline (RUC) continuum. Additionally, partial least squares regression (PLSR) is used to evaluate the collective relationship between multiple sociodemographic variables and population change. This comprehensive approach allows for nuanced predictions about future community composition changes in response to climate-induced migration across diverse geographic contexts in the United States.

3.2 Background

A growing body of literature has emerged to investigate this phenomenon, in which a combination of exposure, vulnerability, and perceived risk associated with climate hazards has already driven, or is expected to drive, individuals and families to relocate within the U.S. (Hauer et al, 2016; Hauer et al, 2019; Robinson et al., 2020; Hauer et al, 2021; Shu et al., 2023). Studies have found that climate migration often follows pathways similar to traditional migration factors, as climate impacts compound with existing socioeconomic drivers such as job opportunities, amenities, and affordability (Black et al., 2011; Fan et al., 2016). Other studies suggest that the ability to relocate in response to environmental pressures is often contingent not only on socioeconomic status but also demographic factors (Fothergill et al., 2002; Fussell et al., 2009; Raker, 2020; Kaczan & Orgill-Meyer, 2020). Thus, it may be predicted that the impacts of climate change will create distinct migratory patterns that vary across sociodemographic groups, potentially reshaping the composition of the populations left behind in areas with escalating climate risk. However, the exact ways sociodemographics might shift with climate-induced population change are less studied.

Recent studies suggest that population shifts driven by climate change may influence the future demographic composition of affected areas in various ways (Hauer, 2017; Hauer et

al., 2024; Best et al., 2023). For example, Hauer et al. (2024) found that climate migration could accelerate population aging in coastal areas vulnerable to flooding as younger populations migrate while older populations remain. Similarly, Best et al. (2023) have found that Black and Hispanic populations face a disproportionate risk of isolation from essential services in areas threatened by sea-level rise, indicating these groups might lack the resources or capabilities to move from affected areas. These findings underscore the complex interactions between climate change, migration, and sociodemographic factors, necessitating more comprehensive understandings of how climate-induced migration relates to various population characteristics.

This section aims to explore the relationship between localized changes in population and shifting sociodemographics across the contiguous United States. To achieve this, we examine the historical relationships between population change and sociodemographic shifts over a 20-year time period (2000 to 2020) as proxies for anticipating the impacts of future climate migration on community profiles. Among the sociodemographic characteristics modeled, we examine demographic and socioeconomic attributes from US Census data including age, education, income, housing, race and ethnicity, and occupation. Bivariate generalized additive models (GAMs) are employed to flexibly trace how sociodemographics have historically moved with population growth or decline, which can serve as predictions for how community composition may continue to transform with future population change. These relationships are also explored in aggregate by employing a partial least squares regression (PLSR) to understand the general direction and magnitude of the relationship with population change when sociodemographics are examined collectively. Mobility and associated sociodemographic shifts are likely to vary across the United States, and depend on the local and geographic context, especially in the face of various climate-related insults. Therefore, our study evaluates these relationships within geographic context by defining a novel set of geographic categories along regional, urban, and coastal divides, characteristic of both the spatial characteristics of population dynamics and climate impacts across the contiguous U.S. Our approach to disaggregating relationships by geographic category leads to more accurate profiles of anticipated changes as population changes across areas of the U.S.

3.3 Methodology

Our main objective for this section was to evaluate the relationship between population change and shifts in community sociodemographics (**Figure 3.1**). These relationships were evaluated across the contiguous US from 2000 to 2020. Since these relationships likely vary by local context, influenced by regional, urban, and coastal trends, we evaluated these relationships separately by geographic context.

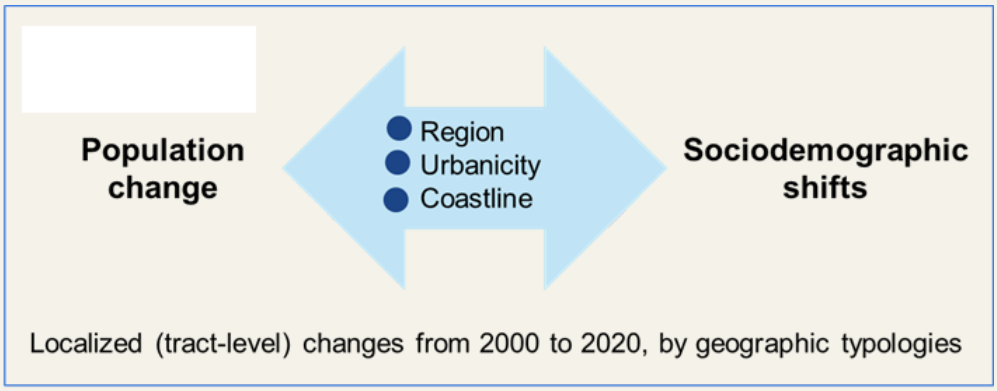

Figure 3.1 Illustration of this section's objective to evaluate the relationship between local changes in population and sociodemographics using historical tract-level data from the U.S. Census Bureau from 2000 to 2020. Relationships evaluated separately in the context of region, urbanicity and coastal proximity.

3.3.1 Data Selection and Sources

We acquired a set of sociodemographic variables of interest from the U.S. Census Bureau, including total population, age, race and ethnicity, sex, income, poverty, education, employment, industry, occupation, housing occupancy and cost (including homeownership and rental costs), and measures of immigration. **Table 3.1** lists the category of outcome variables included in this analysis and their descriptions. We matched variables from 2000 and 2020 that captured the same information over the two time periods, such as median age. Data was collected at the tract-level, the highest resolution available for all demographic variables. Count and percentage data were collected for the larger demographic subgroups (e.g., total population, race and ethnicity, age and sex), while percentage data was pulled for other socioeconomic variables.

Table 3.1 Population and sociodemographic information for tracts across the contiguous U.S. in 2000 and 2020 from the U.S. Census Bureau.

Category	Description
Population	Total population count
Sociodemographics	
Age	Median age, % Age categories (5- or 10-year intervals up to 85+)
Sex	% Male, Female

Race and ethnicity	% White, Black, Asian, Hispanic, Native American or Alaskan, Native Hawaiian or Pacific Islander, other, two or more
Education	% High School, Associate's, College Graduate, Graduate/Terminal Professional Degree
Income	Median income (household), % Income categories (intervals defined by Census)
Poverty	% Poverty families and individuals
Housing occupancy	% Units occupied, Owner occupied, Renter occupied
Housing cost	Median rent, Median value of owner-occupied units % Rent as a ratio of income (intervals defined by Census)
Employment	% Employed, Unemployed
Industry	% Agriculture, Construction, Manufacturing, Wholesale, Retail, Transportation, Information, Finance, Professional/Administrative, Education/Health, Leisure, Public Admin
Occupation	% Professional (management, business, science, and arts occupations), % Labor (natural resources, construction, and maintenance occupations)
Immigration	% Foreign, % Low English proficiency

For comparability across the two decades, sociodemographic data for 2000 and 2020 were reconciled to the geographic boundaries of 2010 tracts. A crosswalk delineating 2000 to 2010 tracts was available from the Longitudinal Tract Database (LTDB). A tract-to-tract crosswalk for 2020 to 2010 was not available at the time of this effort; therefore we used a block group-to-tract crosswalk from the National Historical Geographic Information System (NHGIS). For count data, this required an additional step to disaggregate tract-level data to block groups. This process entailed computing a weight for the proportion of the total tract population within each block group. This weight was then applied to the tract-level count data to estimate counts for each block group. An example of this process is presented in **Table 3.2**. For percentages and medians, we assumed that the value was consistent across all blocks within the same tract.

Table 3.2 Example of disaggregating tract-level count data into block groups.

2020 tractid	2020 blockid	pop_tract	pop_block	weight (pop_block/pop_tract)	hispanic_tract	hispanic_block (hispanic_tract*weight)

1001020400	10010204001	4246	942	0.2219	158	35
1001020400	0010204002	4246	1902	0.4480	158	71
1001020400	0010204003	4246	867	0.2042	158	32
1001020400	0010204004	4246	535	0.1260	158	20

pop_tract= total population within tract

pop_block=total population within each block group

weight=proportion of total tract population within each block group

hispanic_tract=count of Hispanic population within tract

hispanic_block=estimated Hispanic population within each block group

Count data from the origin year (i.e., 2000 or 2020) was then reallocated to 2010 tracts by applying a population weight. In this case, population weight represents the proportion of the population in the origin unit (i.e., tract or block group) belonging to each 2010 tract. These reallocated counts were then aggregated for each 2010 tract. The formula below depicts the crosswalk procedure for 2000 to 2010 tracts.

$$count_{2010\ tract} = \Sigma(count_{2000\ tract} \times popweight_{2000\ tract \rightarrow 2010\ tract}) \quad \text{(Equation 3.1)}$$

Percentage and median data were crosswalked to 2010 tracts by computing a weighted mean. Population weight in this case is the proportion of the population in each 2010 tract that resides in each origin unit relation. Population weight was calculated using the estimated total population in each 2010 tract, computed from the formula above.

$$percent_{2010\ tract} = \frac{\Sigma(percent_{2000\ tract} \times popweight_{2010\ tract \rightarrow 2000\ tract})}{\Sigma(popweight_{2010\ tract \rightarrow 2000\ tract})} \quad \text{(Equation 3.2)}$$

Where $\Sigma(popweight_{2010\ tract \rightarrow 2000\ tract})$ *adds up to 1.*

3.3.2 Statistical Analysis

Estimates for Population and Sociodemographic Change

After data from 2000 and 2020 were reconciled to comparable geographic units of 2010 tracts, we could then directly compute changes in population and demographics over the past two decades.

Population change was expressed as a growth rate (%), indicating declines or increases from a "no change" scenario of 0, calculated as:

$$Population\ growth\ rate\ (\%)\ =\ 100\ x\ (\frac{Total\ population_{2020} - Total\ population_{2000}}{Total\ population_{2000}})$$ (Equation 3.3)

Changes in sociodemographic variables, either expressed as a percentage or median value (e.g., median age, median income), were computed using a straightforward difference from 2000 to 2020:

$$Sociodemographic(i)\ change\ =\ Sociodemographic(i)_{2020}\ -\ Sociodemographic(i)_{2000}$$ (Equation 3.4)

Where i is either expressed as a percentage or median value.

Inclusion Criteria

We included tracts with a total population between 200 and 15,000 people (70,945 of 72,200 tracts; 98.3%). We also excluded outliers with a population growth of 6 times or greater (519 tracts; 0.5%). Our analysis included 70,426 tracts. Distribution of tracts across Region-Urbanicity-Coastline categories are shown in **Table 3.3**.

Table 3.3 Distribution of tracts across Region-Urbanicity-Coastline categories included in our analysis (N=70,426).

Region-Urbanicity-Coastline	Tracts, n (%)
West, Metro, Coast	6,371 (9.0%)
West, Metro, Non-Coast	7,013 (10.0%)
West, Non-Metro	1,529 (2.2%)
Midwest, Metro	12,667 (18.0%)
Midwest, Non-Metro	4,177 (5.9%)

Northeast, Metro, Coast	5,651 (8.0%)
Northeast, Metro, Non-Coast	6,391 (9.1%)
Northeast, Non-Metro	1,275 (1.8%)
South, Metro, Coast	6,922 (9.8%)
South, Metro, Non-Coast	13,530 (19.2%)
South, Non-Metro	4,900 (7%)

Bivariate Population-Sociodemographic Relationships

In order to assess the relationships between population change and sociodemographic factors within a geographical context, such as regional variations, urbanicity differences, and coastal vs. non-coastal comparisons, the change metrics for sociodemographic outcomes and population at the tract level are delineated into the 11 RUC continuums as defined in Section 2.1. Subsequently, we evaluated the bivariate relationship between population change and each demographic variable of interest, separately by RUC classification, using GAMs. The parameters and assumptions employed when using GAMs are described in Section 2.2. From each fitted GAM, we derived predicted values of demographic change across the distribution of population change. Predicted sociodemographic values were centered to a reference point of no population change and plotted along with their 95% confidence intervals (95% CIs). This allows for a clear interpretation of the expected change in a sociodemographic characteristic for a given value of population decline or growth, relative to no growth. Almost all sociodemographic variables had less than 1% missing data; median rent and median value of owner-occupied units was missing about 2% of data.

The model specification for each demographic variable (*i*) within each RUC classification (*j*) is as follows:

$$Sociodemographic\ Change\ (i,j)\ =\ f(Population\ Growth\ Rate(j))\ +\ \varepsilon \quad \text{(Equation 3.5)}$$

where:

-

-

- Demographic(*i*,*j*) change is the change in the demographic variable *i* from 2000 to 2020 in RUC classification *j*
- f() represents a cubic spline smoothing function with a maximum of three knots
- Population Growth Rate(*j*) is the population change from 2000 to 2020 in RUC classification *j*, expressed as a percentage
- ε is the error term

We found relationships between population change and sociodemographics were generally linear. For ease of interpretation, we also plotted coefficients from linear bivariate models using a heat map, to compare the magnitude and direction of the relationship between population change and groupings of sociodemographic variables, such as age categories, income brackets, and educational attainment levels, across the RUC continuum.

Partial Least Squares Regression

To validate our results and provide another way of estimating the magnitude of each sociodemographic variable to population, we evaluated the collective relationship between multiple sociodemographics and population change using a partial least squares regression (PLSR). PLSR is a statistical technique for dimension reduction, modeling the covariance structures between multiple sociodemographics, and the relationship with population change. Advantages of PLSR include: 1) the ability to handle collinearity between sociodemographics, that are likely to cluster together, and 2) being a supervised method that also considers how sociodemographics collectively relate to population change. Sociodemographics in our model include the difference (2020-2000) in median household income ($), % Bachelor's degree or higher, median rent ($), median value of owner-occupied housing units ($), % housing units that are owner-occupied, % individuals below the poverty line, % Hispanic, % Black or African American, % Asian, % White, median age (years), % female, % employed, % in a professional occupation, % in a labor occupation, and % who speak limited English. Population change was included as the outcome. A correlation matrix of variables included in our analysis is presented in **Figure 3.2**. Similar to our bivariate models, we separately modeled tracts according to RUC classification. Sociodemographic variables were scaled before analysis. We focused on evaluating relationships within the first component, which explains the maximum variance in sociodemographics and the relationship with population change. The component includes a loading, or weight, that is estimated for each sociodemographic variable, indicating the magnitude and direction of the relationship with population change. Sociodemographics with a positive loading are associated with population growth, whereas variables with a negative loading are associated with population decline.

See **Equation 1** for more details.

The goal of PLSR is to create a latent variable that consists of a score for each tract, effectively capturing the relationship between collective sociodemographics and population change. These scores are derived from a linear combination of the predictors (sociodemographics) that maximize the covariance with the response variable (population change). As part of this process, a weight is computed for each sociodemographic variable, which is then used to compute the score of the latent variable. A loading can then be computed for each sociodemographic to determine its relative contribution to the composite score that captures the relationship with population change. The process is as follows:

1. **Compute the weight vector** (w)**:**

$$w = \arg arg\ Cov\ (Xw, Y) \quad \text{(Equation 3.6)}$$

Where X is a matrix of predictors (sociodemographics)

Where Y is a single outcome, in this case, population change

The latent variable is derived using the weight vector w to maximize the covariance with the response variable Y

2. **Compute the score Vector** (t)

$$t = Xw \quad \text{(Equation 3.7)}$$

The score vector t represents the latent variable, a linear combination of the original predictors X that captures the most relevant information for predicting Y.

3. **Compute the loadings** (p) **for each predictor in** X**:**

$$p = \frac{X^T t}{t^T t} \quad \text{(Equation 3.8)}$$

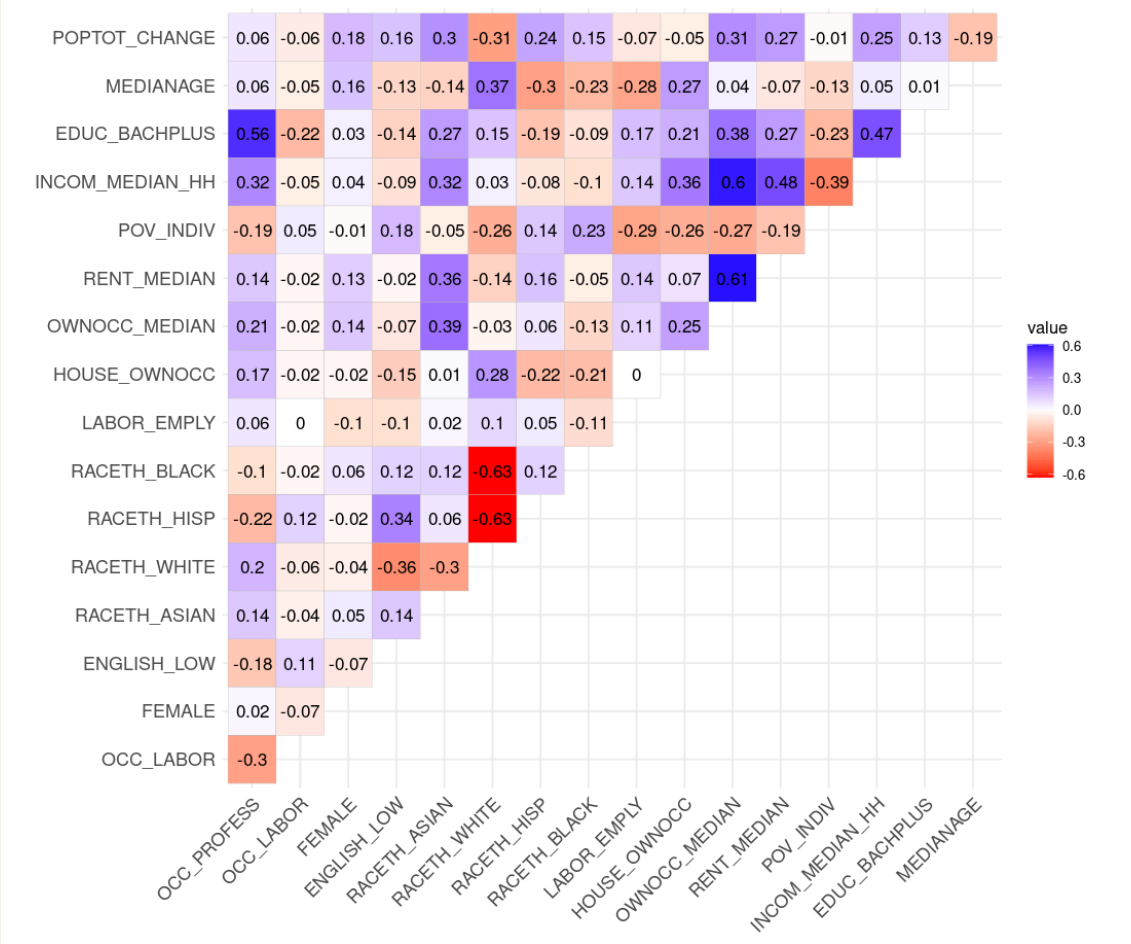

Figure 3.2. Spearman's correlation between tract-level population and sociodemographic changes (2020-2000) included in our partial least squares regression (n tracts with complete information= 67,945).

3.4 Results

3.4.1 Bivariate Relationships

The relationships between sociodemographic variables and population change modeled using GAMs revealed distinct patterns across both categories of variables and RUCs. Socioeconomic characteristics such as income and educational attainment showed consistently positive associations with population growth across RUCs, though the magnitude varied by category. Demographic factors such as age, sex, race, and ethnicity exhibited more varied patterns across different RUC designations. Select sociodemographic outcomes predicted in instances of 50% population growth or decline across RUCs are highlighted below.

Median household income showed a clear positive relationship with population growth across RUCs, with the weakest relationship observed in Northeast coastal areas (**Figure 3.3**). For instance, in Northeast metro coastal areas with a 50% population increase,

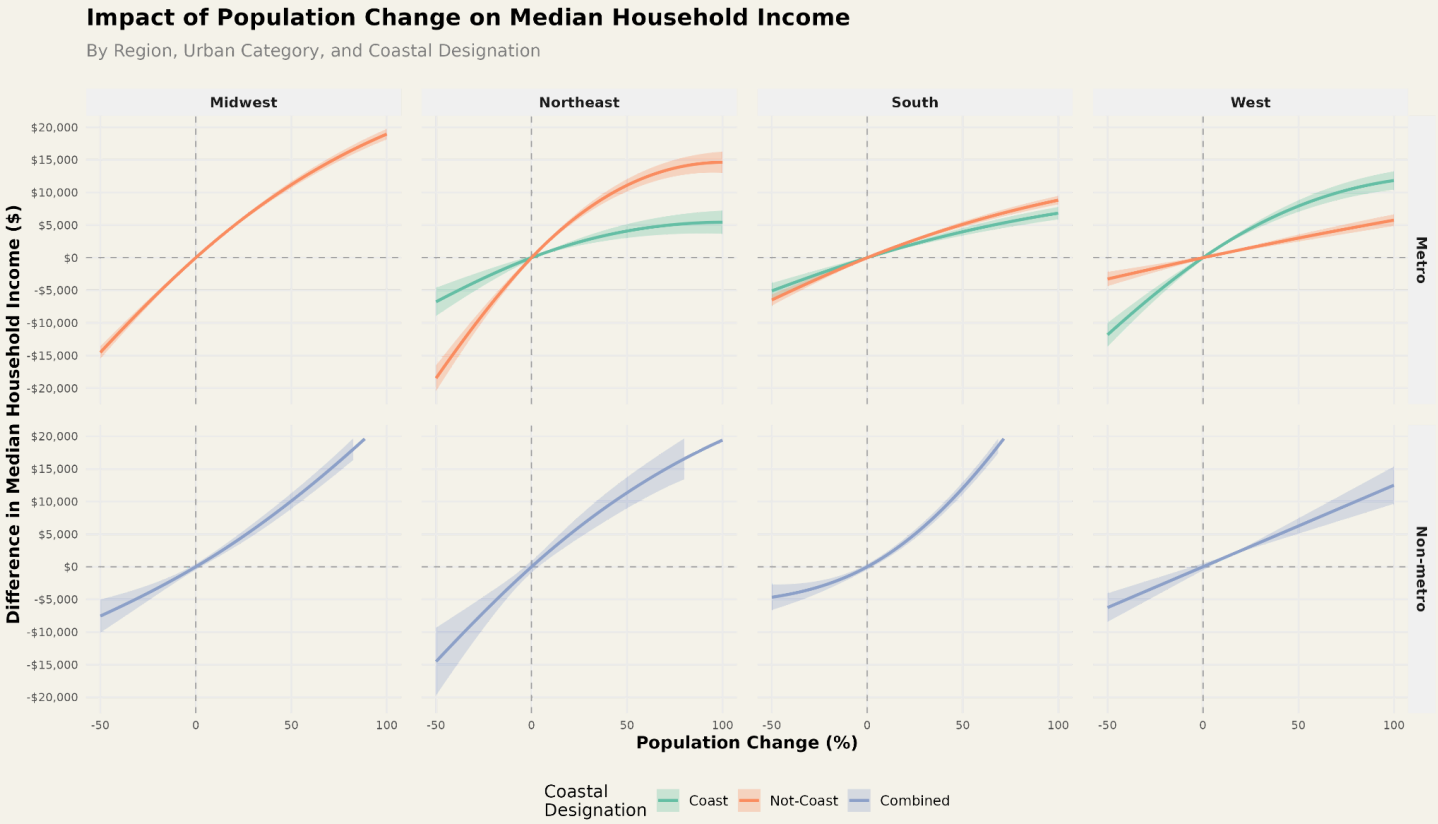

median household income rose by $3,680 (95% CI: $2,665, $4,695), compared to $10,062 (95% CI: $9,181, $10,944) in Northeast metro non-coastal areas.

Figure 3.3 The relationship between population change and median household income for US census tracts from 2000 to 2020, analyzed separately across Region-Urbanicity-Coastline categories. Population change modeled using a cubic spline. X-axis is the population growth factor, where values below 0 indicate a population decline and values above 0 indicate population growth (e.g. 100 represents a 2-fold increase). Y-axis is the expected difference in median income in dollar form from 2000 to 2020 for a given value of population change, relative to no population change.

Similarly, educational attainment increased with population growth across most RUCs, with the strongest relationships observed in Midwest and Southern non-metro areas (**Figure 3.4)**. In Midwestern non-metro areas experiencing 50% population growth, the share of the population with a bachelor's degree increased by 3.16 percentage points (95% CI: 2.81%, 3.51%). This trend was even more pronounced in Southern non-metro areas, with a 3.87 percentage point increase (95% CI: 3.40%, 4.33%).

Figure 3.4. The relationship between population change and percent of the population with a bachelor degree for US census tracts from 2000 to 2020, analyzed separately across Region-Urbanicity-Coastline categories. Population change modeled using a cubic spline. X-axis is the population growth factor, where values below 0 indicate a population decline and values above 0 indicate population growth (e.g. 100 represents a 2-fold increase). Y-axis is the expected difference in percent of the population with a bachelor degree from 2000 to 2020 for a given value of population change, relative to no population change.

Housing occupancy and rental costs showed mixed relationships across RUCs. The percentage of owner-occupied housing units generally decreased with population growth in metropolitan areas and increased in suburban areas (**Figure 3.5**). This contrast was particularly evident in Southern areas: South metro areas with 50% population growth experienced a 1.4 percentage point decrease (95% CI: -1.56%, -1.24%) in non-coastal areas and a 1.9 percentage point decrease (95% CI: -2.13%, -1.67%) in coastal areas in the share of owner-occupied housing. Conversely, non-metro areas of the South saw a 0.56 percentage point increase (95% CI: 0.00%, 0.50%).

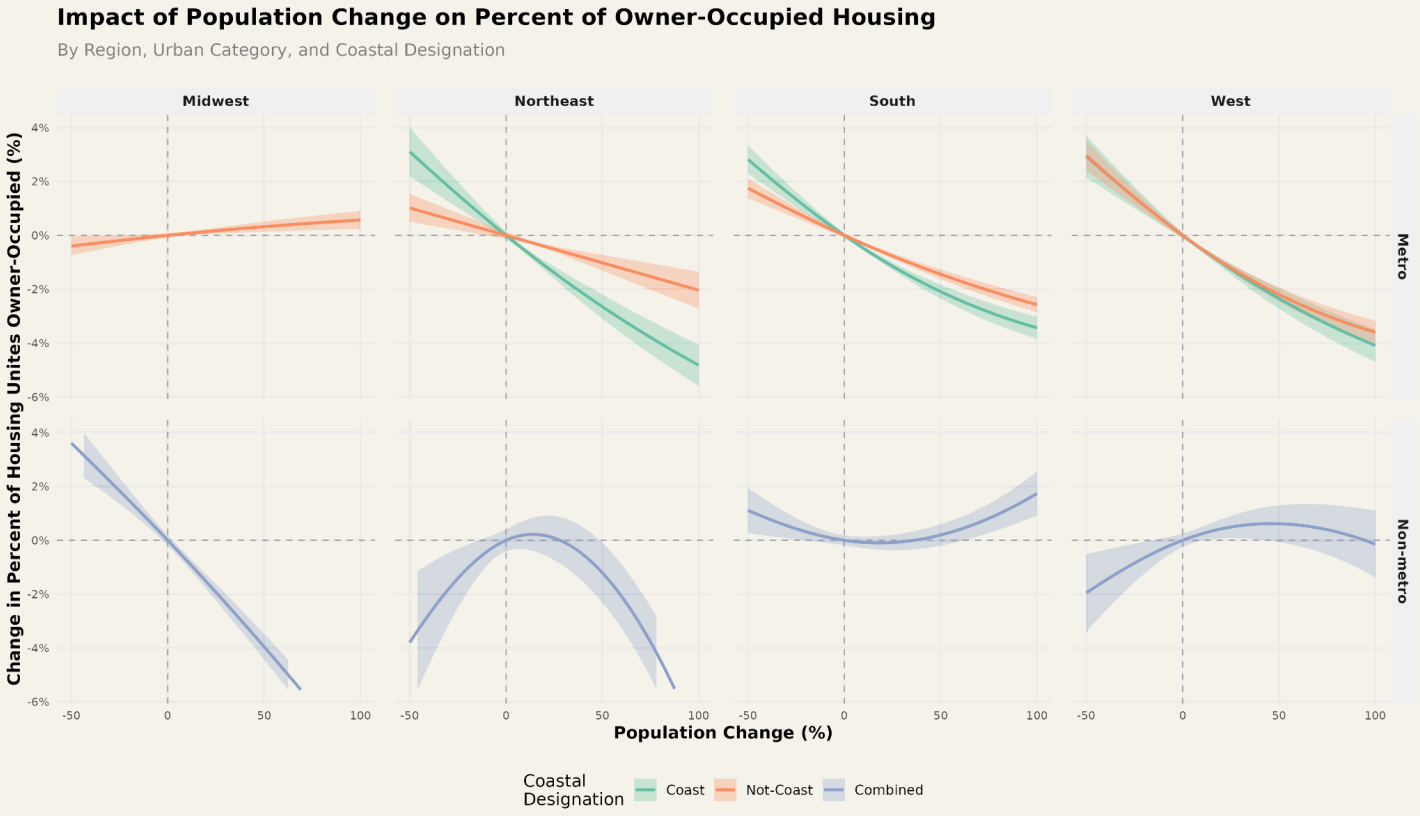

Figure 3.5. The relationship between population change and percent of residential properties that are owner-occupied for US census tracts from 2000 to 2020, analyzed separately across Region-Urbanicity-Coastline categories. Population change modeled using a cubic spline. X-axis is the population growth factor, where values below 0 indicate a population decline and values above 0 indicate population growth (e.g. 100 represents a 2-fold increase). Y-axis is the expected difference in percent of residential properties that are owner-occupied from 2000 to 2020 for a given value of population change, relative to no population change.

Median age showed a clear inverse relationship with population change across all RUCs (**Figure 3.6**). Tracts experiencing population decline showed an increase in median age, while those with population growth exhibited a decrease, at varying rates across regions, urbanicity, and coastal areas. In non-coastal metropolitan areas of the West that experienced a 50% population decline, the median age increased by 0.68 years (95% CI: 0.46, 0.89), relative to no population change. This trend was more pronounced in coastal areas of the same region, with a median age increase of 2.56 years (95% CI: 2.23, 2.89).

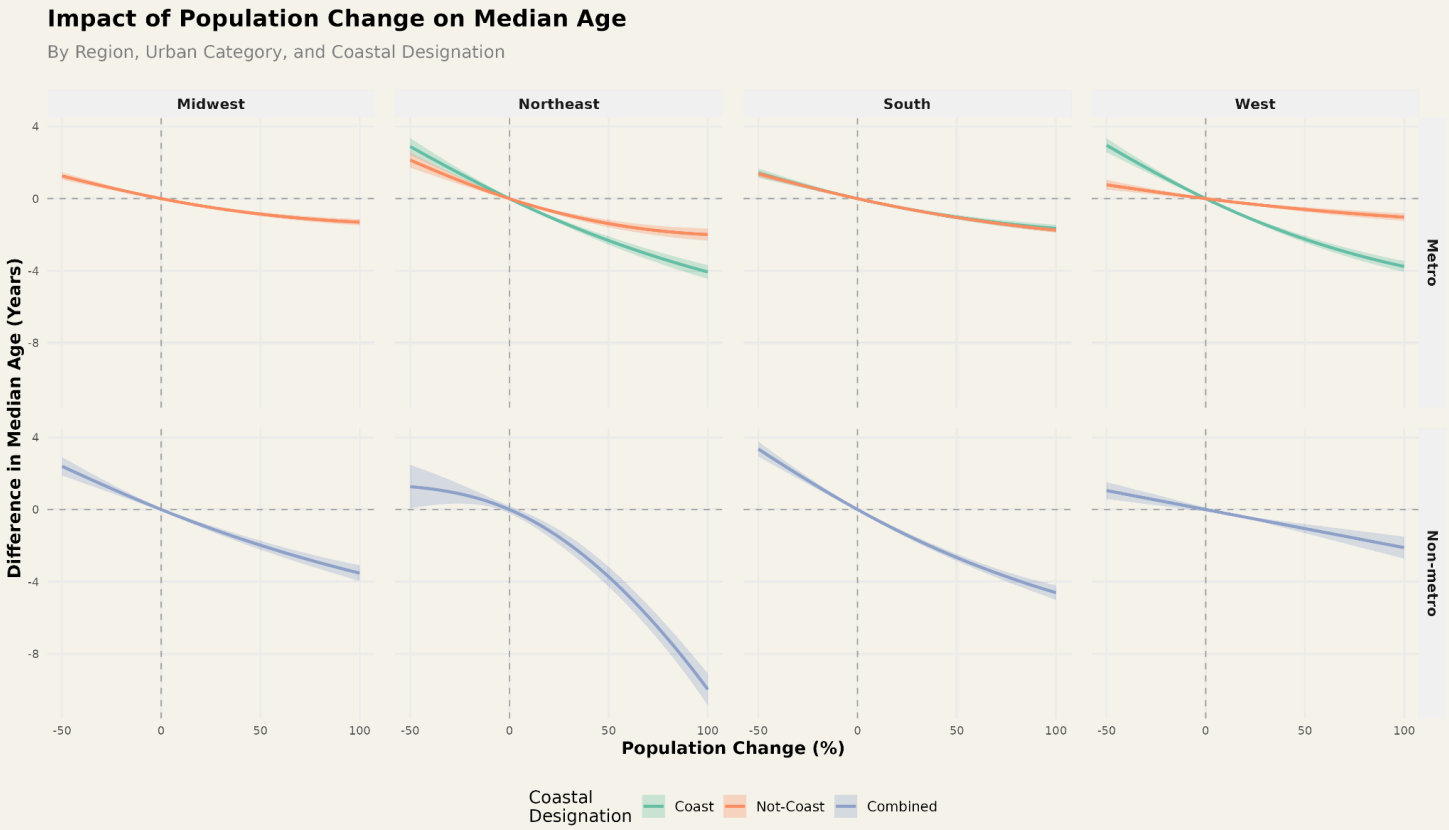

Figure 3.6. The relationship between population change and median age for US census tracts from 2000 to 2020, analyzed separately across Region-Urbanicity-Coastline categories. Population change modeled using a cubic spline. X-axis is the population growth factor, where values below 0 indicate a population decline and values above 0 indicate population growth (e.g. 100 represents a 2-fold increase). Y-axis is the expected difference in median age from 2000 to 2020 for a given value of population change, relative to no population change.

3.4.2 PLSR Relationships

The PLSR analysis between sociodemographic variables and population change revealed patterns that largely corroborated the trends observed in the initial bivariate GAM analyses, while also highlighting some important distinctions. The loading chart for the importance of sociodemographic factors on population change is presented in **Figure 3.7**. For a closer look of how loadings for each sociodemographic characteristic compare across RUC classifications, see **Figure 3.8**.

The PLSR loading charts expand upon the GAM results by providing a comprehensive view of the relationships between population change and multiple sociodemographic

factors simultaneously. While GAMs show individual bivariate relationships, PLSR analyzes all factors together, accounting for potential interactions. The loading charts visually represent the strength and direction of each factor's association with population change, allowing for easy comparison across variables. This approach helps identify which sociodemographic factors have the most significant impact on population dynamics when considered collectively, potentially revealing patterns not apparent when examining factors in isolation. Additionally, it highlights the relative importance of different factors across various geographic contexts.

For example, socioeconomic factors emerged as the strongest predictors of population change. Median household income, median rent, median value of owner-occupied housing, and educational attainment consistently displayed the highest positive loadings across RUC categories, reinforcing their robust positive association with population growth observed in the GAM models. Some new insights were gleaned from the strength of each characteristic’s impact on population growth, as signaled by its loading score. For example, in Northeast metropolitan coastlines, educational attainment emerged as the strongest predictor among all sociodemographic factors, a distinction not apparent in the GAM results. We observed a consistently negative association between poverty rates and population change for all RUCs, except West and South metro coastal areas.

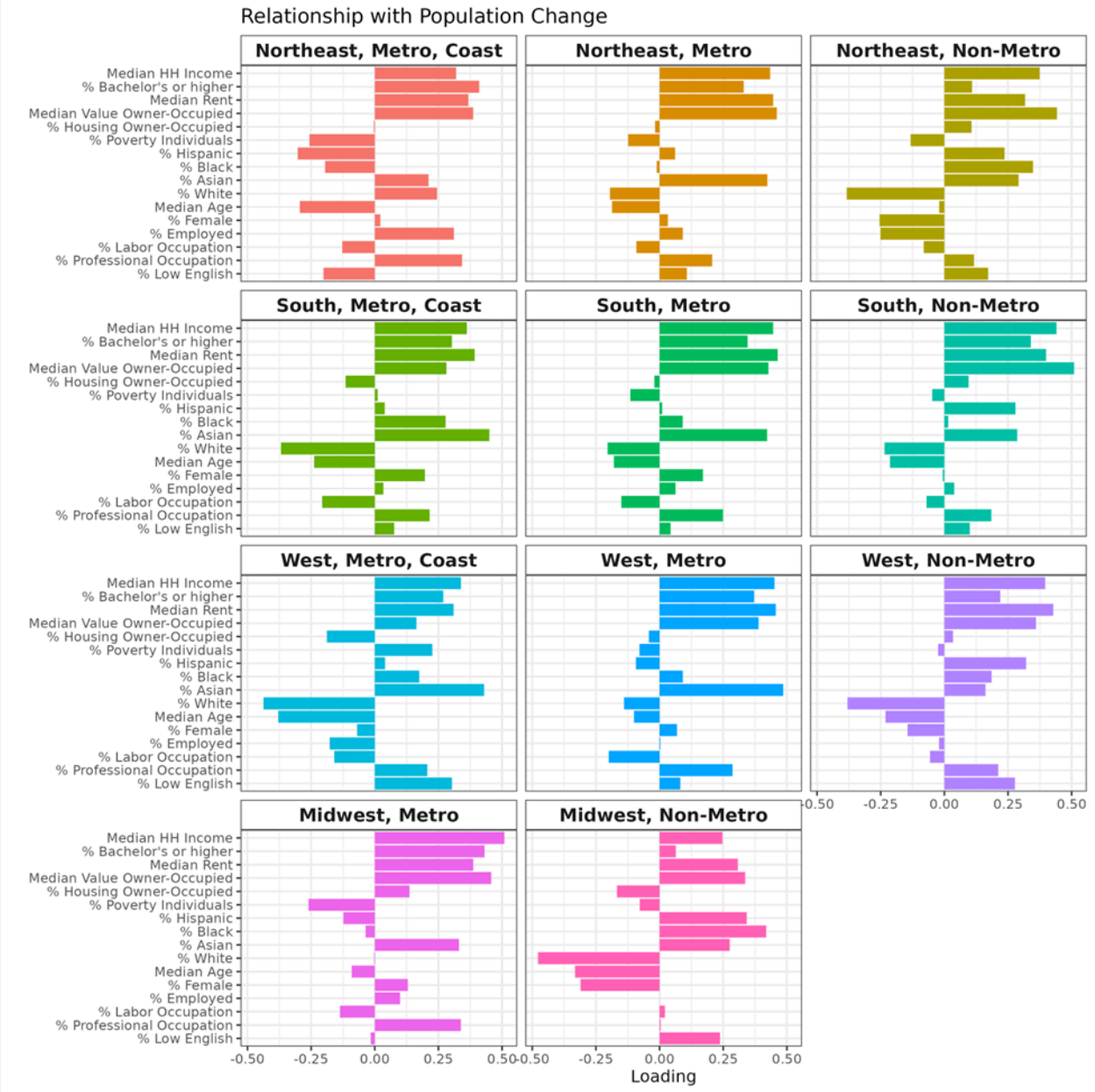

Figure 3.7. Results from the partial least squares (PLS) regression showing the relationship between changes in sociodemographics on population change, separately by Region-Urbanicity-Coastline categories. Among 67,945 Census tracts with complete information (96% of 70,426 total tracts). A loading, or weight, is shown for each sociodemographic variable, indicating the magnitude and direction of the relationship with population. Variables with a positive loading are associated with increases in population (right-hand side of plots), whereas variables with a negative loading are associated with decreases in population (left-hand side of plots).

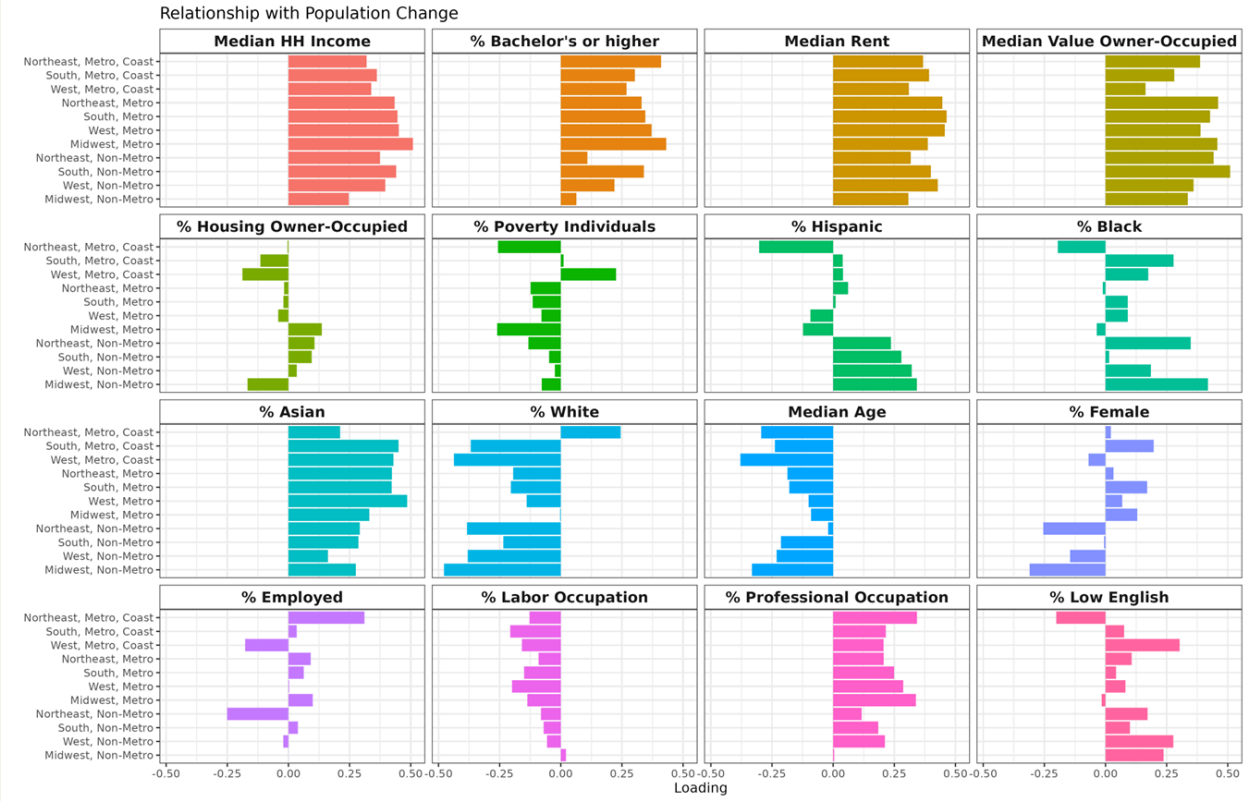

Figure 3.8. Results from the partial least squares (PLS) regression showing the relationship between collective changes in sociodemographics and population change, separately by Region-Urbanicity-Coastline (RUC) categories. Ordered by sociodemographic variable to more easily compare across RUC categories. Among 67,945 Census tracts with complete information (96% of 70,426 total tracts). A loading, or weight, is shown for each sociodemographic variable, indicating the magnitude and direction of the relationship with population change. Variables with a positive loading are positively associated with population change (right-hand side of plots), whereas variables with a negative loading are negatively associated with population change (left-hand side of plots).

4. Economic Implications

4.1 Executive Summary

This analysis investigates the economic implications of climate migration, specifically on economic indicators employed by financial institutions, including Gross Domestic Product (GDP), Housing Price Index (HPI), and Debt-to-Income (DTI) ratio across the contiguous U.S. The purpose of this analysis is to estimate the economic impacts of shifting populations used by banks and other financial institutions when making decisions about the housing market and tie those impacts to the indirect effects of climate exposure via combined climate model outputs. The methodology integrates estimates from various federal sources to create separate models for each economic-population relationship that employs bivariate modeling techniques. The relationships are analyzed along Rural-Urban-Coastline (RUC) boundaries to investigate variations across regional, urbanicity, and coastal parts of the U.S. Key findings reveal generally positive relationships between changes in population and GDP and HPI and a negative relationship between changes in population and DTI, with varying sensitivities across the economic variables of interest and RUCs.

4.2 Background

Climate migration within the U.S. could have significant impacts on economic indicators in areas affected by such population dynamics. As populations shift domestically, patterns of economic activity, housing demand, and financial behaviors change, potentially affecting GDP, housing prices, and debt levels. These perceived indirect impacts of population change are supported by several economic theories on the intersection of population characteristics and economic outcomes. Specifically, Neoclassical Growth Theory, developed by Solow and Swan (1956), suggests that economic growth is driven in part by changes in the labor force which in turn could shift as populations grow or decline. Similarly, Urban Economics and Amenity Theory developed by Roback (1982) and Glaser et al. (2001) explains how the attractiveness of a location, based on its amenities and economic conditions, affects migration to an area as well as housing prices in that area. Lastly, Life Cycle Theory of Consumption and Saving proposed by Modigliana and Brumberg (1954) suggests that individuals make consumption and saving decisions based on their expected lifetime income, meaning borrowing decisions vary depending on a person’s age or life-stage, which in turn could impact aggregate debt-to-income ratios in areas as migration shifts age structures (as shown by the results of our Demographic Change model in Section 3.4.1.

These patterns have been observed in literature. For example, Bell and Charles-Edwards (2014) find that GDP per capita is strongly correlated with both short-term and medium term migration intensities across a several developed and developing countries, including the U.S. In the housing market, several studies have demonstrated that immigration into the US is associated with increased housing prices, i.e., HPI (Xu, 2020; Mussa et al., 2017; Saiz, 2007). Studies assessing the associations between internal migration and housing prices are less available in the U.S., but studies from other countries have suggested similar positive associations (Erol and Unal, 2022). Regarding debt, research by Fulford and Schuh (2015) shows that credit and debt levels change over the life cycle and with local economic conditions, which could be influenced by migration patterns. Similarly, Demyank et al. (2017) demonstrate that existing debt levels and access to credit affect internal migration decisions, which in turn could impact debt levels of areas with high or low levels of migration. Furthermore, Fan et al. (2018) apply a spatial equilibrium model to examine the economic impacts of sea-level rise-induced migration at the county level in the U.S., finding significant effects on wages, housing prices, and local GDP in both origin and destination counties.

4.3 Methodology for GDP

4.3.1 Data Inputs

Data on county-level Gross Domestic Product (GDP) were obtained from the U.S. Bureau of Economic Analysis (BEA) regional accounts, specifically from the CAGDP9 dataset. This dataset provides annual GDP estimates for all counties in the U.S., broken down by major industry sectors according to the North American Industry Classification System (NAICS).

The data collected covers the period from 2001 to 2019, offering a near 20-year span for analysis. GDP figures are reported in thousands of chained 2012 dollars, providing inflation-adjusted values for accurate comparison over time. **Table 4.1** presents a breakdown of all NAICS sectors included in the analysis, including all sectors in aggregate.

To smooth out short-term fluctuations and test relationships at different levels of smoothing, multi-year averages were calculated. These included 3-year and 5-year averages at the start of the period (2001-2003 and 2001-2005 respectively) and at the end of the period (2017-2019 and 2015-2019 respectively). Single year data, including 2001 and 2019 were also kept. While data was available for the years 2020 to 2021, they were omitted in order to avoid capturing any irregularities caused by the COVID-19 pandemic.

Table 4.1 NAICS Sectors Included in GDP Modeling.

Sector Name	NAICS Code
All sectors	00
Agriculture, Forestry, Fishing and Hunting	11
Utilities	22
Construction	23
Manufacturing	31-33
Wholesale Trade	42
Retail Trade	44-45
Transportation and Warehousing	48-49
Information	51
Finance and Insurance	52
Real Estate and Rental and Leasing	53
Professional, Scientific, and Technical Services	54
Management of Companies and Enterprises	55
Administrative and Support and Waste Management and Remediation Services	56
Educational Services	61

Health Care and Social Assistance	62
Arts, Entertainment, and Recreation	71
Accommodation and Food Services	72
Other Services (except Public Administration)	81

Population data for years 2000 and 2020 were collected and reconciled to comparable geographic units of 2010 tracts as discussed in the demographic change Section 3.3.1. Historical data on population change estimates over those 20 years were integrated directly from data generated for the demographic change model, as described in Section 3.3.2. Historical population data at the tract level was merged with the GDP data at the county level on county FIPS code, thereby expanding GDP estimates for counties to fill all rows in corresponding tracts.

4.3.2 Statistical Analysis

Estimating GDP and Population Change

To quantify economic growth and change over time, several change metrics were calculated. A one-year change metric was computed by comparing GDP values from 2001 to 2019 using the formula

$$GDP\ Change_{1-year} = \frac{GDP_{2019} - GDP_{2001}}{GDP_{2001}} \quad \text{(Equation 4.1)}$$

A three-year average change metric was derived using the formula

$$GDP\ Change_{3-year} = \frac{GDP_{2017-2019} - GDP_{2001-2003}}{GDP_{2001-2003}} \quad \text{(Equation 4.2)}$$

Similarly, a five-year average change was calculated as

$$GDP\ Change_{5-year} = \frac{GDP_{2015-2019} - GDP_{2001-2005}}{GDP_{2001-2005}} \quad \text{(Equation 4.3)}$$

These change metrics were calculated for each county and each NAICS sector.

Consistent with the methods used in the demographic change analysis, population change is then expressed as a growth factor where:

$$Population\ Growth\ Factor\ (Change) = \left(\frac{Total\ Population_{2020} - Total\ Population_{2000}}{Total\ Population_{2000}}\right) \quad \text{(Equation 4.4)}$$

Values below 0 indicate a decline in population and values above 0 indicate an increase in population.

Test regressions were run between population change and the three different GDP change estimates using single year, three-year, and five-year smoothing to determine goodness-of-fit based on variance explained. Ultimately, the three-year smoothed GDP change estimates were chosen due to their higher R-squared value compared to the other two variables' relationships with population change.

Inclusion Criteria

Input data into the model was filtered to the 98% confidence range for 3-year smoothed GDP change, excluding the top and bottom 1% of GDP change observations. This filtering excluded 1,866 counties (2.6% of all counties in the data). This resulted in less error in the modeling results and tighter confidence bounds.

Bivariate Modeling

Change metrics of county GDP and population at the tract level were delineated into the 11 RUC continuums as defined in Section 2.1 in order to explore regional variations, urbanicity differences, and coastal vs. non-coastal comparisons. Similar to proceeding sections, bivariate GAMs are employed to evaluate the impact of growth factors in population on county GDP for each sector interacted by each of the RUCs. The parameters and assumptions employed when using GAMs are described in Section 2.2. From each fitted GAM, we derived predicted values of sectoral county GDP change across the distribution of population change. Predicted county GDP change values were centered to a reference point of no population change and plotted along with their 95% confidence intervals. The resulting predictions produce conversion tables that translate changes in population into changes in county GDP for each sector and RUC.

4.4 Methodology for DTI

4.4.1 Data Inputs

Data on Debt-to-Income (DTI) ratios were obtained from the Home Mortgage Disclosure Act (HMDA) dataset, which is maintained by the Consumer Financial Protection Bureau (CFPB). This dataset provides loan-level information on mortgage applications and originations across the U.S., including borrower characteristics and DTI ratios. The HMDA data covers a wide range of financial institutions and offers insights into lending patterns and borrower financial profiles at various geographic levels, including census tracts,

counties, and metropolitan statistical areas. Specifically, DTI ratios reflect the proportion of a mortgage applicant's monthly income that goes towards paying debts, providing insight into the applicant's ability to manage additional mortgage payments.

HMDA Loan/Application Register (LAR) data for 2018 and 2022 was used to collect census tract-level DTI estimates. Initial data preparation involved filtering and cleaning to refine and structure the HMDA dataset across both years. Data was filtered to focus exclusively on home purchase loans by selecting only those entries where the loan purpose was home purchase (code 1). From these filtered datasets, only the census tract identifier and DTI ratio fields were retained for further analysis.

The DTI data then underwent a cleaning process to standardize the values and prepare them for statistical analysis. Entries marked as "Exempt" were removed from the dataset to ensure all remaining data points were comparable. The DTI values, originally recorded in categorical ranges, were converted to numerical estimates. For instance, the "<20%" category was assigned a value of 15, "20%-<30%" was assigned 25, "30%-<36%" was assigned 33, "50%-60%" was assigned 55, and ">60%" was assigned a value of 65.

In order to assess the relationship between DTI and population, historical data on population change at the tract level from 2000 to 2020 were integrated directly from data generated for the demographic change model, as described in Section 3.3.2. Historical population data and DTI data were merged on each census tract to produce the final input data for modeling. The final input data was structured similarly to that of proceeding analyses–each row in the data frame represented a tract, with DTI change and population change as columns.

4.4.2 Statistical Analysis

Estimating DTI change

To quantify DTI growth and change over time, a change metric was computed by comparing DTI values from 2018 to 2022 using the formula

$$DTI\ Change = \frac{DTI_{2022} - DTI_{2018}}{DTI_{2018}} \quad \text{(Equation 4.5)}$$

Inclusion Criteria

Input data into the model was filtered to the 98% confidence range for DTI change, excluding the top and bottom 1% of DTI change observations. This filtering excluded 958 tracts (2.0% of all census tracts in the data). This resulted in less error in the modeling results and tighter confidence bounds.

Bivariate Modeling

Change metrics of DTI and population at the tract level were delineated into the 11 RUC continuums as defined in Section 2.1 in order to explore regional variations, urbanicity differences, and coastal vs. non-coastal comparisons. Different from other analyses, the relationships between population change and DTI change was derived using linear regressions to better capture the direction of the associations between these factors to produce generalizable estimates. GAM models were tested using a similar approach as described in Section 2.2, but the results overfit the historical data, limiting the predictive power of the models. The linear regressions were run by RUC to create RUC-specific estimates of how trends in population change are associated with DTI change within regional, urban, and coastal bounds. From each fitted linear regression, we derived predicted values of DTI change across the distribution of population change for each RUC. Predicted DTI change values were centered to a reference point of no population change and plotted along with their 95% confidence intervals (95% CIs). The resulting predictions produce conversion tables that translate changes in population into changes in DTI for each RUC.

4.5 Methodology for HPI

4.5.1 Data Inputs

Data on Housing Price Index (HPI) were obtained from the Federal Housing Finance Agency (FHFA), which maintains a comprehensive database of home price trends across the U.S. The FHFA HPI is a broad measure of the movement of single-family house prices, calculated using repeat sales and refinancings of the same properties. The index, which is based on transactions involving conforming, conventional mortgages purchased or securitized by Fannie Mae or Freddie Mac, offers insights into home price fluctuations and appreciation rates across different regions and time periods.

Raw data on HPI was collected from the FHFA at a quarterly frequency for the years 2000 and 2020 for 3-digit ZIP codes. A 3-digit ZIP code refers to the first three digits of a full 5-digit ZIP code. These first three digits designate a sectional center facility (SCF) or a central mail processing facility within a larger geographical region. As the data was quarterly, annual averages were developed to produce single estimates for each year and ZIP code. A crosswalk from 3-digit ZIP codes to 2010 census tracts was then used to be able to merge in data on population change and RUC designations. Historical data on population change at the tract level over those 20 years were integrated directly from data generated for the demographic change model, as described in Section 3.3.2.

This data was aggregated up to the county level and merged with the HPI data to produce the final input data for modeling.

Annual estimates of HPI were also standardized by dividing each HPI observation for each ZIP code HPI and each year by the average HPI for that year across all observations in order to smooth out any extreme values and possible mismatches from the crosswalk. For example, 2020 HPI estimates were standardized using the formula:

$$HPI\ Standardized_i = \frac{HPI\ 2020_i}{HPI\ 2020\ avg} \quad \text{(Equation 4.6)}$$

Where, i represents HPI at each census tract.

The final input data was structured similarly to that of proceeding analyses–each row in the data frame represented a tract, with HPI change and population change as columns.

4.5.2 Statistical Analysis

Estimating HPI Change

To quantify HPI growth and change over time, a change metric was computed by comparing HPI values from 2000 to 2020 using the formula

$$HPI\ Change = \frac{HPI_{2020} - HPI_{2010}}{HPI_{2010}} \quad \text{(Equation 4.7)}$$

Inclusion Criteria

Input data into the model was filtered to the 98% confidence range for HPI change, excluding the top and bottom 1% of HPI change observations. This filtering excluded 2,677 tracts (1.3% of all tracts in the data). This resulted in less error in the modeling results and tighter confidence bounds.

Bivariate Modeling

Change metrics of HPI and population at the county level were delineated into the 11 RUC continuums as defined in Section 2.1 in order to explore regional variations, urbanicity differences, and coastal vs. non-coastal comparisons. Similar to proceeding sections, bivariate GAMs are employed to evaluate the impact of growth factors in population on HPI interacted by each of the RUCs. The parameters and assumptions employed when using GAMs are described in Section 2.2. From each fitted GAM, we derived predicted

values of HPI change across the distribution of population change for each RUC. Predicted HPI change values were centered to a reference point of no population change and plotted along with their 95% confidence intervals (95% CIs). The resulting predictions produce conversion tables that translate changes in population into changes in HPI for each RUC.

4.6 Results

4.6.1 County GDP Results

Results for county GDP varied across NAICS sectors (**Figure 4.3**). For example, county GDP for the agriculture sector saw largely negative relationships with population change across most RUCs, while the information sector saw mostly positive relationships. Overall, the relationship between population change and county GDP growth was positive when looking at aggregate GDP across all sectors, with non-metropolitan GDP showing more sensitivity to population growth. In the Northeast metro non-coastal areas experiencing 50% population growth, county GDP rose by 8.4 percentage points (95% CI: 7.23%, 9.67%). However, in Northeast non-metro areas with 50% population gain, county GDP rose by 20.75 percentage points (95% CI: 16.81%, 24.68%).

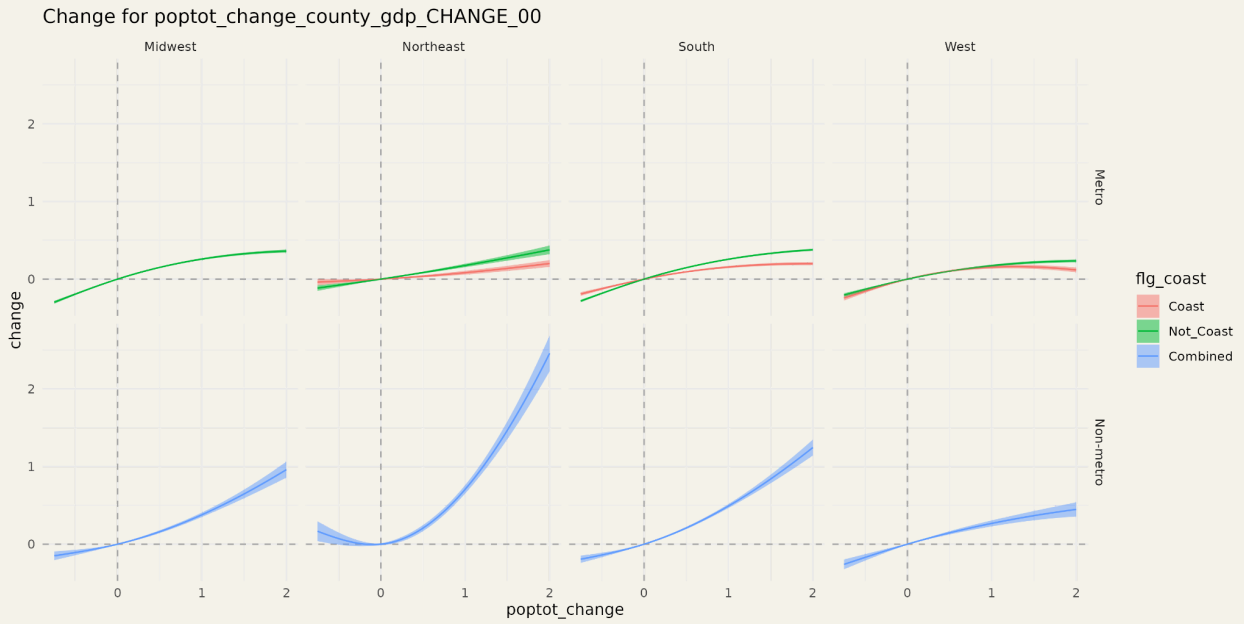

Figure 4.3 The relationship between population change and county GDP for US counties from 2000 to 2020, analyzed separately across Region-Urbanicity-Coastline categories. Population change modeled using a cubic spline. X-axis is the population growth factor, where values below 0 indicate a population decline and values above 0 indicate population growth (e.g. 100 represents a 2-fold increase). Y-axis is the expected change

in county GDP from 2000 to 2020 for a given value of population change, relative to no population change.

4.6.2 DTI Results

Select results for DTI are presented here, specifically for metropolitan areas (**Figure 4.4**). Generally, the relationship between changes in population and changes in DTI across all RUCs showed negative trends. This suggests that in growing areas, incomes are rising faster than debt levels, possibly due to economic growth, improved job opportunities, and an influx of financially stable residents. The latter may also suggest selective migration among individuals or families in better financial standing. Such trends indicate that population growth is often associated with economic vitality and improved financial health for residents. However, Northeast metro coastal areas exhibit a divergent trend, with DTI increasing alongside population growth. This unique pattern could be attributed to the exceptionally high cost of living in these desirable locations, where housing prices and other expenses may be outpacing income growth. These contrasting trends highlight the complex interactions between population dynamics, economic factors, and geographic characteristics in shaping financial outcomes across different regions.

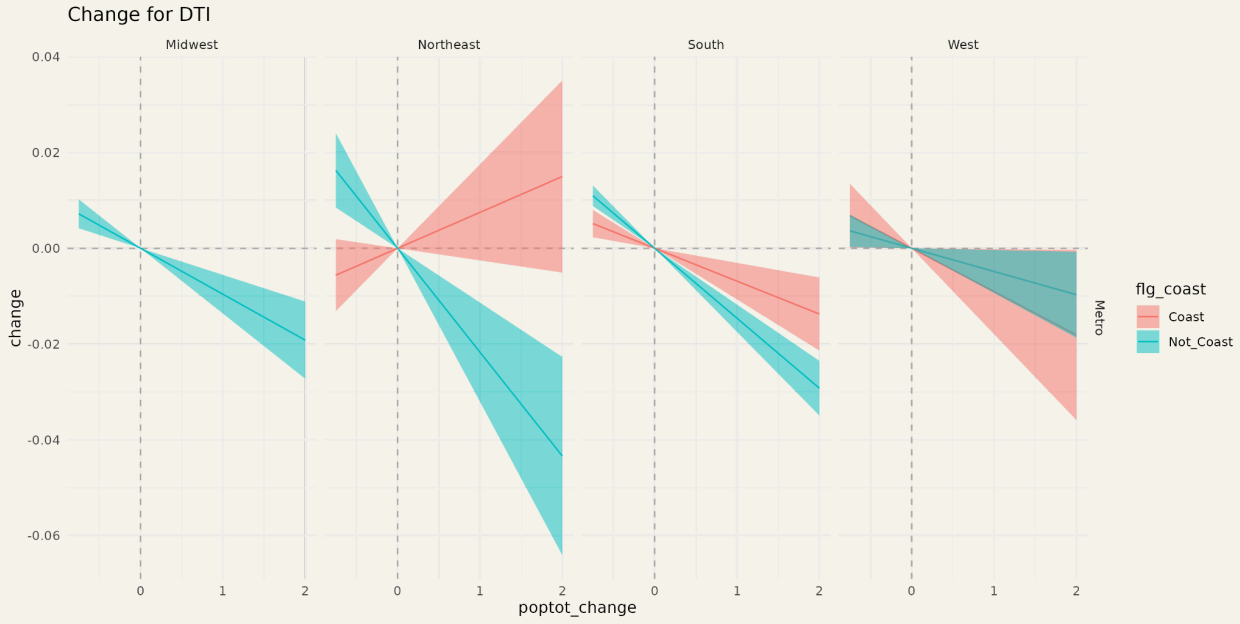

Figure 4.4 The relationship between population change and HPI for U.S. tracts from 2000 to 2020, analyzed separately across Region-Urbanicity-Coastline categories, for metropolitan areas specifically. Population change modeled using a cubic spline. X-axis is the population growth factor, where values below 0 indicate a population decline and values above 0 indicate population growth (e.g. 100 represents a 2-fold increase). Y-axis

is the expected change in DTI from 2000 to 2020 for a given value of population change, relative to no population change.

4.6.2 HPI Results

Results for HPI growth given population change were largely positive across RUCs, with non-metropolitan HPI showing more sensitivity to population growth (**Figure 4.5**). This suggests that while housing prices generally increase with population growth across all areas, non-metropolitan regions experience a more pronounced effect on housing prices even with smaller population increases. This heightened sensitivity in non-metro areas may be due to factors such as limited housing supply, less developed infrastructure to accommodate growth, or the relative scarcity of new residents compared to more populous urban areas. West non-metro areas showed some negative outcomes at high levels of population growth over 100%, but such levels of population growth are rarely expected from our combined model. In the West non-metro areas experiencing 50% population growth, HPI rose by 14.4 percentage points (95% CI: 8.75%, 19.99%). Moreso, in West non-coastal metro areas with 50% population gain, HPI rose by 19.88 percentage points (95% CI: 17.67%, 22.08%).

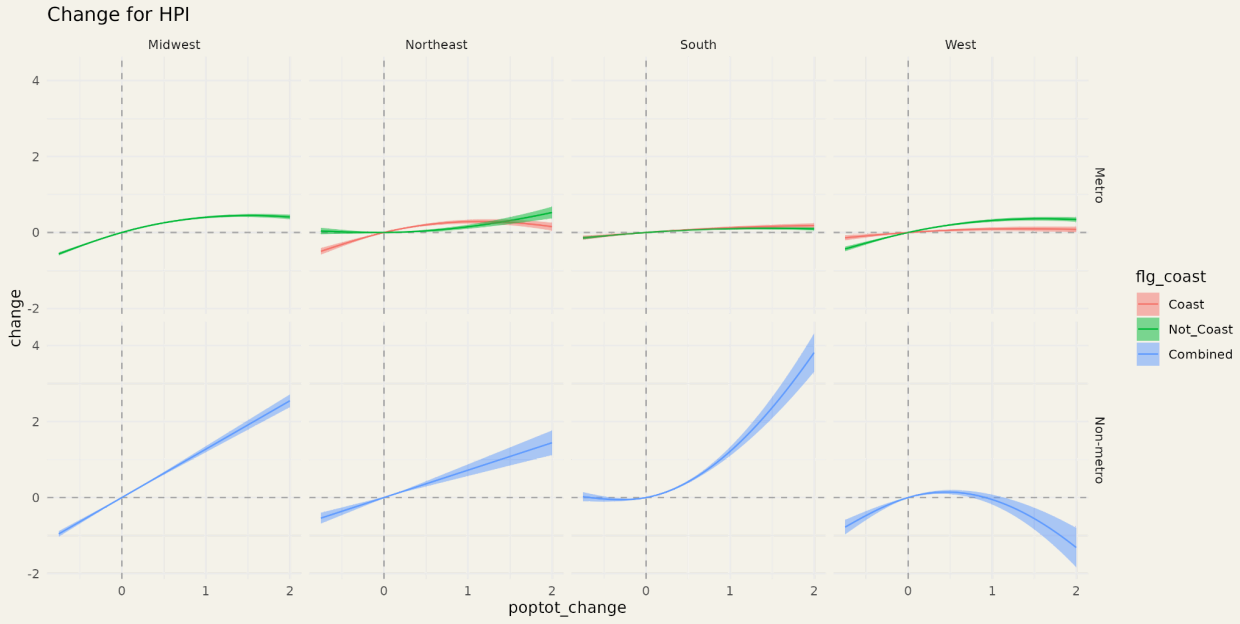

Figure 4.5 The relationship between population change and HPI for U.S. counties from 2000 to 2020, analyzed separately across Region-Urbanicity-Coastline categories. Population change modeled using a cubic spline. X-axis is the population growth factor, where values below 0 indicate a population decline and values above 0 indicate population growth (e.g. 100 represents a 2-fold increase). Y-axis is the expected change

in HPI from 2000 to 2020 for a given value of population change, relative to no population change.

5. Commercial Implications

5.1 Executive Summary

This analysis investigates the commercial implications of climate-induced demographic shifts, focusing on the relationship between changes in sectoral labor force composition and business outcomes across the contiguous U.S. The purpose of this analysis is to estimate the market impacts of shifting populations and resulting demographics spurred by climate exposure, to paint a comprehensive picture of the indirect impacts of climate risk to communities. The study evaluates five key commercial metrics: employment counts, establishment counts, payroll, revenue, and costs across most major North American Industry Classification System (NAICS) sectors. The methodology integrates various business statistics from federal sources in aggregate, interpolating and downscaling data as necessary to create a comprehensive dataset. Statistical analysis employs bivariate Generalized Additive Models (GAMs) for each sector and Rural-Urban-Coastline (RUC) continuum, similar to previous studies, but using industry labor force as the explanatory variable rather than population change. Key findings reveal generally positive relationships between changes in industry labor force share and commercial outcomes, with varying sensitivities across different RUCs, sectors, and outcome types.

5.2 Background

Downstream impacts of climate-induced migration may come in the form of impacts to businesses and industries located in areas with population inflows or outflows and shifting demographic characteristics. As the composition of a community changes, so too may its consumption patterns, labor force characteristics, and entrepreneurial activities (Liang et al., 2018; Goetz et al., 2010; Aguiar & Hurst, 2013), impacting overall commercial viability, including employment, payroll, business revenue, and business expenses. This analysis aims to explore the dynamic between demographic shifts and commercial impacts by modeling the implications of climate change-induced sectoral labor force changes, or professional migration, on relevant commercial outcomes across sectors.

Several studies have sought to explore the indirect impacts of climate migration on economic outcomes in the U.S. (Fan et al., 2018; Fan & Davlasheridze, 2019). These studies conclude that climate migration impacts the economic welfare of certain areas,

including changes in consumption patterns and wage rates. For instance, an influx of climate migrants from coastal areas to inland regions might alter local consumer demand and labor markets, while the loss of population in climate-vulnerable areas could lead to a shrinking tax base and reduced public services, potentially creating a feedback loop of further out-migration and economic decline (Hauer et al., 2019; Fan et al., 2018). Changes in age structure due to selective migration could affect local labor supplies and economic productivity differently across US regions (Maestas et al., 2016). Apart from climate-related impacts, evidence exists relating the impact of domestic professional migration within the U.S. on commercial viability. Several studies examine the impact of between-state migration on business dynamism or new business formation, finding associations between the migration of skilled workers and commercial activity (Baughn et al., 2012; Decker et al., 2016). Other studies assess trends in geographic mobility among professionals across sectors and differences across labor markets and occupation types (Choudhury, 2022; Reisinger, 2003, Molloy & Smith, 2019).

The findings from these studies suggest domestic migration may impact the commercial viability of an area, with differences existing across sectors. Findings from our demographic change analysis described above, further suggest that professional migration exists in the wake of population growth or decline. When coupled with climate-driven migration, climate conditions may dictate, to some extent, the flow of professional migration and thus commercial viability. Therefore, this analysis seeks to evaluate the historical relationship between climate-induced professional occupational migration and business outcomes, including employment counts, establishment counts, payroll, revenue and costs, across all major sectors and the contiguous U.S. (CONUS) from 2000 to 2020, using county-level Census data. Following a similar approach as was employed in the demographic change analysis, these relationships were evaluated along the Rural-Urban-Coastline (RUC) continuum to explore whether trends vary across geographic designations in the U.S.

5.3 Methodology

5.3.1 Data Inputs

Data on aggregate business statistics at the county- and state-level in CONUS were pulled from the U.S. Census Bureau's County Business Patterns (CBP) and Economic Census (ECN) as well as the U.S. Department of Agriculture's (USDA) Agricultural Census. The CBP is an annual program that compiles population data from the Business Registrar of all U.S. employer businesses across all NAICS sectors. Data gathered from this dataset included employment figures, number of establishments, and annual payroll, by North American Industry Classification System (NAICS) 2-digit sector and county from 1999 to 2021. **Table 5.1** presents a breakdown of all NAICS sectors. Data on business revenue and

expenditures were gathered from the ECN for 2017 at the state level, the highest resolution available, for all sectors except the agricultural sector (NAICS 11). The ECN is a survey of roughly 4.2 million employer and nonemployer businesses conducted every five years (specifically in years ending in "2" and "7"). Revenue and expenditure data for the agricultural sector was pulled from the Agricultural Census for 2017 at the county-level. The Agricultural Census provides detailed information on agricultural businesses in the U.S. and is similarly conducted every five years along the same years as the ECN.

Table 5.1 NAICS Sectors Included in Commercial Modeling.

Sector Name	NAICS Code
Agriculture, Forestry, Fishing and Hunting	11
Construction	23
Manufacturing	31-33
Wholesale Trade	42
Retail Trade	44-45
Transportation and Warehousing	48-49
Information	51
Finance and Insurance	52
Professional, Scientific, and Technical Services	54
Administrative and Support and Waste Management and Remediation Services	56
Educational Services	61
Health Care and Social Assistance	62

Arts, Entertainment, and Recreation	71
Accommodation and Food Services	72
Other Services (except Public Administration)	81

As data from the ECN and Agricultural Census was only pulled for 2017, macroeconomic indices from the Bureau of Labor Statistics (BLS) were extracted from the Major Sector Total Factor Productivity Metrics and used to interpolate a 20-year time series of business revenue and expenditures from 1999 to 2019 to link back to the CBP data. Specifically, an index of real sectoral output was used to proxy fluctuations in business revenue over time, and an index of total factor productivity was used to proxy trends in business expenditure. Both indices are normalized at the year 2017 (where 2017 = 100.0) and reflect national trends. Therefore, we assume these trends hold when being applied to state-level dynamics over the 20 years from from 1999 to 2019. Real sectoral output represents each sector's share of GDP for each year, thus illustrating the value of the goods and services it produced, making it an appropriate proxy for fluctuation in revenue. Total factor productivity is defined as the efficiency at which combined inputs, including labor, capital, energy, etc., are used to produce goods and services. Sectoral costs in these inputs are assumed to fluctuate along with their combined productivity at the national level.

In order to assess the relationships in the model at a higher resolution, the state time series of ECN business revenue and expenditures were downscaled to the county-level (corresponding to the CBP data) by using a simple county-to-state proportion. County-level estimates of agricultural business revenue and expenditures were already available through the Agricultural Census. The aggregate county annual payroll relative to aggregate state annual payroll was used to proxy the distribution of business revenue and expenditure estimates from the state- to the county-level. The intuition behind this choice lies in the assumption that businesses with higher payrolls typically have more employees or higher-paid staff, indicating larger-scale operations and higher overall expenditures. This thought process is further bolstered by the fact that labor costs comprise the vast majority of business expenditures in most sectors (Paycor, 2022). Therefore, a county’s share of overall state annual payroll is assumed to adequately downscale and redistribute the aggregate totals for business revenue and expenditure. Further, this approach was validated against available ECN county-level data for certain sectors and the differences between the predicted and actual values for those counties were insignificant. Data for all sectors, variables and years were merged into one file used in further manipulation to prep the data for modeling.

Data related to business metrics were pulled from public sources and manipulated, as described above, and served as dependent outcomes in the model. The independent variables driving the change in business outcomes were derived from the demographic change model, which captured the change in industry share of an area's labor force over the 20-year time period from 2000 to 2020 for each sector and at the tract-level. Data was merged at the county-level (the highest resolution at which business data was available) and expanded long to fill all the rows corresponding to tracts within that county. The RUCs described in Section 2.1 applied to the demographic change model were also merged in this process. The data was structured wide such that each row corresponded to a census tract and each column represented either a business outcome or sectoral labor share change.

5.3.2 Statistical Analysis

Estimating changes in commercial outcomes

In order to translate shifts in industry population shares to impacts on business outcomes, "change" metrics, or growth factors over time, were calculated for each commercial variable, calculated in a similar fashion as the change metrics used in the demographic change model. Change in employment counts, establishment counts, payroll, revenue, and business expenditure were estimated using a 20-year change ratio from 1999 to 2019, selecting years that wouldn't capture the impact of economic shocks, particularly over the COVID-19 pandemic, which resulted in unusual business patterns. The following formula illustrates the growth factor estimated for commercial outcomes from 1999 to 2019:

$$Commercial\ outcome\ growth\ factor\ (Change) = \left(\frac{Business\ outcome_{2019} - Business\ outcome_{1999}}{Business\ outcome_{1999}}\right) + 1$$

(Equation 5.1)

Thus, for each county and sector, corresponding growth factors in employment, number of establishments, payroll, revenue, and expenditure were estimated over the period from 1999 to 2019. When combined with the data inputs from the demographic change model at the census tract level, each sector-specific commercial outcome corresponded with a percentage point difference in industry share of an area's labor force over a similar 20-year period from from 2000 to 2020.

$$Industry\ labor\ force\ growth\ factor\ (Difference) = Industry\ Share_{2020} - Industry\ Share_{2000}$$

(Equation 5.2)

Bivariate modeling

Change metrics of business outcomes and industry population shares at the tract level were delineated into the 11 RUC continuums defined in Section 2.1 in order to explore regional variations, urbanicity differences, and coastal vs. non-coastal comparisons. Similar to preceding sections, bivariate GAMs are employed to evaluate the impact of growth factors in industry shares of the labor force on each commercial outcome variable interacted by each of the RUCs. The parameters and assumptions employed when using GAMs are described in Section 2.2.

Predictions about the outcome of commercial metrics from changes in industry share of the labor force are made using the fitted GAM model for each relationship. The values of industry labor share variables are expanded into a sequence of values within the 90% central range of each variable divided into 0.05 percentage point steps. The predicted commercial outcomes are mapped to each of the industry labor share values to estimate the predicted value of the outcomes along with their standard errors and resulting 95% confidence intervals. The resulting predictions produce conversion tables that translate percent changes in industry shares of the labor force into percent changes in commercial outcomes across revenue, expenditure, payroll, employment, and number of establishments for each sector and RUC.

5.4 Results

Results from the commercial implications model show that commercial outcomes and industry labor force generally share a positive relationship. While varying levels of sensitivity/magnitude to changes in the labor force exist across commercial outcomes in different RUCs, sectors, and outcome types, the average relationships across these variables are in a positive direction. This positive relationship is intuitive because a larger labor force often indicates growing demand for an industry's products or services. As more workers enter an industry, new businesses may form, leading to increases in establishments, employment, and revenue. We highlight some examples of the employment, expenditure and revenue curves for the Manufacturing industry (NAICS 31-33) below to illustrate these positive relationships across **Figures 5.2 - 5.4**.

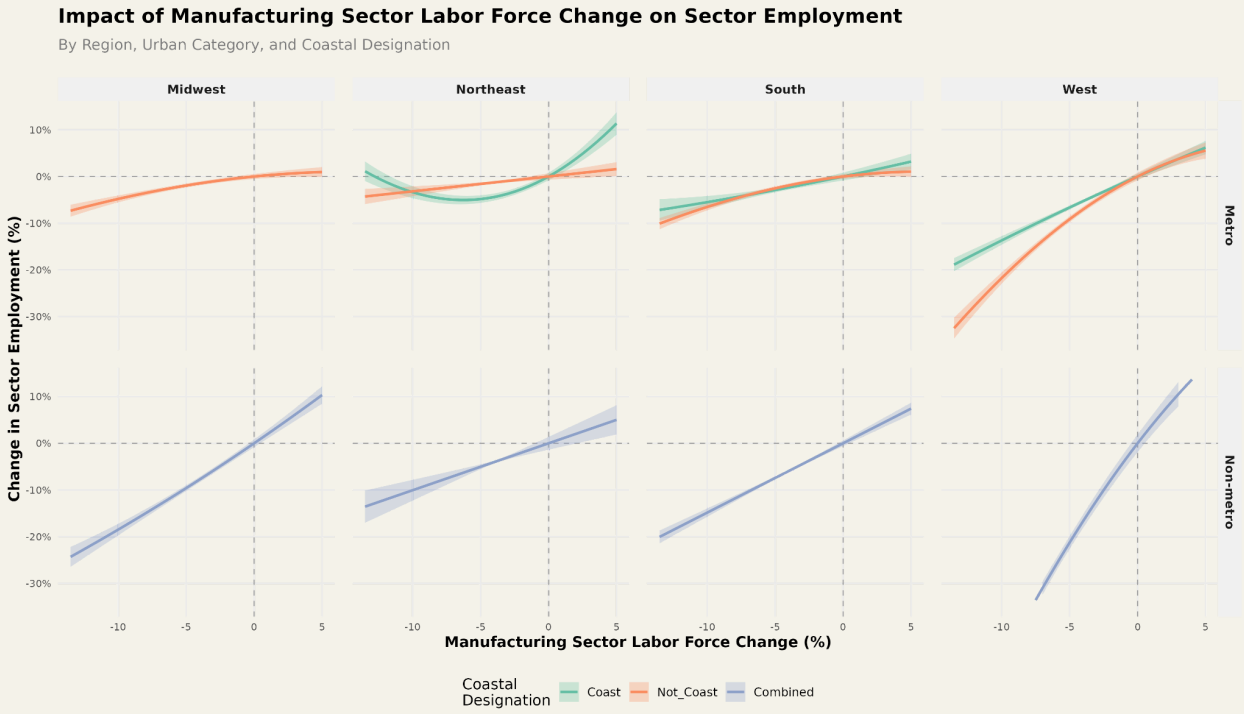

Figure 5.2 The relationship between share of the labor force represented by the manufacturing industry and the manufacturing industry's employment levels for US counties from 2000 to 2020, analyzed separately across Region-Urbanicity-Coastline categories. Population change modeled using a cubic spline. X-axis is the growth factor in the share of the labor force represented by the manufacturing industry, where values below 0 indicate a population decline and values above 0 indicate population growth (e.g. 100 represents a 2-fold increase). Y-axis is the expected change in the manufacturing industry's employment levels from 2000 to 2020 for a given value of population change, relative to no population change.

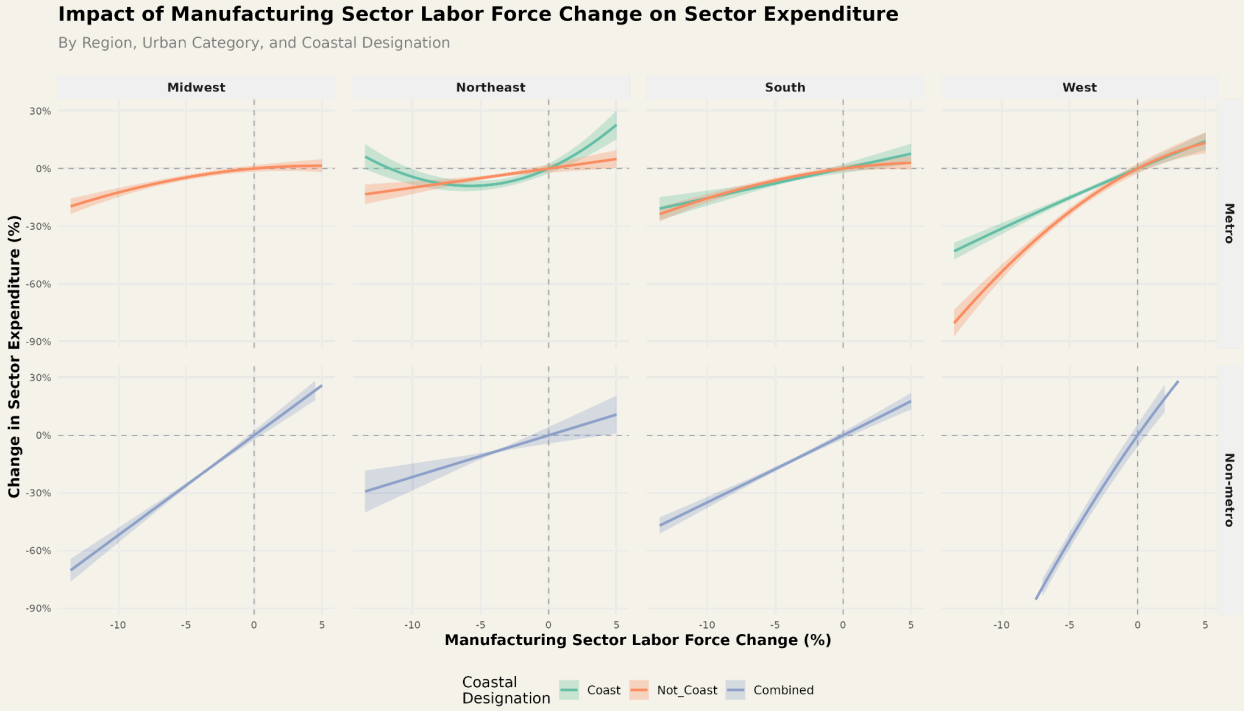

Figure 5.3 The relationship between share of the labor force represented by the manufacturing industry and the manufacturing industry's number of establishments for US counties from 2000 to 2020, analyzed separately across Region-Urbanicity-Coastline categories. Population change modeled using a cubic spline. X-axis is the growth factor in the share of the labor force represented by the manufacturing industry, where values below 0 indicate a population decline and values above 0 indicate population growth (e.g. 100 represents a 2-fold increase). Y-axis is the expected change in the manufacturing industry's number of establishments from 2000 to 2020 for a given value of population change, relative to no population change.

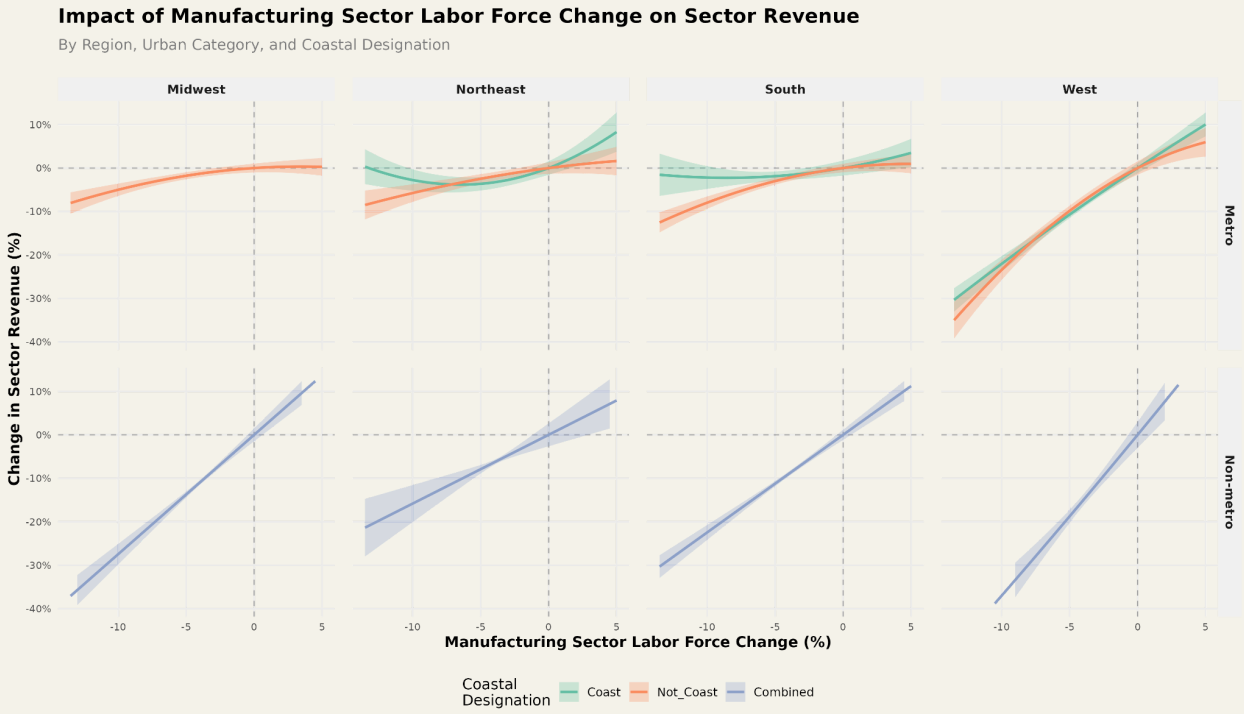

Figure 5.4 The relationship between share of the labor force represented by the manufacturing industry and the manufacturing industry's revenue for US counties from 2000 to 2020, analyzed separately across Region-Urbanicity-Coastline categories. Population change modeled using a cubic spline. X-axis is the growth factor in the share of the labor force represented by the manufacturing industry, where values below 0 indicate a population decline and values above 0 indicate population growth (e.g. 100 represents a 2-fold increase). Y-axis is the expected change in the manufacturing industry's revenue from 2000 to 2020 for a given value of population change, relative to no population change.

6. Property Value Change

6.1 Executive Summary

This analysis examines the impact of climate-induced population changes and direct hazard exposure on property values and tax revenues across the contiguous United States. The study has three main components:

1. Pre-Exposure Market Impacts: Investigates the relationship between historical population changes (2000-2020) and property value trends before climate hazard exposure using a generalized additive models (GAMs) applied within the Region-Urbanicity-Coastline (RUC) framework outlined in Section 2. This analysis provides insights into how population dynamics influence property markets across different geographic contexts.
2. Post-Exposure Hazard Impacts: Evaluates the effects of specific climate hazards (flood, tropical cyclone wind, and wildfire) on property transaction values over time using difference-in-differences estimators. This component assesses both short-term and long-term impacts of hazard events on property values.
3. Tax and Revenue Implications: Estimates potential changes in property tax revenues and overall local government finances resulting from flood-induced property value declines by applying elasticity of tax revenue to property sale prices.

By integrating high-resolution climate hazard data from First Street's models, property transaction records, historical population change estimates, and local government financial data, this methodology comprehensively assesses the implications climate change may have on property values and those implications on governments via tax revenue.

6.2 Background

Population changes have a significant impact on regional economic activity (Glaeser & Gottlieb, 2009; World Bank, 2020; Kline & Moretti, 2014). When the population in an area grows, it generally leads to an increase in demand for goods and services, which can stimulate economic activity and lead to job creation. This, in turn, can lead to further population growth as more people are attracted to the area due to the availability of jobs. On the other hand, a decrease in the population can have the opposite effect. As the number of people in an area decreases, there may be less demand for goods and services, leading to a decrease in economic activity and job losses. This can create a

downward spiral, as the loss of jobs can lead to more people leaving the area, which can further decrease the population and economic activity. If a city is unable to attract and retain residents, it may struggle to support businesses and provide essential services, which can have negative consequences for the local economy and quality of life. Directly connected, a slowing population can lead to declining property values, which can affect the city's tax base and ability to fund important services. On the other hand, increased property values also serve to reduce population growth, as discussed in urban economics and spatial equilibrium theory.

Property values are profoundly affected by various hazards such as flooding, tropical cyclone winds, and wildfires, each imparting unique and lasting consequences. Flooding, for example, can swiftly devalue properties in flood-prone areas due to the immediate risk and potential damage costs (Bin and Polasky, 2004). The financial burdens of repairs, elevated insurance premiums, and fears of recurrent damage deter potential buyers, resulting in decreased demand and depressed property prices (Crichton, 2008). Over time, repeated flooding events can stigmatize an area, prolonging the depreciation of property values amid negative media coverage and heightened public awareness (Tascón-González et.al, 2020).

Windstorms, including hurricanes and tornadoes, also pose substantial risks to property values. Properties in storm-prone regions face immediate devaluation following significant wind damage, as reconstruction costs rise and insurance premiums escalate (Michel-Kerjan and Kunreuther, 2011). The long-term impact includes the perception of heightened risk, potentially diminishing property desirability and market appeal over time (Hauer, 2019).

Similarly, wildfires can significantly impact property values, especially in fire-prone regions. Direct damage to properties from flames and smoke can lead to immediate declines in value due to repair costs and insurance implications (Nie, 2023). The enduring effects of fire risk can further erode property values as insurance premiums increase and market perception shifts, affecting broader real estate dynamics in these areas (O'Neill and Handmer, 2012).

Policy responses to these hazards, such as stricter building codes and zoning regulations, aim to mitigate risks but can increase construction costs and reduce property market attractiveness (O'Neill and Handmer, 2012). Higher insurance premiums and limited access to insurance coverage also contribute to decreased property values and market stability in hazard-prone regions (Kousky, 2010; Michel-Kerjan & Kunreuther, 2011).

Beyond financial impacts, these hazards disrupt local economies, displace residents, and damage infrastructure, which collectively diminish community appeal and property values (Bagstad et al., 2007). This comprehensive view underscores the profound and multifaceted effects of flooding, windstorms, and wildfires on property markets and community resilience, highlighting the critical interplay between environmental risks, economic development, and urban planning strategies.

6.3 Data Inputs

We integrate data on historic flood, tropical cyclone winds, wildfire exposure, and population enumeration with a series of indicators related to demographic conditions. Historic hazard exposure was accounted for using tract-level data from the sources detailed in Lai et al. (2022), and from the NOAA Storm Events Database. By leveraging these sources, we are able to construct a foundation for assessing climate-related risks at a high resolution for the Contiguous United States, while accounting for neighborhood exposures and their impact on property transactions.

The modeling procedures discussed below all took place at the property transaction level. However, it's essential to note that while certain data elements, such as historical flooding data, were aggregated at a higher level of geographic granularity, like the Census Tract, they were treated as "repeated measures" for all properties within the same higher-level unit. This approach ensures that the broader context of geographic regions and their historical flood exposure is considered when examining individual property transactions.

Property transaction values and property characteristics over time are provided through proprietary data from Lightbox. Residential properties are investigated in this analysis through limits set on the property-associated land use IDs. For residential properties, only transactions for properties that meet certain criteria are used in the analysis. The International Residential Code (IRC), which is the most widely adopted residential building code in the US, requires that all homes have at least one room with 70 square feet of habitable space (IRC, 2021). Additionally, to reduce noise from outliers as well as potential data errors, an upper limit of 6,000 square feet was chosen to represent the maximum size of a single-family residential property. As such, and as property values are operationalized as transaction price by square foot, any property records with under 70 square feet or over 6,000 square feet are removed from the sample. An additional limit for the number of units associated with a property is also added, with only properties kept that have 5 or fewer units reported.

Further processing was dependent on whether the sample is being used for pre- or post-exposure analysis, this being described in the sections below.

In order to understand the downstream implications of changing property values, local tax revenue data, including sources of that revenue, are provided through the US Census Bureau's State and Local Government Finance Survey (U.S. Census Bureau, 2023). These data provide sub-housing market indicators of the proportion of all local revenue directly tied to property valuation. The data further allow for an understanding of the elasticity of tax revenues in their relationships to shifting property values, as described below.

6.4 Pre-Exposure: Market Impacts on Property Values

For the purposes of this modeling effort, the interest is the relationship between pre-flood exposure property transactions and historical population change from 2000-2020. This allows for a comprehensive understanding of the impact of population change on property values, underscoring the impact of an area's amenities and/or disamenities.

6.4.1 Methods + Model

In order to find property value change across the pre-exposure period, greater than 2 transactions have had to occur at a unique property ID before any flood exposure in order to be included in the analysis. We also removed outlier $/sq.ft values by calculating the 1 and 99th percentile values and only keeping transactions that fit this criteria. The range of the values include from $22.10 to $497.30. After property transactions (4,347,828 of them) were grouped by property IDs, and distributed into categories across the Region-Urbanicity-Coastline (RUC) continuum, as described later, the number of unique properties included are 1,941,614.

6.4.2 Statistical Analysis

Tracts were included meeting the specified property level conditions, where the square footage had to be greater than 70 square feet and under 6,000 square feet. An additional limit for the number of units associated with a property is also added, with only properties kept that have 5 or fewer units reported. The number of included tracts in this analysis are 6,791, out of the total potential 72,200 tracts (or 9.4%). Distribution of tracts across Region-Urbanicity-Coastline categories are shown in **Table 6.1**.

Table 6.1. Distribution of tracts (N=6,791) and properties (N=1,941,614) across Region-Urbanicity-Coastline categories included in our analysis.

Region-Urbanicity-Coastline	Tracts	% of sample	Properties	% of sample

West, Metro, Coast	**133**	**1.96**	**66620**	**3.43**
West, Metro, Not_Coast	**437**	**6.43**	**196190**	**10.10**
West, Non-Metro, Combined	**91**	**1.34**	**20849**	**1.07**
Midwest, Metro, Not_Coast	**1516**	**22.3**	**402848**	**20.75**
Midwest, Non-Metro, Combined	**396**	**5.83**	**58071**	**3**
Northeast, Metro, Coast	**787**	**11.6**	**194498**	**10.02**
Northeast, Metro, Not_Coast	**1263**	**18.6**	**328376**	**16.91**
Northeast, Non-Metro, Combined	**260**	**3.83**	**43515**	**2.24**
South, Metro, Coast	**513**	**7.55**	**233776**	**12.04**
South, Metro, Not_Coast	**1112**	**16.4**	**349957**	**18.02**
South, Non-metro, Combined	**283**	**4.17**	**46914**	**2.42**

Transaction and Property Specific Ratios

To gain a holistic understanding of a property's value within a more granular area (tract) at the first transaction pre-exposure, a ratio is created such that:

$$FTR_{i,y} = \frac{PPSF_{i,y}}{PPSF_{j,y}} \quad \text{(Equation 6.1)}$$

Where:

$FTR_{i,y}$: $First\ Transaction\ Ratio\ at\ property\ i\ in\ year\ y$

$PPSF_{i,y}$: $Price\ per\ square\ foot\ at\ property\ i\ in\ year\ y$

$PPSF_{j,y}$: $Price\ per\ square\ foot\ at\ tract\ j\ in\ year\ y$

This same ratio is created for the last transaction pre-exposure, such that:

$$LTR_{i,y} = \frac{PPSF_{i,y}}{PPSF_{j,y}} \quad \text{(Equation 6.2)}$$

Where:

$LTR_{i,y}$: $Last\ Transaction\ Ratio\ at\ property\ i\ in\ year\ y$

$PPSF_{i,y}$: $Price\ per\ square\ foot\ at\ property\ i\ in\ year\ y$

$PPSF_{j,y}$: $Price\ per\ square\ foot\ at\ tract\ j\ in\ year\ y$

These two ratios are then used to calculate the relative percentage change in the transaction bounds at a property where,

$$Ratio\ Change\ \% = \frac{LTR_{i,y} - FTR_{i,y}}{FTR_{j,y}} \times 100 \quad \text{(Equation 6.2)}$$

Where:

$LTR_{i,y}$: $Last\ Transaction\ Ratio\ at\ property\ i\ in\ year\ y$

$FTR_{i,y}$: $First\ Transaction\ Ratio\ at\ property\ i\ in\ year\ y$

This metric, the Normalized Percentage Change in Property Value Ratio, ultimately describes the relative change from the first to the last transaction, accounting for changes in the average price per square foot over time in a properties specific spatial area (tract), and the real dollar value change of the price per square foot sales price at a specific property. It considers the ratio of the real sales price per square foot to the average price per square foot at both the earliest and latest transaction dates. This percentage change in this ratio is then used as a proxy for actual percentage change in property value.

Estimating Population Change

Population data for years 2000 and 2020 were collected and reconciled to comparable geographic units of 2010 tracts as discussed in the demographic change Section 3.3.2.

Consistent with the methods used in the demographic change analysis, population change is then expressed as a growth factor where:

$$Population\ Growth\ Factor\ (Change) = \left(\frac{Total\ population_{2020} - Total\ population_{2000}}{Total\ population_{2000}}\right) \quad \text{(Equation 6.3)}$$

Values below 0 indicate a decline in population and values above 0 indicate an increase in population.

Bivariate Modeling

Change metrics for property value and population at the tract level were delineated into the 11 RUC continuums as defined in Section 2.1 in order to explore regional variations, urbanicity differences, and coastal vs. non-coastal comparisons. Similar to proceeding sections, bivariate GAMs are employed to evaluate the impact of growth factors in population on property values interacted by each of the RUCs. The parameters and assumptions employed when using GAMs are described in Section 2.2. From each fitted GAM, we derived predicted values of HPI across the distribution of population change for each RUC. Predicted property value estimates were centered to a reference point of no population change and plotted along with their 95% confidence intervals (95% CIs). The resulting predictions produce conversion tables that translate changes in population into changes in property value for each RUC.

6.4.3 Results

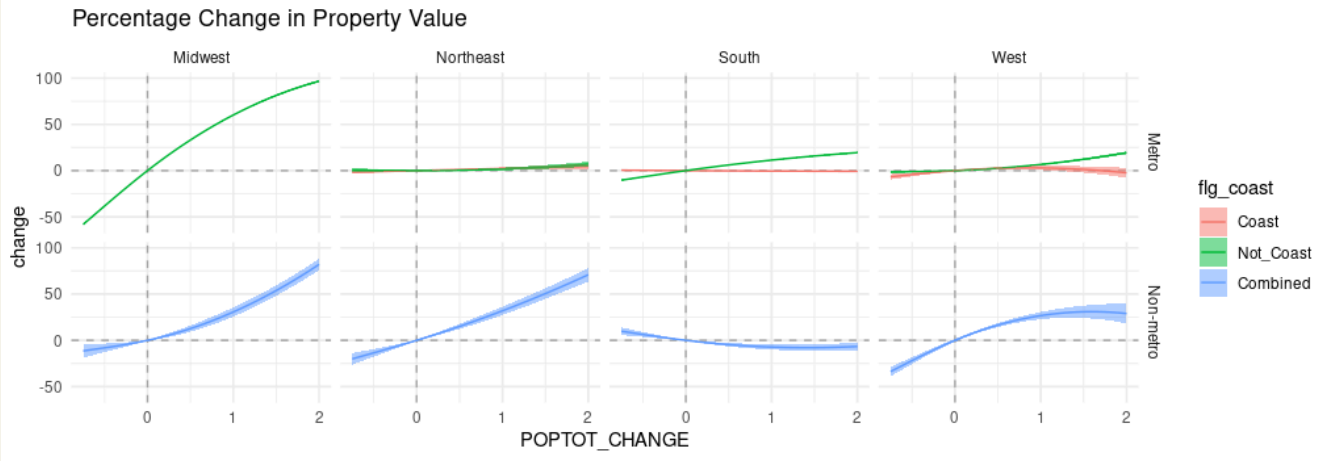

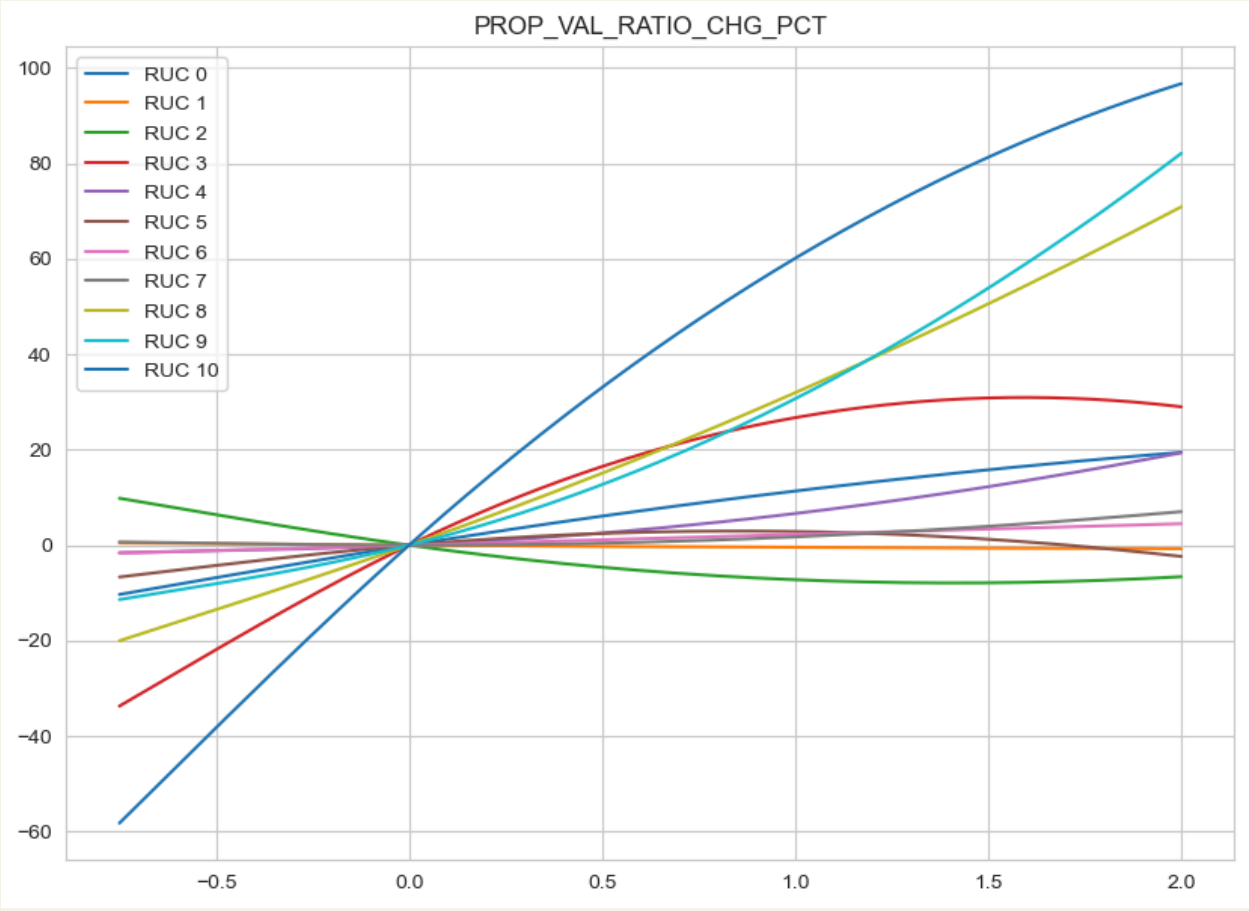

Figure 6.1. The relationship between population change and percentage change in property value across US census tracts from 2000 to 2020, analyzed separately across Region-Urbanicity-Coastline categories. Population change is modeled using a cubic

spline. X-axis is the population growth factor, where values below 1 indicate a population decline (e.g., 0.5 represents a 50% decline) and values above 1 indicate population growth (e.g., 2 represents a 2-fold increase). Y-axis is the expected percentage difference in property value from 2000 to 2020 for a given value of population change, relative to no population change.

We observed mainly positive relationships between population change and property value change from 2000 to 2020 (**Figure 6.1**). Tracts across the midwest and northeast had clear positive relationships, where population growth occurred so did the change in property value. For example, in the non-metro midwest areas that experienced a 50% population increase, the median property value increase was 12.7% (95%CI = 9.33%,16.05%), relative to no population change. In the south, there is a slight divergence in trend between the coast and not-coast categories, with the coast being close to no change given any level of population change. In the west, the non-coastal region has a strong positive relationship with population change, whereas the coastal region has a tipping point in areas that have increased population at or above 175% growth with the median property value increase at .002% (95%CI = -4.21%, 4.22%), with a slight decrease with higher levels of population growth.

Given the outputs from the Climate Migration Model that adjusts future SSP projections with their climate impact, within the confines of SSP2, the percentage change in property value is depicted in **Figure 6.2**. The overall property value change over the next 30 years can be projected to be in the -49.5% to 80.6% range. Since property value change was modeled at the RUC designation, the trends seen in **Figure 6.2** are directly as a result of the trend associated with the RUC presented in **Figure 6.1**. In areas with a strong positive relationship between population change and property value, like that seen in the midwest, a larger expected population decline at the tract level will result in a decline in property values in the region, as shown in **Figure 6.2**.

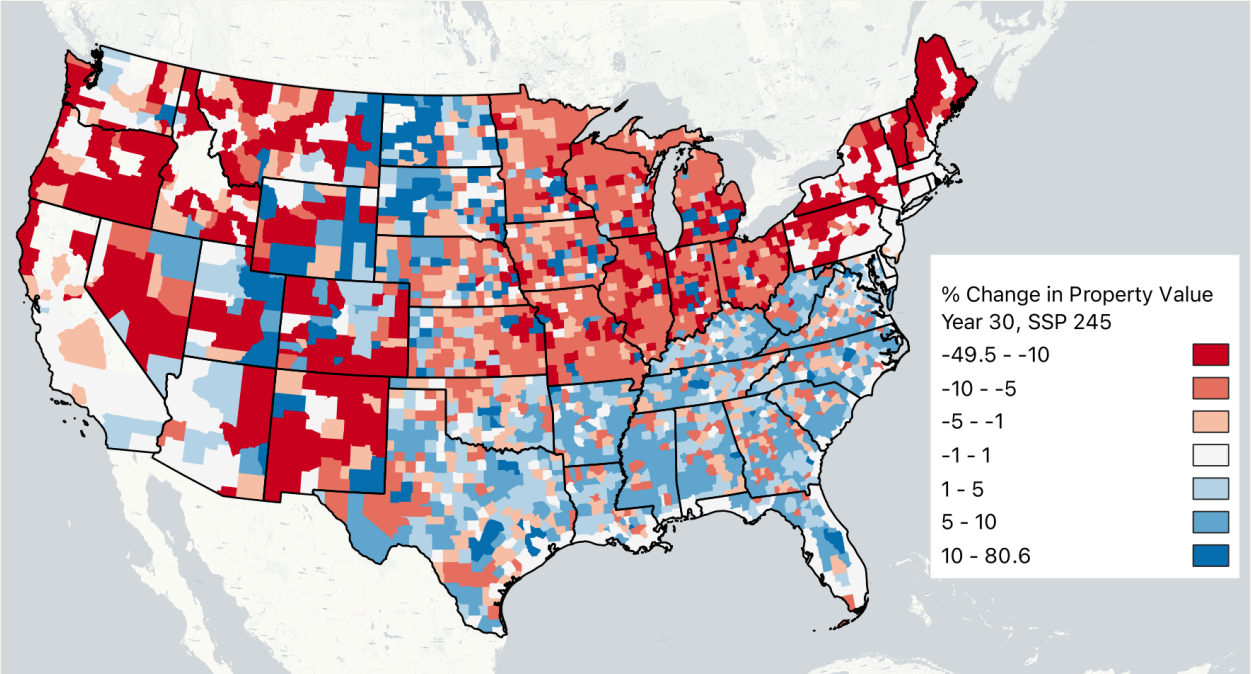

Figure 6.2. Map of the contiguous U.S. colored by expected percentage change in property value over the 2025-2055 time period across SSP 2-4.5.

6.5 Post-Exposure: Impact of Hazard Exposure on Property Values

For the purposes of this modeling effort, the interest is the relationship between pre- and post- hazard exposure property transactions for flood, tropical cyclone wind, and wildfire exposed properties. We also account for within tract population growth or decline as a potential bias factor, which allows for a comprehensive understanding of the hazard's impact on the trajectory of property values in these growth/decline communities once exposed.

6.5.1 Methods + Model

Pre-Exposure Migration. To assess how pre-exposure migration patterns impact the trajectory of property sale prices following a flood event, we begin by calculating the difference between the population counts in the 2010 and 2000 decennial censuses at the tract level. This calculation helps determine whether property transactions occur within census tracts experiencing population growth or decline. We then estimate separately equation (3) for properties located in growing and declining census tracts.

Main Estimand. We aim to understand how past exposure to hazards affects property transactions over time. In other words, we aim to estimate the average treatment effect

on the treated (ATT) of historic exposure on a property transaction, i, valuation dynamics, Y, for cohort, g, at event time $e \equiv t - g$, which is defined as:

$$\text{ATT}_{g,e} \equiv E\left[Y_{i,t+e}(g) - Y_{i,t+e}(\times) \mid G_i = g \right] \qquad \text{(Equation 6.4)}$$

Where, $E[\ \bullet\ ]$, is the expected value operator, $Y_{i,t+e}(g)$, is the observed outcome of interest for a *treated* property transaction, i, located within a census tract impacted by a hazard event, during event time, e. $Y_{i,t+e}(\times)$ is the observed outcome of interest for a *control* property transaction, i. Note that $\text{ATT}_{g,e}$ identifies the average treatment effect on the treated cohort, g, at event time $e \equiv t - g$, and we are interested in the ATT across treated cohorts for a given event time, i.e., ATT_e, which we obtain as the weighted mean of each $\text{ATT}_{g,e}$:

$$\text{ATT}_e \equiv \sum_g \varrho_{g,e}\, \text{ATT}_{g,e} \qquad \text{Where: } \varrho_{g,e} \equiv \frac{\sum_i 1\{G_i = g\}}{\sum_i 1\{G_i = -\times\}} \qquad \text{(Equation 6.5)}$$

$\sum_i 1\{G_i = g\}$ represents the number of properties in the cohort g, whereas, $\sum_i 1\{G_i = -\times\}$, is the number of properties that received treatment at one point in time. Thus, when aggregating $\text{ATT}_{g,e}$ to ATT_e, estimates from cohorts with a higher number of treated units will receive a higher weight.

Estimator. To identify the ATT_e, we rely on Sun and Abraham's (2021) generalized difference-in-differences event study estimator, which has as a unit of observation the property transaction, i, in the year, t, taking the following empirical form:

$$\ln(Y_{it}) = \alpha_0 + \sum_{g=0}^{G} \sum_{e=-7}^{12} \beta_g^e D_{it}^e + \lambda_i + \theta_t + e_{it} \qquad \text{(Equation 6.6)}$$

Where $ln(Y_{it})$ is the natural logarithm of outcome of the transaction, i, in the year, t. $D_{it}^{e} = 1\{t - \text{Cohort}_i = e\}$ is an event study dummy that takes the value of 1 if the unit is, e, periods away from the treatment (i.e., being located within a census tract impacted by a flood event) and 0 otherwise. Period $e = -1$ is the baseline. λ_i and θ_t are property and year/month fixed-effects, respectively. Property-level fixed effects control for all time-invariant characteristics of a property, whereas year/month fixed-effects control for year characteristics impacting the whole United States, such as economic shocks or consumer sentiment and for seasonal effects. Standard errors are clustered at the census tract level. To go from β_g^e to β^e, we use the weight, $\varrho_{g,e}$, defined in equation (2) for event time, e. The causal identifying assumption for $\beta^e = \text{ATT}_e$ is that outcomes within census tracts impacted by a hazard would have continued along the same trajectory without exposure. To formally test this assumption, we jointly test the null hypothesis: $\beta^{-7} = \ldots = \beta^{-2}$.

6.5.2 Results

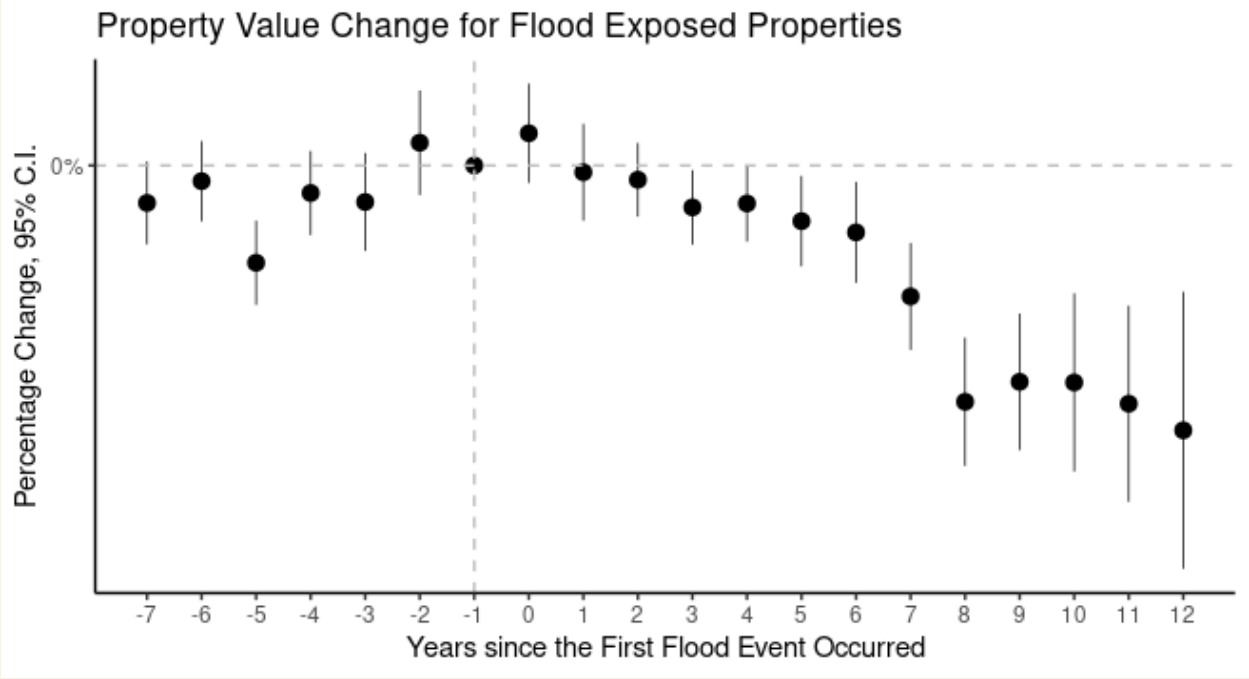

Figure 6.3. Flooding Events and Sale Prices per Square Feet: *Percentage Change Relative to Period, One Year Prior to Exposure (-1).*

Event	Years after Event	Lower Bound (%)	Median (%)	Upper Bound (%)
Flood	1	-3.3%	-0.4%	2.5%
Flood	5	-6.1%	-3.4%	-0.6%
Flood	10	-18.6%	-13.2%	-7.8%

Our analysis shows that following a flood event, properties within an impacted census tract sell at lower prices per square foot (**Figure 6.3**). The change in sale prices per square foot keeps decreasing as years pass. Five years after a flood event occurred, properties get sold at -3.4% less (95%CI: -6.1%, -0.6%) ($p < .0001$), relative to identical properties located within non-flooding census tracts, whereas, ten years after the flooding event occurred, the difference reaches -13.2% (95%CI: -18.6%, -7.8%) ($p < .0001$).

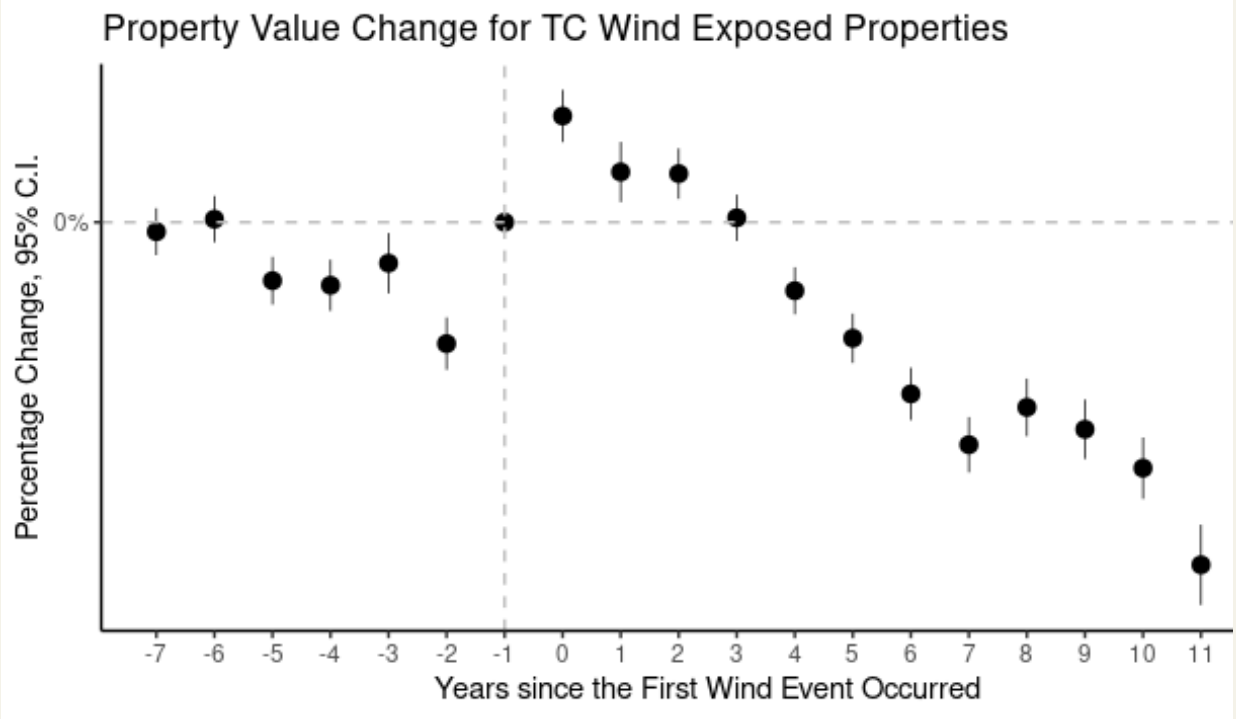

Figure 6.4. Tropical Cyclone Wind Events and Sale Prices per Square Feet: *Percentage Change Relative to Period, One Year Prior to Exposure (-1).*

Event	Years after Event	Lower Bound (%)	Median (%)	Upper Bound (%)
Wind	1	1.1%	2.7%	4.3%
Wind	5	-7.4%	-6.1%	-4.8%
Wind	10	-14.6%	-13.0%	-11.4%

Our analysis shows that following a tropical cyclone wind event, properties within an impacted census tract sell at lower prices per square foot (**Figure 6.4**). Five years after a TC wind event occurred, properties get sold at -6.1% less (95%CI: -7.4%, -4.8%) ($p < .0001$), relative to identical properties located within non-wind impacted census tracts, whereas, ten years after the TC wind event occurred, the difference reaches -13% (95%CI: -14.6%, -11.4%) ($p < .0001$).

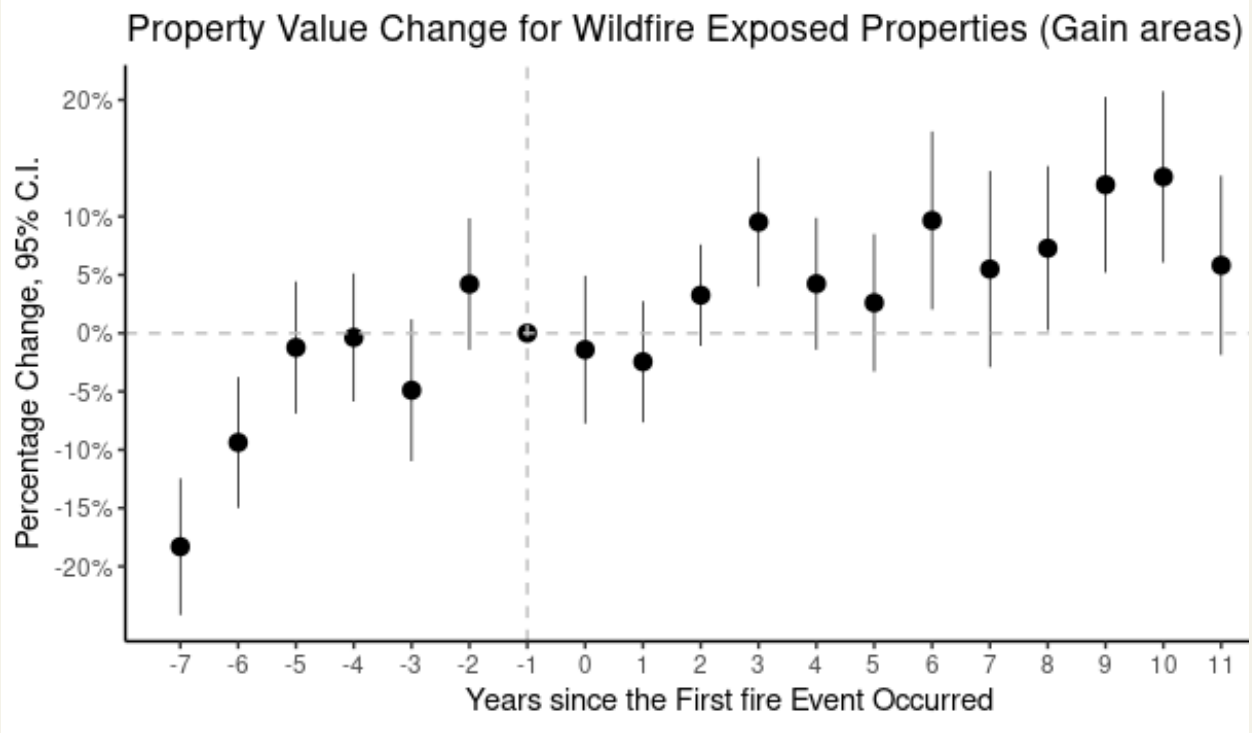

Figure 6.5. Wildfire Events (in historically gaining communities) and Sale Prices per Square Feet: *Percentage Change Relative to Period, One Year Prior to Exposure (-1).*

Event	Years after Event	Lower Bound (%)	Median (%)	Upper Bound (%)
Fire - Gain	1	-7.6%	-2.5%	2.7%
Fire - Gain	5	-3.3%	2.6%	8.5%
Fire - Gain	10	6.1%	13.4%	20.7%

Our analysis shows that following a wildfire event in areas that have historically gained population, properties are more resilient long-term and are sold at lower prices per square foot in the short-term (**Figure 6.5**). For example, one year after a wildfire, properties are sold at -2.5% less (95%CI: -7.6%, 2.7%), relative to identical properties in non-fire impacted census tracts. Although, in these historically growing communities, the amenities tend to overshadow some of the disamenities. Five years after a wildfire event occurred, properties get sold at 2.6% more (95%CI: -3.3%, 8.5%) ($p < .0001$), relative to identical properties located within non-wind impacted census tracts, whereas, ten years after the wildfire event occurred, the difference reaches 13.4% (95%CI: 6.1%, 20.7%) ($p < .0001$).

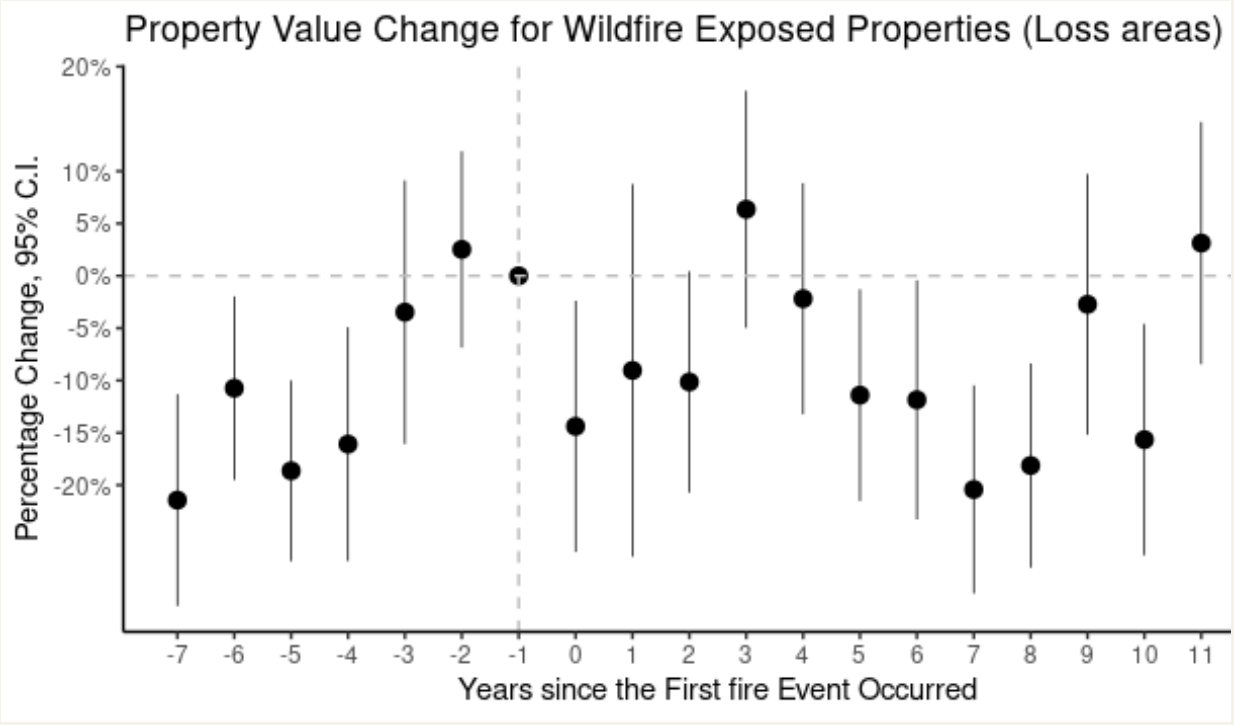

Figure 6.6. Wildfire Events (in historically abandoned communities) and Sale Prices per Square Feet: *Percentage Change Relative to Period, One Year Prior to Exposure (-1).*

Event	Years after	Lower Bound	Median (%)	Upper Bound

	Event	(%)		(%)
Fire - Loss	1	-26.8%	-9.0%	8.8%
Fire - Loss	5	-21.5%	-11.4%	-1.3%
Fire - Loss	10	-26.7%	-15.7%	-4.6%

Our analysis shows that following a wildfire event in areas that have historically lost population, properties are sold at lower prices per square foot over time (**Figure 6.6**). For example, one year after a wildfire, properties are sold at -9% less (95%CI: -26.8%, 8.8%), relative to identical properties in non-fire impacted census tracts. Five years after a wildfire event occurred, properties get sold at -11.4% less (95%CI: -21.5%, -1.3%) ($p < .0001$), relative to identical properties located within non-fire impacted census tracts, whereas, ten years after the wildfire event occurred, the difference reaches -15.7% (95%CI: -26.7%, -4.6%) ($p < .0001$).

6.6 Tax and Revenue Implications of Housing Price Declines from Flood Exposure

Flood events can also impact property taxes and, consequently, local revenues. When a region is hit by a flood, property values often experience a significant drop due to both the tangible damage to structures and the perceived risk of future flood events. This decrease in property values could lead to lower sale prices when these properties transact. As property tax assessments are typically based on properties' assessed value or sale price, municipalities may witness a substantial dip in their property tax collections post-flood. This revenue shortfall can pose challenges for local governments as they struggle to fund essential public services when the community's restoration and rebuilding demands peak.

6.6.1 Methods + Model

To evaluate the potential consequences of declining property values on property tax revenues following flood events, we operate under the assumption that either every property within a county is impacted by flooding or that there is a ripple effect on property values in a county due to properties affected by flooding. We then employ the following methodology to estimate the potential decrease in property tax revenues due to flooding events:

1. As we lack access to an annual nationwide historical parcel tax assessments database, we depend on aggregated county-level historical data concerning tax

collections and sale prices to estimate the elasticity of tax revenue in response to changes in sale prices, using the following empirical form:

$$ln(Y_{st}) = \alpha_0 + \xi_s ln(X_{st}) + \theta_t + e_{st} \quad \text{(Equation 6.7)}$$

- Where, $ln(Y_{st})$ and $ln(X_{st})$, are the natural logarithm of the mean sale price of residential properties and total property tax collection in state, s, during year, t, respectively. θ_t represents year fixed-effects. Standard errors are clustered at the county level. The coefficients of interest are, ξ_s, which tells us the elasticity of property tax revenue to sale price fluctuations for state, s. Running separate regressions for each state provides flexible elasticity measures specific to each state, helping to account for differences in tax policies, property tax rates, and assessment practices.

2. Using the estimated elasticity of tax revenue to sale prices, $\hat{\xi}_g$, from equation (4) and the impact of flood exposure on a property transaction, $\hat{\beta}^e$, from equation (3), we estimate the potential downfall, D_C, in annual property tax collection, PT_c, in county, c, from a flooding event as $D_C = \hat{\xi}_s \cdot \hat{\beta}^e \cdot PT_{Ct}$. To better understand the relative impact of a decline in property taxes, we present the potential downfalls as percentage decreases of both total tax collections and total revenues.

This is combined with the most current tax information from the U.S. Census' Annual Survey of State and Local Government Finances where the property taxes, total taxes, and total revenues are inflation adjusted based on their given entry year. The output presents real property taxes, real total taxes, and real total revenues for each county, as well as a percentage change decrease value for property taxes, total taxes, and total revenues as a result of flood exposure.

6.6.2 Results

Property tax change is presented as a single value across the nation (-13%), where total taxes and revenues are dynamic based on the county in question but have a maximum effect of 13% (**Figure 6.7 and 6.8**)

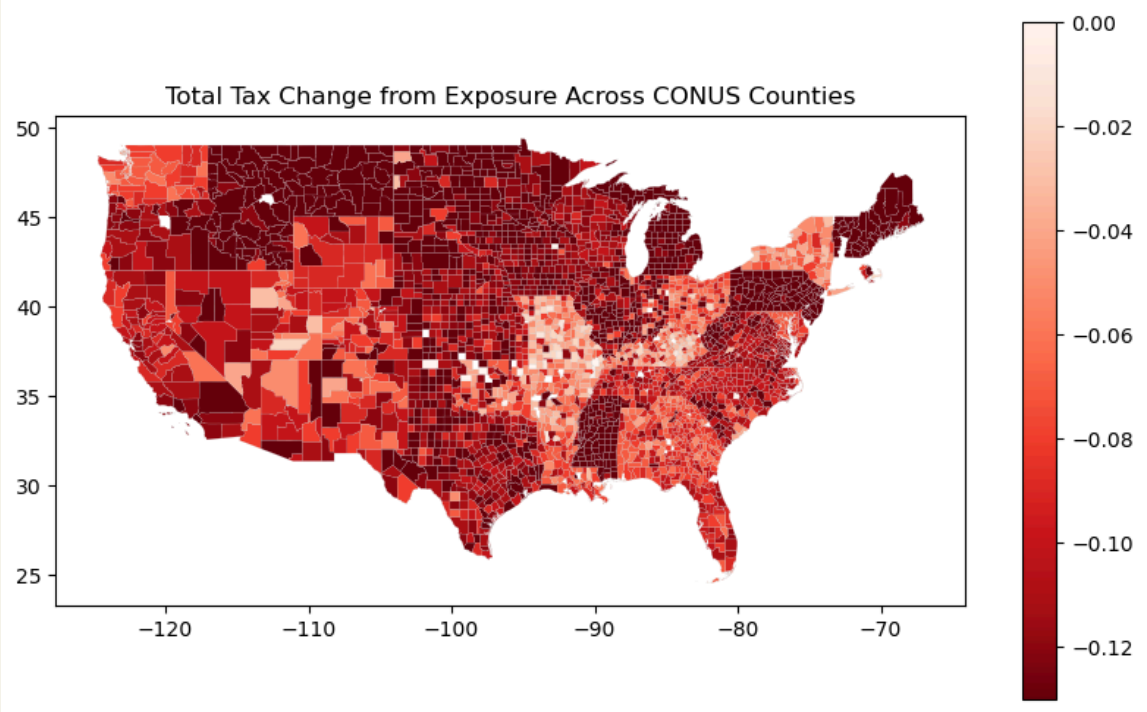

Figure 6.7 Expected Percentage Change in Total Taxes as a result of flood exposure to CONUS counties.

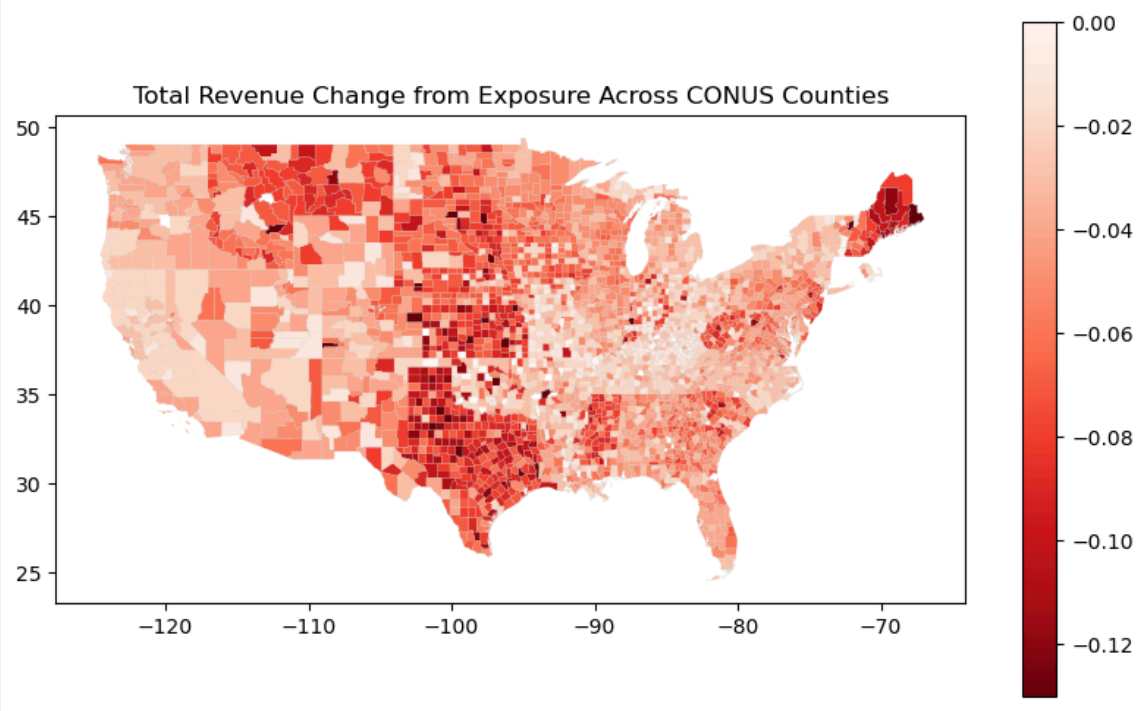

Figure 6.8 Expected Percentage Change in Total Revenues as a result of flood exposure to CONUS counties.

First Street

First Street

References

2021 International Residential Code (IRC) (no date). Available at: https://codes.iccsafe.org/content/IRC2021P2(Accessed: 4 August 2024).

Aguiar, M. and Hurst, E. (2013) 'Deconstructing Life Cycle Expenditure', *Journal of Political Economy*, 121(3), pp. 437–492. Available at: https://doi.org/10.1086/670740.

Ambinakudige, S. and Parisi, D. (2017) 'A Spatiotemporal Analysis of Inter-County Migration Patterns in the United States', *Applied Spatial Analysis and Policy*, 10(1), pp. 121–137. Available at: https://doi.org/10.1007/s12061-015-9171-1.

Bagstad, K.J., Stapleton, K. and D'Agostino, J.R. (2007) 'Taxes, subsidies, and insurance as drivers of United States coastal development', *Ecological Economics*, 63(2), pp. 285–298. Available at: https://doi.org/10.1016/j.ecolecon.2006.09.019.

Baughn, C.C., Neupert, K.E. and Sugheir, J.S. (2013) 'Domestic migration and new business creation in the United States', *Journal of Small Business & Entrepreneurship*, 26(1), pp. 1–14. Available at: https://doi.org/10.1080/08276331.2012.761799.

Beck, N. and Jackman, S. (1998) 'Beyond linearity by default: Generalized additive models', *American Journal of Political Science*, 42(2), pp. 596–627. Available at: https://doi.org/10.2307/2991772.

Bell, M. and Charles-Edwards, E. (2014) *Measuring Internal Migration around the Globe: A Comparative Analysis*. KNOMAD Working Paper 3. Global Knowledge Partnership on Migration and Development.

Best, K. *et al.* (2023) 'Demographics and risk of isolation due to sea level rise in the United States', *Nature Communications*, 14(1), p. 7904. Available at: https://doi.org/10.1038/s41467-023-43835-6.

Bin, O. and Polasky, S. (2004) 'Effects of Flood Hazards on Property Values: Evidence before and after Hurricane Floyd', *Land Economics*, 80(4), pp. 490–500. Available at: https://doi.org/10.2307/3655805.

Black, R. *et al.* (2011) 'Climate change: Migration as adaptation', *Nature*, 478(7370), pp. 447–449. Available at: https://doi.org/10.1038/478477a.

Choudhury, P. (Raj) (2022) 'Geographic Mobility, Immobility, and Geographic Flexibility: A Review and Agenda for Research on the Changing Geography of Work', *Academy of Management Annals*, 16(1), pp. 258–296. Available at: https://doi.org/10.5465/annals.2020.0242.

Clark, M.B., Nkonya, E. and Galford, G.L. (2022) 'Flocking to fire: How climate and natural hazards shape human migration across the United States', *Frontiers in Human Dynamics*, 4. Available at: https://doi.org/10.3389/fhumd.2022.886545.

Crichton, D. (2008) 'Role of Insurance in Reducing Flood Risk', *The Geneva Papers on Risk and Insurance - Issues and Practice*, 33(1), pp. 117–132. Available at: https://doi.org/10.1057/palgrave.gpp.2510151.

Davies, W.K.D. (1992) 'Berry, B.J.L. 1967: Geography of market centers and retail distribution. Englewood Cliffs, NJ: Prentice-Hall', *Progress in Human Geography*, 16(2), pp. 219–222. Available at: https://doi.org/10.1177/030913259201600204.

Decker, R.A. *et al.* (2016) 'Declining Business Dynamism: What We Know and the Way Forward', *American Economic Review*, 106(5), pp. 203–207. Available at: https://doi.org/10.1257/aer.p20161050.

Demyanyk, Y. *et al.* (2017) 'Moving to a Job: The Role of Home Equity, Debt, and Access to Credit', *American Economic Journal: Macroeconomics*, 9(2), pp. 149–181. Available at: https://doi.org/10.1257/mac.20130326.

de' Donato, F.K. *et al.* (2015) 'Changes in the Effect of Heat on Mortality in the Last 20 Years in Nine European Cities. Results from the PHASE Project', *International Journal of Environmental Research and Public Health*, 12(12), pp. 15567–15583. Available at: https://doi.org/10.3390/ijerph121215006.

Edward L. Glaeser, J.K. (2001) 'Consumer city', *Journal of Economic Geography*, 1(1), pp. 27–50.

EPA (2021) *Climate Change and Social Vulnerability in the United States: A focus on Six Impacts*. EPA 430-R-21-003. U.S. Environmental Protection Agency. Available at:

https://primarysources.brillonline.com/browse/climate-change-and-law-collection/climate-change-and-social-vulnerability-in-the-united-states-a-focus-on-six-impacts;cccc016620210513(Accessed: 30 July 2024).

Erol, I. and Unal, U. (2023) 'Internal migration and house prices in Australia', *Regional Studies*, 57(7), pp. 1207–1222. Available at: https://doi.org/10.1080/00343404.2022.2106363.

Fan, Q. and Davlasheridze, M. (2019) 'Economic impacts of migration and brain drain after major catastrophe: the case of hurricane katrina', *Climate Change Economics*, 10(01), p. 1950004. Available at: https://doi.org/10.1142/S2010007819500040.

Fan, Q., Fisher-Vanden, K. and Klaiber, H.A. (2018) 'Climate Change, Migration, and Regional Economic Impacts in the United States', *Journal of the Association of Environmental and Resource Economists*, 5(3), pp. 643–671. Available at: https://doi.org/10.1086/697168.

Flood Insurance Protects You All Year Long | FEMA.gov (2024). Available at: https://www.fema.gov/fact-sheet/flood-insurance-protects-you-all-year-long (Accessed: 14 July 2024).

Fothergill, A., Maestas, E.G.M. and Darlington, J.D. (1999) 'Race, Ethnicity and Disasters in the United States: A Review of the Literature', *Disasters*, 23(2), pp. 156–173. Available at: https://doi.org/10.1111/1467-7717.00111.

Fulford, S.L. and Schuh, S. (no date) 'Consumer revolving credit and debt over the life-cycle and business cycle'.

Fussell, E., Sastry, N. and VanLandingham, M. (2010) 'Race, socioeconomic status, and return migration to New Orleans after Hurricane Katrina', *Population and Environment*, 31(1), pp. 20–42. Available at: https://doi.org/10.1007/s11111-009-0092-2.

Glaeser, E.L. and Gottlieb, J.D. (2009) 'The Wealth of Cities: Agglomeration Economies and Spatial Equilibrium in the United States', *Journal of Economic Literature*, 47(4), pp. 983–1028. Available at: https://doi.org/10.1257/jel.47.4.983.

Goetz, S.J. *et al.* (2010) 'U.S. commuting networks and economic growth: Measurement and implications for spatial policy', *Growth and Change*, 41(2), pp. 276–302. Available at: https://doi.org/10.1111/j.1468-2257.2010.00527.x.

Gosnell, H. and Abrams, J. (2011) 'Amenity migration: diverse conceptualizations of drivers, socioeconomic dimensions, and emerging challenges', *GeoJournal*, 76(4), pp. 303–322. Available at: https://doi.org/10.1007/s10708-009-9295-4.

Gourevitch, J.D. *et al.* (2023) 'Unpriced climate risk and the potential consequences of overvaluation in US housing markets', *Nature Climate Change*, 13(3), pp. 250–257. Available at: https://doi.org/10.1038/s41558-023-01594-8.

Hallegatte, S. *et al.* (no date) *Unbreakable : building the resilience of the poor in the face of natural disasters*. World Bank Group. Available at: http://documents.worldbank.org/curated/en/512241480487839624/Unbreakable-building-the-resilience-of-the-poor-in-the-face-of-natural-disasters.

Hauer, M.E. (2017) 'Migration induced by sea-level rise could reshape the US population landscape', *Nature Climate Change*, 7(5), pp. 321–325. Available at: https://doi.org/10.1038/nclimate3271.

Hauer, M.E. (2019) 'Population projections for U.S. counties by age, sex, and race controlled to shared socioeconomic pathway', *Scientific Data*, 6(1), p. 190005. Available at: https://doi.org/10.1038/sdata.2019.5.

Hauer, M.E. *et al.* (2020) 'Sea-level rise and human migration', *Nature Reviews Earth & Environment*, 1(1), pp. 28–39. Available at: https://doi.org/10.1038/s43017-019-0002-9.

Hauer, M.E. *et al.* (2021) 'Assessing population exposure to coastal flooding due to sea level rise', *Nature Communications*, 12(1), p. 6900. Available at: https://doi.org/10.1038/s41467-021-27260-1.

Hauer, M.E., Evans, J.M. and Mishra, D.R. (2016) 'Millions projected to be at risk from sea-level rise in the continental United States', *Nature Climate Change*, 6(7), pp. 691–695. Available at: https://doi.org/10.1038/nclimate2961.

Hauer, M.E., Jacobs, S.A. and Kulp, S.A. (2024) 'Climate migration amplifies demographic change and population aging', *Proceedings of the National Academy of Sciences of the*

United States of America, 121(3), p. e2206192119. Available at: https://doi.org/10.1073/pnas.2206192119.

Hoegh-Guldberg, O. *et al.* (2018) 'Impacts of 1.5°C of Global Warming on Natural and Human Systems', in *Global Warming of 1.5°C. An IPCC Special Report on the impacts of global warming of 1.5°C above pre-industrial levels and related global greenhouse gas emission pathways, in the context of strengthening the global response to the threat of climate change, sustainable development, and efforts to eradicate poverty*.

IDMC (2021) *2021 Global Report on Internal Displacement*. Internal Displacement Monitoring Centre.

Jeremy Porter (2023) *Climate Abandonment Areas*. First Street. Available at: https://firststreet.org/research-library/climate-abandonment-areas (Accessed: 14 July 2024).

Johnson, K. and Cromartie, J. (2006) 'The Rural Rebound and Its Aftermath: Changing Demographic Dynamics and Regional Contrasts', in *Population change and rural society*. Springer, pp. 25–49. Available at: https://scholars.unh.edu/soc_facpub/65.

Johnson, K., Winkler, R. and Rogers, L. (2013) 'Age and lifecycle patterns driving U.S. migration shifts', *Carsey School of Public Policy* [Preprint]. Available at: https://dx.doi.org/10.34051/p/2020.192.

Johnson, K.M. *et al.* (2005) 'Temporal and spatial variation in age-specific net migration in the United States', *Demography*, 42(4), pp. 791–812. Available at: https://doi.org/10.1353/dem.2005.0033.

Johnson, K.M. and Lichter, D.T. (2019) 'Rural Depopulation: Growth and Decline Processes over the Past Century', *Rural Sociology*, 84(1), pp. 3–27. Available at: https://doi.org/10.1111/ruso.12266.

Kaczan, D.J. and Orgill-Meyer, J. (2020) 'The impact of climate change on migration: a synthesis of recent empirical insights', *Climatic Change*, 158(3), pp. 281–300. Available at: https://doi.org/10.1007/s10584-019-02560-0.

Kearns, E.J. *et al.* (2022) 'The Construction of Probabilistic Wildfire Risk Estimates for Individual Real Estate Parcels for the Contiguous United States', *Fire*, 5(4), p. 117. Available at: https://doi.org/10.3390/fire5040117.

Keenan, J.M., Hill, T. and Gumber, A. (2018) 'Climate gentrification: from theory to empiricism in Miami-Dade County, Florida', *Environmental Research Letters*, 13(5), p. 054001. Available at: https://doi.org/10.1088/1748-9326/aabb32.

Kenneth M. Johnson and Calvin L. Beale (2002) *Nonmetro Recreation Counties: Their Identification and Rapid Growth*. Volume 17, Issue 4. USDA ERS. Available at: https://www.ers.usda.gov/webdocs/publications/46984/19347_ra174b_1_.pdf?v=0.

Kline, P. and Moretti, E. (2014) 'People, Places, and Public Policy: Some Simple Welfare Economics of Local Economic Development Programs', *Annual Review of Economics*, 6(1), pp. 629–662. Available at: https://doi.org/10.1146/annurev-economics-080213-041024.

Kousky, C. (2010) 'Learning from Extreme Events: Risk Perceptions after the Flood', *Land Economics*, 86(3), pp. 395–422. Available at: https://doi.org/10.3368/le.86.3.395.

Kousky, C. and Shabman, L. (2015) *Understanding Flood Risk Decisionmaking: Implications for Flood Risk Communication Program Design*. SSRN Scholarly Paper 2561374. Resources for the Future. Available at: https://papers.ssrn.com/abstract=2561374 (Accessed: 30 July 2024).

Liang, J., Wang, H. and Lazear, E.P. (2018) 'Demographics and Entrepreneurship', *Journal of Political Economy*, 126(S1), pp. S140–S196. Available at: https://doi.org/10.1086/698750.

Lichter, D.T. and Johnson, K.M. (2023) 'Urbanization and the Paradox of Rural Population Decline: Racial and Regional Variation', *Socius*, 9, p. 23780231221149896. Available at: https://doi.org/10.1177/23780231221149896.

Linden, S.L. van der *et al.* (2015) 'The Scientific Consensus on Climate Change as a Gateway Belief: Experimental Evidence', *PLOS ONE*, 10(2), p. e0118489. Available at: https://doi.org/10.1371/journal.pone.0118489.

Maestas, N., Mullen, K. and Powell, D. (2016) *The Effect of Population Aging on Economic Growth, the Labor Force and Productivity*. w22452. Cambridge, MA: National Bureau of Economic Research, p. w22452. Available at: https://doi.org/10.3386/w22452.

McAlpine, S.A. and Porter, J.R. (2018) 'Estimating Recent Local Impacts of Sea-Level Rise on Current Real-Estate Losses: A Housing Market Case Study in Miami-Dade, Florida', *Population Research and Policy Review*, 37(6), pp. 871–895. Available at: https://doi.org/10.1007/s11113-018-9473-5.

McGranahan, D. (1999) *Natural Amenities Drive Rural Population Change*. Agricultural Economic Report No. (AER-781). USDA ERS, p. 27. Available at: http://www.ers.usda.gov/publications/pub-details/?pubid=41048 (Accessed: 14 July 2024).

McLeman, R. and Smit, B. (2006) 'Migration as an Adaptation to Climate Change', *Climatic Change*, 76(1), pp. 31–53. Available at: https://doi.org/10.1007/s10584-005-9000-7.

Michel-Kerjan, E. and Kunreuther, H. (2011) 'Redesigning Flood Insurance', *Science*, 333(6041), pp. 408–409. Available at: https://doi.org/10.1126/science.1202616.

Modigliani, F. and Brumberg, R. (1955) 'Utility analysis and the consumption function: An interpretation of cross-section data', *Post-Keynesian economics* [Preprint].

Molloy, R., Smith, C.L. and Wozniak, A. (2011) 'Internal Migration in the United States'. Available at: https://www.federalreserve.gov/econres/feds/internal-migration-in-the-united-states.htm (Accessed: 29 July 2024).

Mussa, A., Nwaogu, U.G. and Pozo, S. (2017) 'Immigration and housing: A spatial econometric analysis', *Journal of Housing Economics*, 35, pp. 13–25. Available at: https://doi.org/10.1016/j.jhe.2017.01.002.

Myers, N. (2002) 'Environmental refugees: a growing phenomenon of the 21st century.', *Philosophical Transactions of the Royal Society B: Biological Sciences*, 357(1420), pp. 609–613. Available at: https://doi.org/10.1098/rstb.2001.0953.

Nawrotzki, R.J. *et al.* (2014) 'Wildfire-Migration Dynamics: Lessons from Colorado's Fourmile Canyon Fire', *Society & natural resources*, 27(2), pp. 215–225. Available at: https://doi.org/10.1080/08941920.2013.842275.

Nie, X. *et al.* (2023) 'Perception of Increasing Wildfire Risk Lowers Appreciation of Residential Real Estate in California'. Available at: https://doi.org/10.2139/ssrn.4540783.

O'Neill, B.C. *et al.* (2014) 'A new scenario framework for climate change research: the concept of shared socioeconomic pathways', *Climatic Change*, 122(3), pp. 387–400. Available at: https://doi.org/10.1007/s10584-013-0905-2.

O'Neill, S.J. and Handmer, J. (2012) 'Responding to bushfire risk: the need for transformative adaptation', *Environmental Research Letters*, 7(1), p. 014018. Available at: https://doi.org/10.1088/1748-9326/7/1/014018.

Pörtner, H.-O. *et al.* (eds) (2022) *Climate Change 2022: Impacts, Adaptation and Vulnerability. Contribution of Working Group II to the Sixth Assessment Report of the Intergovernmental Panel on Climate Change.*

Raker, E.J. (2020) 'Natural Hazards, Disasters, and Demographic Change: The Case of Severe Tornadoes in the United States, 1980–2010', *Demography*, 57(2), pp. 653–674. Available at: https://doi.org/10.1007/s13524-020-00862-y.

Rappaport, J. (2007) 'Moving to nice weather', *Regional Science and Urban Economics*, 37(3), pp. 375–398. Available at: https://doi.org/10.1016/j.regsciurbeco.2006.11.004.

Reisinger, M.E. (2003) 'Sectoral Shifts and Occupational Migration in the United States', *The Professional Geographer*, 55(3), pp. 383–395. Available at: https://doi.org/10.1111/0033-0124.5503014.

Rickman, D.S. and Wang, H. (2017) 'US regional population growth 2000–2010: Natural amenities or urban agglomeration?', *Papers in Regional Science*, 96(S1), pp. S69–S90. Available at: https://doi.org/10.1111/pirs.12177.

Roback, J. (1982) 'Wages, Rents, and the Quality of Life', *Journal of Political Economy*, 90(6), pp. 1257–1278.

Robinson, C., Dilkina, B. and Moreno-Cruz, J. (2020) 'Modeling migration patterns in the USA under sea level rise', *PLOS ONE*, 15(1), p. e0227436. Available at: https://doi.org/10.1371/journal.pone.0227436.

Saiz, A. (2007) 'Immigration and housing rents in American cities', *Journal of Urban Economics*, 61(2), pp. 345–371. Available at: https://doi.org/10.1016/j.jue.2006.07.004.

Shu, E.G. *et al.* (2022) 'The Economic Impact of Flood Zone Designations on Residential Property Valuation in Miami-Dade County', *Journal of Risk and Financial Management*, 15(10), p. 434. Available at: https://doi.org/10.3390/jrfm15100434.

Shu, E.G. *et al.* (2023) 'Integrating climate change induced flood risk into future population projections', *Nature Communications*, 14(1), p. 7870. Available at: https://doi.org/10.1038/s41467-023-43493-8.

Smith, A. (2019) '2018's Billion Dollar Disasters in Context | NOAA Climate.gov', 2 July. Available at: http://www.climate.gov/news-features/blogs/beyond-data/2018s-billion-dollar-disasters-context (Accessed: 30 July 2024).

Solow, R.M. (1956) 'A Contribution to the Theory of Economic Growth', *The Quarterly Journal of Economics*, 70(1), pp. 65–94. Available at: https://doi.org/10.2307/1884513.

Swan, T.W. (1956) 'ECONOMIC GROWTH and CAPITAL ACCUMULATION', *Economic Record*, 32(2), pp. 334–361. Available at: https://doi.org/10.1111/j.1475-4932.1956.tb00434.x.

Tascón-González, L. *et al.* (2020) 'Social Vulnerability Assessment for Flood Risk Analysis', *Water*, 12(2), p. 558. Available at: https://doi.org/10.3390/w12020558.

The Biggest Cost of Doing Business: A Closer Look at Labor Costs (no date) *Paycor*. Available at: https://www.paycor.com/resource-center/articles/closer-look-at-labor-costs/ (Accessed: 29 July 2024).

The Precipitation Problem (2023). First Street. Available at: https://firststreet.org/research-library/the-precipitation-problem.

'U.S. Billion-Dollar Weather and Climate Disasters' (2024). NOAA National Centers for Environmental Information. Available at: https://doi.org/10.25921/STKW-7W73.

U.S. Census Bureau. (2023) *Annual Survey of State and Local Government Finances*, *Census.gov*. Available at: https://www.census.gov/programs-surveys/gov-finances.html (Accessed: 4 August 2024).

USDA ERS (no date) 'Rural-Urban Continuum Codes'. Available at: https://www.ers.usda.gov/data-products/rural-urban-continuum-codes/ (Accessed: 14 July 2024).

van Vuuren, D.P. *et al.* (2011) 'A special issue on the RCPs', *Climatic Change*, 109(1), p. 1. Available at: https://doi.org/10.1007/s10584-011-0157-y.

Wilson, B. *et al.* (2022) 'High-Resolution Estimation of Monthly Air Temperature from Joint Modeling of In Situ Measurements and Gridded Temperature Data', *Climate*, 10(3), p. 47. Available at: https://doi.org/10.3390/cli10030047.

Winkler, R.L., Winkler, R.L. and Johnson, K.M. (2015) 'Migration signatures across the decades: Net migration by age in U.S. counties, 1950-2010', *Demographic Research*, 32, pp. 1065–1080. Available at: https://doi.org/10.4054/DemRes.2015.32.38.

World Bank (2020) *World Development Report 2020: Trading for Development in the Age of Global Value Chains*. Washington, DC: World Bank. Available at: https://doi.org/10.1596/978-1-4648-1457-0.

Xu, A. (2020) 'Changing faces, changing places: understanding immigration, housing market and native out-migration in established and new destinations in the United States.', *The University of Louisville's Institutional Repository* [Preprint]. Available at: https://doi.org/10.18297/etd/3577.

First Street

Appendix

Appendix Table 1. List of Variable Outputs Across Macroeconomic Implications Models

Variable	Granularity of Outputs	Unit of Outputs
Climate Migration Model		
Flood Impact in Population	block group	count, %
Wind Impact on Population	block group	count, %
Smoke Impact on Population	block group	count, %
Wildfire Impact on Population	block group	count, %
Heatwave Impact on Population	block group	count, %
Drought Impact on Population	block group	count, %
Climate-Adjusted Future Population (SSP's 1-5)	block group	count, %
Demographic Characteristics		
White Population Share	block group	%
Black Population Share	block group	%
Asian Population Share	block group	%
Hispanic Population Share	block group	%
"Other" Population Share	block group	%
Share of Households Owner Occupied	block group	%
Share of Households Renter Occupied	block group	%
Share of Occupied Housing Units	block group	%
Male Population Share	block group	%
Female Population Share	block group	%
Median Age	block group	number of years
Population Share by Age Category (5-15 year intervals--min 5, max 85+)	block group	%
Population Share with High School Diploma	block group	%
Population Share with Associates Degree	block group	%
Population Share with Bachelor's Degree	block group	%
Population Share with Graduate/Terminal Degree	block group	%
Unemployed Population Share	block group	%
Labor Share in a Professional Occupation	block group	%

Labor Share in a Service Occupation	block group	%
Labor Share in a Laborer Occupation	block group	%
Labor Share in a Farm Occupation	block group	%
Labor Share in a Transportation Occupation	block group	%
Labor Share Working in the Agriculture Industry	block group	%
Labor Share Working in the Construction Industry	block group	%
Labor Share Working in the Manufacturing Industry	block group	%
Labor Share Working in the Wholesale Industry	block group	%
Labor Share Working in the Retail Industry	block group	%
Labor Share Working in the Transportation Industry	block group	%
Labor Share Working in the Information Industry	block group	%
Labor Share Working in the Finance Industry	block group	%
Labor Share Working in the Professional/Administrative Industry	block group	%
Labor Share Working in the Education/Health Industry	block group	%
Labor Share Working in the Leisure Industry	block group	%
Labor Share Working in Other Industries (except Public Admin)	block group	%
Labor Share Working in the Public Administration Industry	block group	%
Median Household Income	block group	$
Median Family Income	block group	$
Population Share by Income Categories ($10k intervals--min $10k, max $200k)	block group	%
Population Share in Poverty	block group	%
Median Rent	block group	$
Gross Rent as a Percent of Household Income (5% intervals--15%-35%)	block group	%
Population Share Born in the US	block group	%
Population Share Where English in the Primary Language	block group	%
Property Value Metrics		
Exposure Property Value Change (By Peril)	county	%
Market Property Value Change	county	%
Tax Revenue Metrics		
Total Taxes Collected	county	%
Total Revenue	county	%
Total Expenditures	county	%
Economic Metrics		

Debt-to-Income (DTI) ratio	county	%
Housing Price Index (HPI)	county	%
Gross Domestic Product (County total and by Sector)	county	%
Commercial Viability		
Number of Employees (By Sector)	county	%
Number of Establishments (By Sector)	county	%
Annual Payroll (By Sector)	county	%
Revenue (Receipts and Total Sales) (By Sector)	county	%
Total Business Expenditures (By Sector)	county	%